KTO KARATAY UNIVERSITY
THE SCHOOL FOR GRADUATE STUDIES
DEPARTMENT OF ELECTRICAL AND COMPUTER ENGINEERING
MASTER'S PROGRAM WITH THESIS

INNOVATIVE STANDALONE MASSIVE CHANNEL TEMPERATURE MONITORING SYSTEM FOR CMS DETECTOR

Hatice TEKİŞ

Master of Science

KONYA

June 2021

INNOVATIVE STANDALONE MASSIVE CHANNEL TEMPERATURE MONITORING SYSTEM FOR CMS DETECTOR

Hatice TEKİŞ

KTO Karatay University
The School for Graduate Studies
Department of Electrical and Computer Engineering
Master's Program with Thesis

Master of Science

Thesis Supervisor: Assist. Prof. Dr. Semih YUMUŞAK
Thesis Co-Supervisor: Dr. Andromachi TSIROU

Konya
June 2021

BİLDİRİM

Enstitü tarafından onaylanan Yüksek Lisans tezimin tamamını veya herhangi bir kısmını basılı veya dijital biçimde arşivleme ve aşağıda belirtilen koşullar dahilinde erişime açma iznini KTO Karatay Üniversitesine verdiğimi bildiririm. Bu izinle, Üniversiteye verilen kullanım hakları dışındaki tüm fikri mülkiyet haklarım bende kalacak ve gelecekteki çalışmalar (makale, kitap, lisans, patent vb.) için tezimin tamamının veya bir bölümünün kullanım hakları yalnızca bana ait olacaktır.

Tezimin bütünüyle kendi çalışmam olduğunu, başkalarının haklarını ihlal etmediğimi ve tezimin tek yetkili sahibi olduğumu beyan ve taahhüt ederim. Telif hakkı bulunan ve sahiplerinden yazılı izinle kullanılması zorunlu olan kaynakları, yazılı izin alarak kullandığımı ve istenildiğinde izinlerin suretlerini Üniversiteye teslim etmeyi taahhüt ederim.

Yükseköğretim Kurulu tarafından yayımlanan "Lisansüstü Tezlerin Elektronik Ortamda Toplanması, Düzenlenmesi ve Erişime Açılmasına İlişkin Yönerge" kapsamında, tezim, aşağıda belirtilen koşullar haricince, YÖK Ulusal Tez Merkezi ve KTO Karatay Üniversitesi Açık Erişim Sisteminde erişime açılır.

☐ Enstitü / Fakülte Yönetim Kurulu kararı ile tezimin erişime açılması mezuniyet tarihimden itibaren 2 yıl ertelenmiştir.[1]

☐ Enstitü / Fakülte Yönetim Kurulunun gerekçeli kararı ile tezimin erişime açılması mezuniyet tarihimden itibaren ... ay ertelenmiştir.[2]

☐ Tezimle ilgili gizlilik kararı verilmiştir.[3][4]

7th of June 2021

Hatice TEKİŞ

[1] MADDE 6(1) Lisansüstü tezle ilgili patent başvurusu yapılması veya patent alma sürecinin devam etmesi durumunda, tez danışmanının önerisi ve enstitü anabilim dalının uygun görüşü üzerine enstitü veya fakülte yönetim kurulu iki yıl süre ile tezin erişime açılmasının ertelenmesine karar verebilir.

[2] MADDE 6(2) Yeni teknik, materyal ve metotların kullanıldığı, henüz makaleye dönüşmemiş veya patent gibi yöntemlerle korunmamış ve internetten paylaşılması durumunda 3. şahıslara veya kurumlara haksız kazanç imkanı oluşturabilecek bilgi ve bulguları içeren tezler hakkında tez danışmanının önerisi ve enstitü anabilim dalının uygun görüşü üzerine enstitü veya fakülte yönetim kurulunun gerekçeli kararı ile altı ayı aşmamak üzere tezin erişime açılması engellenebilir.

[3] MADDE 7(1) Ulusal çıkarları veya güvenliği ilgilendiren, emniyet, istihbarat, savunma ve güvenlik, sağlık vb. konulara ilişkin lisansüstü tezlerle ilgili gizlilik kararı, tezin yapıldığı kurum tarafından verilir. Kurum ve kuruluşlarla yapılan işbirliği protokolü çerçevesinde hazırlanan lisansüstü tezlere ilişkin gizlilik kararı ise, ilgili kurum ve kuruluşun önerisi ile enstitü veya fakültenin uygun görüşü üzerine üniversite yönetim kurulu tarafından verilir. Gizlilik kararı verilen tezler Yükseköğretim Kuruluna bildirilir.

[4] MADDE 7(2) Gizlilik kararı verilen tezler gizlilik süresince enstitü veya fakülte tarafından gizlilik kuralları çerçevesinde muhafaza edilir, gizlilik kararının kaldırılması halinde Tez Otomasyon Sistemine yüklenir.

ETHICAL STATEMENT

I hereby declare that all the data, information, documents, evaluations, analyzes, findings, and results in this thesis document supervised under Dr. Semih Yumuşak and prepared following Thesis Preparation and Writing Rules of the School for Graduate Studies in KTO Karatay University has been obtained and presented within the framework of scientific rules and ethical conduct. I also declare that, as required by these rules and conduct, I have fully cited and referenced all material and results that are not original to this work.

7thof June, 2021

Hatice TEKİŞ

To my beloved family and my dear supervisor, Andromachi

ACKNOWLEDGMENTS

First and foremost, it was an honor and a privilege for me to do my master's studies at such a prestigious institute, CERN under the supervision of Dr. Andromachi Tsirou and Piero Giorgio Verdini. I had a great chance to meet, know and work with wonderful people during CERN 2020 Technical & 2019 Summer Student Programmes. I would like to thank those helping, inspiring, supporting me, and making this environment a very friendly one particularly throughout difficult pandemic times.

I would like to express heartfelt gratitude to my amazing supervisor Dr. Andromachi Tsirou. The completion of this thesis would not have been possible without her help and nurturing. She was the best supervisor I've ever met and is not only for being my advisor but also for her continuing support and invaluable guidance during my Master's of Science. She was more than a supervisor to me from beginning to end.

I would also like to express my most sincere gratitude to my co-supervisor Piero Giorgio Verdini for his guidance and for inspiring me with his professional experience. He patiently helped me throughout the process of learning new tools.

I acknowledge my university advisor Dr. Semih Yumuşak for accepting me as a master's student and guiding me. I would like to express my deepest appreciation to my jury committee; Dr. Bora Akgün and Dr. H. Oktay Altun for their unwavering support and valuable advice.

I am also grateful for the time I spent with lab mates; Wassef Karimeh, Tanya Angelova, and Amar Kapic. I enjoyed my time in the lab, and I am thankful for creating a supportive, enjoyable lab environment. I particularly wish to thank my friend Jakub Lukasz Wieczorek who helped me design a PCB card for this project. We had so much fun while working together, and I have never forgotten those moments. In addition, I would like to a special thank all my physicist and engineer friends who were with me during our time at CERN.

Last but not least, I am deeply indebted to my beautiful parents and brother, Ahmet Emir for endless support and always standing beside me in any condition. A very big thank goes to my dear friends Merve Şafak, Ünal Akar, Başak Dursun and Kübra Çalık for always staying beside me along this way from miles away.

7^{th} of June, 2021
Hatice TEKİŞ

ABSTRACT

Hatice TEKİŞ

Innovative Standalone Massive Channel
Temperature Monitoring System for CMS Detector

Master of Science Thesis

Konya, 2021

Compact Muon Solenoid (CMS) experiment has been preparing for Upgrade-2 and High Luminosity-Large Hadron Collider (HL-LHC) projects during Long Shutdown 2 (LS2) by replacing and enhancing electronics and the components of its detector. The Upgrade-2 project will implement high intensities in the collisions, which results in a highly integrated luminosity of about 2500 fb^{-1} at the heart of the detector. Moreover, the experiment will gather more data with the HL-LHC, which enables an additional integrated luminosity by a factor of 10 beyond the current luminosity value of the Large Hadron Collider (LHC) after 2027. Higher luminosity values bring about higher temperature onto electronics of the detector, therefore controlling and monitoring the temperature around the detector environment under challenging operating conditions plays a crucial role. This temperature monitoring has been fulfilled by the Programmable Logic Controller (PLC) up to this point in time. However, a new and optimum monitoring system is made essential because PLC-based monitoring is more expensive and takes much more place. The work presented in this thesis addresses the above-mentioned issues and proposes a novel temperature monitoring system using embedded systems. In this approach, we developed a Massive Temperature Monitoring System (MTRS), including sensor choices, designing readout circuitry, hardware and software implementations, and optimizing the issues to have arisen, as well as providing communication between MTRS and Detector Control System (DCS) via Open Platform Communications Unified Architecture (OPC UA) server. This dissertation discusses the reasons why the MTRS is essential for the future upgrades of the detector and furnishes the ways of embedded-based approach.

Keywords: OPC-UA, network programming, embedded systems, internet of things, integrated circuit design

ÖZET

Hatice TEKİŞ

CMS Algıcı İçin Yenilikçi Bağımsız Çok Kanallı Sıcaklık İzleme Sistemi

Yüksek Lisans Tezi

Konya, 2021

Kompakt Müon Solenoid (CMS) deneyi, elektronikleri ve dedektörünün bileşenlerini değiştirerek ve geliştirerek ikinci uzun kapatma dönemi (LS2) sırasında ikinci aşama güncelleme ve Yüksek Parlaklık-Büyük Hadron Çarpıştırıcısı (HL-LHC) projeleri için hazırlanmaktadır. Yükseltme-2 projesi, daha yüksek yoğunlukta çarpışma gerçekleştirecek ve bu da dedektörün kalbinde yüksek parlaklık ile sonuçlanacaktır. Dahası, deney, 2027'den sonra Büyük Hadron Çarpıştırıcısı'nın (LHC) mevcut parlaklık değerinin ötesinde 10 kat daha fazla entegre parlaklık sağlayan HL-LHC ile daha fazla veri toplayacaktır. Daha yüksek parlaklık değerleri, elektroniklerin ısınmasına yol açacaktır, bu nedenle dedektörün çevresindeki sıcaklığın kontrol edilmesi ve izlenmesi çok önemli bir rol oynamaktadır. Bu sıcaklık izleme, zaman içinde bu noktaya kadar Programlanabilir Mantık Denetleyicisi (PLC) tarafından yerine getiriliyordu. Fakat, PLC tabanlı izlemenin daha pahalı olması ve çok daha fazla yer kaplaması nedeniyle yeni ve optimum bir izleme sisteminin geliştirilmesi zorunlu hale getirilmiştir. Bu tezde sunulan çalışma, yukarıda belirtilen konuları ele almakta ve gömülü sistemler kullanarak yeni bir sıcaklık izleme sistemi önermektedir. Bu yaklaşımda, sensör seçimlerini, okuma devresini, donanımın ve yazılım uygulayan ve ortaya çıkacak sorunları optimize eden, ayrıca OPC- UA sunucusu aracılığıyla MTRS ve Algıç Kontrol Sistemleri (DCS) arasındaki iletişimi sağlayan MTRS sistem geliştirilmiştir. Bu tez, MTRS'nin dedektörün gelecekteki yükseltmeleri için neden gerekli olduğunu tartışmakta ve gömülü tabanlı yaklaşımın yollarını sunmaktadır.

Anahtar kelimeler: OPC-UA, ağ programlama, gömülü sistemler, nesnelerin interneti, entegre devre tasarımı

TABLE OF CONTENTS

ACCEPTANCE AND APPROVAL i

BİLDİRİM ii

ETHICAL STATEMENT iii

ABSTRACT vi

ÖZET vii

LIST OF TABLES xii

LIST OF FIGURES xiii

LIST OF ACRONYMS/ABBREVIATIONS xvi

LIST OF SYMBOLS xix

1. INTRODUCTION 1

2. LARGE HADRON COLLIDER 6
   - 2.1. Overview of Particle Accelerators 6
     - 2.1.1. Energy in centre-of-momentum (COM) frame 7
     - 2.1.2. A Performance Parameter: Luminosity 10
     - 2.1.3. Acceleration Methods 11
   - 2.2. Overview of LHC and its Status 14
     - 2.2.1. Upgrades and Schedule of LHC 16
     - 2.2.2. High Luminosity LHC (HL-LHC) 18
   - 2.3. The Layout of LHC 18

2.3.1. Journey from Proton Source to Vacuum Chamber 18
2.3.2. Accelerator Complex at CERN 19
2.3.3. Beam Collimation and Arc Layout at LHC 21

3. COMPACT MUON SOLENOID (CMS) 24
3.1. Structure of CMS Detector 26
3.2. Tracker 28
3.3. Electromagnetic Calorimeter (ECAL) 30
3.4. Hadronic Calorimeter (HCAL) 32
3.5. Muon System 34
3.6. Trigger and DAQ System 35
3.7. HL-LHC Upgrade of CMS 37
3.7.1. Upgrade of CMS Tracker 38
3.7.2. Upgrade of CMS Calorimeters 38
3.7.3. Upgrade of Muon System 39
3.7.4. Upgrade of the Trigger and DAQ system 39

4. CONCEPTS OF THE CMS MONITORING SYSTEM 40
4.1. Temperature Monitoring System for Silicon Detectors 40
4.2. CMS Detector Readout and Monitoring System 42
4.3. CMS Detector Control System 43
4.4. CMS Detector Safety System 45
4.5. CMS Detector Readout System 46
4.6. CMS Cold Detector System 47

5. MASSIVE TEMPERATURE READOUT SYSTEM 49
5.1. Evaluation of the LTC2984 50
5.1.1. Overview of the LTC2984 Chip 51
5.1.2. Testing the LTC2984 with the DC2420 Kit 53
5.2. The First Stage of the MTRS 56
5.3. The Readout Card Design of MTRS-I 57
5.4. The DAQ of the MTRS-I 59
5.4.1. Configuration of the Sense Resistor 61
5.4.2. Configuration of the RTD Sensor 61

6. THE FIRST RESULTS OF THE MTRS 68
6.1. Results and Challenges of the MTRS Stage 1 68
6.2. Proposed Solutions for the Stage 1 Boards 68
6.3. The Second Version of the MTRS Boards 72

7. DATA TRANSMISSION: RPi to DCS 78
7.1. Overview of Socket Programming 79
7.2. Development of the Socket Programming 80
7.3. The OPC UA for the MTRS 81
7.4. Overview of the OPC UA 82
7.5. Specifications of OPC UA 84
7.5.1. OPC UA Data Access Specification 84
7.5.2. OPC UA Alarm and Conditions (AC) Specification 86
7.5.3. OPC UA Historical Access (HA) Specification 86
7.5.4. OPC UA Program Specifications 87
7.6. Information Model of OPC UA 87
7.6.1. Address Space 88
7.7. Development of OPC UA Server and Client 89

8. CONCLUSION 92

9. TÜRKÇE GENİŞLETİLMİŞ ÖZET 94
9.1. Giriş 94
9.2. LHC ve Parçacık Hızlandırıcılar 97
9.2.1. Parçacık Hızlandırıcılara Genel Bir Bakış 97
9.2.2. Büyük Hadron Çarpıştırıcısı 99
9.3. Kompakt Müon Selonoid (CMS) 100
9.4. CMS'in Detektör Kontrol ve Güvenlik Sistemleri 102
9.5. Çok Kanallı Sıcaklık Sensörlerini Okuma Sistemi 104
9.5.1. MTRS Aşama 1 Kartlarından Verilerin Elde Edilmesi 107
9.6. MTRS Aşama 1'nin Sonuçları ve Getirdiği Problemler 108
9.6.1. MTRS Aşama 1'nin Sonuçları ve Değerlendirilmesi 108
9.6.2. MTRS Aşama-2 Tasarlanması 109
9.7. RPi'den DCS'e Veri Akışı 109
9.8. Sonuç 110

REFERENCES 112

APPENDIX 1. EDA-04119-V1-0 SCHEMATIC DRAW 121

APPENDIX 2. EDA-04119-V1-0 PCB MATERIALS 123

APPENDIX 3. EDA-04119-V2-0 SCHEMATIC DRAW 124

CURRICULUM VITAE 127

LIST OF TABLES

Table 2.1 The nominal operation parameters of the LHC ring. 15

Table 4.1 Si-sensor operating temperatures of the multi-purpose LHC detectors. 42

Table 5.1 The excitation current values corresponding to RTD wire types. . 63

Table 5.2 The most significant 5 bits of the sense resistor channel assignment word consisting of 32 bits. 64

Table 5.3 Sense resistor value (1 kΩ) representation with binary notation. . . 64

LIST OF FIGURES

Figure 2.1 Instantaneous luminosity is calculated by taking the geometry of the bunches of protons and the parameters of the beam into consideration. 10

Figure 2.2 A circular accelerator with RF cavities, bending and focusing magnets. 12

Figure 2.3 Design of a linear accelerator. 13

Figure 2.4 Accelerator complex at CERN. 14

Figure 2.5 Instantaneous the LHC luminosity over 10 years with the evolution of possible peak luminosity at LHC. 17

Figure 2.6 The schedule of LHC upgrades. 18

Figure 2.7 The cross section of LHC ultra-high vacuum pipe. 20

Figure 2.8 Arc layout of the LHC. 22

Figure 2.9 F and Q type quadrupole magnets. 23

Figure 2.10 The structure of each arc cell at the LHC. Dipole magnets aims to keep the beams inside the ring and quadrupole magnets focus them in both directions. 23

Figure 3.1 Labelled schema of the CMS detector. 24

Figure 3.2 CMS cavern consists of UXC (experimental cavern) and USC (underground cavern). 25

Figure 3.3 (a) Illustration of the longitudinal scattering angle θ_{CM} is presented (left) and (b) a variety of pseduraphidity corresponding to different values of θ_{CM} is given (right). 26

Figure 3.4 Sublayers of CMS detector with different signatures of the particles. 27

Figure 3.5 Schematic view of CMS Tracker in r-z plane. 29

Figure 3.6 The barrel part of CMS Tracker in xy plane. 30

Figure 3.7 The ECAL sublayer of CMS detector. 31

Figure 3.8 A schematic view of the HCAL. 33

Figure 3.9 The muon chamber with its three gaseous detectors. 35
Figure 3.10 CMS triggering and DAQ system. 36
Figure 3.11 Data flow in L1 triggering system of the CMS detector. 37
Figure 4.1 A schematic view of main CMS DCS with its sub-DCS. 44
Figure 4.2 Overview of HGCAL Detector Safety System. 46
Figure 4.3 CMS Cold Detector Safety System. 48
Figure 5.1 The development steps of the MTRS project. 50
Figure 5.2 The LTC2984 chip measuring various temperature sensors with high accuracy. 51
Figure 5.3 Blok diagram of the LTC2984 chip. 52
Figure 5.4 The DC2420 evaluation kit comprises of Linduino, DC2399 circuit including LTC2984 chip and DC2210 circuit for connection of six RTD sensors. 54
Figure 5.5 Configuration of five RTD PT-1000 and a RTD PT-100 sensors tied to LTC2984 board. 55
Figure 5.6 Configuration of a RTD sensor tied to Channel-4 is performed using QuikEval software. 56
Figure 5.7 The first stage of the MTRS board. 59
Figure 5.8 The block diagram of temperature sensors readout procedure for MTRS Stage 1. 60
Figure 5.9 The five MSBs of the channel assignment word are set as RTD types configuration. 61
Figure 5.10 Bits B13 and B12 are assigned as the RTD curve and are the corresponding *Callendar-Van Dusen* constants. 63
Figure 5.11 The global configuration register of the LTC2984 chip is used for defining the notch frequency and temperature format. 65
Figure 6.1 Sensors values from chip-1 at different times. 69
Figure 6.2 RTD values reading from Chip-4 located onto the first version of MTRS board. 69
Figure 6.3 It is the first version of MTRS board which were connected Arduino to the first VME input and tied chiller via sensors to its second VME input. 70

Figure 6.4 The temperatures reading with Arduino connecting the a single MTRS board. 70
Figure 6.5 Adaptor Board including RS485 and ATMEGA328P is connected to RS422/RS485 Modbus shield onto Raspberry Pi 4B+. 72
Figure 6.6 Three different communication protocols were used with Atmega328P. 72
Figure 6.7 PLC structure consists of 32 crates and each crates has 8 modules. Each module associates with a number of channels (depends upon the system) and each channel gets data with some information–id, type, flag. 73
Figure 6.8 An overview of MTRS structure. 74
Figure 6.9 Board connectivity with minimal implementation (adaptor board). 75
Figure 6.10 The limited implementation of the MTRS. 75
Figure 6.11 The rich implementation of the MTRS with intermediary partner. 76
Figure 6.12 PLC system communicates its slaves over Modbus protocol. . . . 76
Figure 6.13 The Stage 2 of the MTRS board. 77
Figure 7.1 The sensor data flow from the boards to the DCS by developing socket server/client and OPC UA server/client. 78
Figure 7.2 The OPC UA structure that composed variety layers. 85
Figure 7.3 The node model of OPC UA within the framework of address space model. 88
Figure 7.4 The object model of OPC UA. 89
Figure 7.5 FreeOpcUa GUI OPC UA Client with its nodes, objects, and variables. 91
Figure 9.1 MTRS Phase 1 circuit design for SPI communication, board and chip selections. 121
Figure 9.2 A LTC2984 IC connections by two VME connectors (Raspberry Pi and sensors) in MTRS Phase 1. 122
Figure 9.3 Materials used for PCB design of MTRS Phase 1. 123
Figure 9.4 VME sensor connections by four LTC2984 ICs, and ATMEGA328P SPI, UART and I^2C connections with four LTC2984 chips in MTRS Phase 2 circuit design. 124

Figure 9.5 MTRS Phase-2 circuit design continues with connections between ATMEGA328 and RS485 TTL circuit. 125
Figure 9.6 A LTC2984 IC connections by VME connectors (sensor connections) and ATMEGA328P in MTRS Phase 2. 126

LIST OF ACRONYMS/ABBREVIATIONS

AC	Alternating Current.
AD	Antiproton Decelerator.
ADC	Analog-to-Digital Converter.
ALICE	A Large Ion Collider Experiment.
APD	Avalanche Photodiode.
ATLAS	A Toroidal LHC ApparatuS.
BPIX	Barrel Pixel.
CERN	Conseil Européen pour la Recherche Nucléaire.
CLK	Clock.
CM	Center-of-Mass.
CMS	Compact Muon Solenoid.
CNGS	CERN Neutrinos to Gran Susso.
COM	Center-of-Momentum.
COTS	Commercial Off-The-Shelf.
CSC	Cathode Strip Chambers.
DAQ	Data Acquisition.
DC	Direct Current.
DCS	Detector Control System.
DCU	Detector Control Unit.
DSS	Detector Safety System.
DT	Drift Tubes.
EB	Electromagnatic Barrel.
ECAL	Electromagnatic Calorimeter.
EE	Electromagnatic Endcap.
FPIX	Forward Pixel.
GBT-SCA	Gigabit Transceiver-Slow Control Adaptor.
GUI	Graphical User Interface.

HB	Hadronic Barrel.
HCAL	Hadronic Calorimeter.
HGCAL	High Granularity Calorimeter.
HL-LHC	High Luminosity-Large Hadron Collider.
HLT	High-Level Trigger.
HMI	Human-Machine Interface.
HO	Hadronic Outer.
ICs	Integrated Circuit.
IoT	Internet of Things.
IP	Interaction Point.
ISOLDE	ISotope Separator Online Device.
L1	Level 1.
LEIR	Low-Energy Ion Ring.
LHC	Large Hadron Collider.
LHCb	Large Hadron Collider beauty.
Linac	Linear Accelerator.
LS	Long Shutdown.
M2M	Machine-to-Machine.
MISO	Master Input Slave Output.
MOSI	Master Output Slavee Input.
MTD	MIP Timing Detector.
MTRS	Massive Temperature Readout System.
OPC	Open Platform Communication.
OPC UA	Open Platform Communication Unified Architecture.
PLC	Programmable Logic Controller.
PS	Proton Synchrotron.
PSB	Proton Synchrotron Booster.
RPC	Resistive Plate Chamber.
RPi	Raspberry Pi.
RTD	Resistive Temperature Detector.
SCADA	Supervisory Control and Data Acquisition.
SM	Standard Model.
SoC	System on Chip.

SPI	Serial Peripheral Interface.
SPS	Super Proton Synchrotron.
SUSY	Supersymmetry.
TCP/IP	Transmission Control Protocol/Internet Protocol.
TEC	Two EndCaps.
TIB	Tracker Inner Barrel.
TID	Two Inner Disks.
TOB	Tracker Outer Barrel.
UDP	User Datagram Protocol.
USC	Underground Service Cavern.
UXC	Underground Experimental Cavern.
WinCC OA	WinCC Open Architecture.

LIST OF SYMBOLS

c	Speed of light in a vacuum
E	Energy
E_1	Energy of 1st particle
E_2	Energy of 2nd particle
f	Number of revolution per second
h	Planck constant
m	Mass
m_1	Mass of 1st particle
m_2	Mass of 2nd particle
$\dot{\mathscr{N}}$	Number of collision in a certain time
n	Number of bunch
N_1	Number of particle inside the Beam-1
N_2	Number of particle inside the Beam-2
$\overrightarrow{p}$	Momentum of any particle
p_i	Momentum of i^{th} particle
$\overrightarrow{p_1}$	Momentum of 1st particle
$\overrightarrow{p_2}$	Momentum of 2nd particle
T	Temperature
$\sqrt{s}$	Mandelstam variable
$\mathscr{L}$	Luminosity
$\mathscr{L}_{int}(t_1 - t_0)$	Integrated luminosity
η	Psedurapidity
θ	Incident angle where two beams collide
λ	Wavelength
σ	Cross-sectional area
ϕ	Azimuthal angle

1. INTRODUCTION

The world's foremost particle and accelerator physics laboratory, Conseil Européen pour la Recherche Nucléaire (CERN) has been conducting researches on groundbreaking discoveries concerning physics beyond the Standard Model (SM) (Langacker, 1986) explaining sub-atomic particles and their interactions or Supersymmetry (SUSY) (Fayet & Ferrara, 1977) forecasting partner of every particle in the Standard Model. The world's largest accelerator Large Hadron Collider (LHC) accelerator with its state-of-art experiments, has been operating for twelve years including Long Shutdown (LS) phases (which are maintenance phases for both the LHC and its detectors). Recently, the LHC is in the ongoing LS2 phase for upcoming Run 3 (which also known as Phase 2) so as to reach 14 TeV of center-of-mass (CM) energy and $2 \cdot 10^{-34}\ cm^{-2} \cdot s^{-1}$ of instantaneous luminosity. (Tsirou, 2020-12-05).

Following Run 3, it will go into the LS3 phase, in which the instantaneous luminosity will be increased two or even three times. That's why the LHC and its detectors have been upgraded for both Run 3 and High Luminosity-LHC (HL-LHC)(Béjar Alonso et al., 2020) phases. The goal of reaching high luminosities and CM energies is to advance our understanding regarding behavior, interactions, and decays of the Higgs boson discovered in 2012. Therefore, two multi-purpose detectors of the LHC; A Toroidal LHC ApparatuS (ATLAS) and Compact Muon Solenoid (CMS) are deployed to perform this purpose.

Currently, the CMS experiment has been preparing for what is called Upgrade 2 during which the accelerator will provide CMS an additional integrated luminosity of about 2500 fb^{-1} over 10 years of operation, starting in 2028. (Akgun, 2021-05-03).

The HL-LHC project aims to enhance the performance of LHC in order to increase the potential for discoveries. The objective is to increase integrated luminosity by ten-

fold beyond the LHC's nominal design values, enhancing the potential for physics discoveries(Béjar Alonso et al., 2020). For this objective, the CMS detector comes up against some issues stated below and will arrive at the solutions here below.

The CMS detector is being prepared for

1. Upgrading the sub-detectors to cope with the high radiation environment which necessitates.
    i The CMS Tracker and the end-cap calorimeters will be completely replaced, starting with replacing the Tracker Pixel detector.
    ii The barrel ECAL will operate at below-cavern-dewpoint temperatures for reasons of Avalanche Photodiode (APD) noise mitigation. It will operate at 100°C while the cavern dewpoint is 130°C.
    iii There will also be major electronics overhaul and consolidation of the barrel calorimeters and muon systems.
2. Handling the expected high pile-up will require:
    i Improving readout granularity.
    ii Novel techniques mitigate the pile-up[1] effect using 30 ps precision timing detectors.

(Tsirou, 2020-12-05).

Accompanied by the sub-detectors and systems upgrades, new front-end electronics have to be developed for readout, monitoring and controlling the "environmental" sub-detector parameters. These parameters are very important for the operation and the services of the detector but are equally important during the sub-detector evaluation, testing, and assembly phases. The parameters are namely temperature, dewpoint, radiation,

[1] Pile-up is simultaneous inelastic scattering event per 25 ns spaced bunch crossing (Fartoukh, 2014).

traces of other gases, and the composition of the drying gas.

The traces of the other gases can appear due to the CO_2 based cooling systems. Moreover, the composition of the drying gas, which is used permanently inside the detector in order to avoid electrical fires when the detector is operating and has to allow personnel to work in the detector premises when the detector is in a review phase (O_2, smoke). Thus, the above-stated parameters require the development of new electronic systems in order to handle the problems mentioned above.

In this thesis, a promising temperature monitoring system will be discussed as it is of paramount importance in all the Si-based sub-detector developments –Tracker, HGCAL, partially ECAL –but not only, since the increase in granularity and irradiation impacts the importance of standalone temperature monitoring both for the sub-detectors as well for the supporting systems (cooling, dry gas, Si-detector storing cabinets).

It can be emphasized that the Phase 1 CMS Si-based sub-detectors are equipped with detailed temperature monitoring employing two temperature sensor technologies; integrated thermistor sensors in the Detector Control Unit (DCU) that are used for monitoring the Tracker readout electronics temperature and whose data is available via the data acquisition (DAQ) streams and resistive temperature detector (RTD) sensors ($\sim$ 1000) attached at strategically important parts of the detector and its services that are attached to the Detector Safety System (DSS) Programmable Logic Controller (PLC)-based control. (Yousaf Shah et al., 2009).

The sensor of preference is RTD because of its interchangeability and its excellent behavior under irradiation, being the affordable sensor of choice in many nuclear installations. The 4-wire type of RTD sensors is utilized to monitor the temperature of the detector environment on account of reasons of accuracy and the fact that even if in our "demanding" installations one wire breaks the three provide adequate accuracy for our type of measurements.

Same functionality PLC-based systems have been accompanying several CMS Tracker facilities outside the detector site (Yousaf Shah et al., 2009). However, using PLCs for sensor-based monitoring is not at all an optimized use of this indispensable industrial safety tool. The cost is above 50 CHF per channel which means a significant cost for a system that can very well consist of more than 100 sensors. A PLC installation is meant for a more permanent implementation and has significant hardware requirements; this translates to space requirements as well. Data monitored via a PLC would be available to the user via a CERN-wise Supervisory Control and Data Acquisition (SCADA) system which also means some serious overhead in software development. Having therefore be comprehended the need for a temperature monitoring system that:

- Could be deployed without much effort and provide between some tens and some hundreds of temperature measurements.
- Could function as a standalone system or part of a Detector Control System (DCS) environment or be integrated into a DSS.
- Keeps the RTD as a sensor of preference given its very satisfactory attitude over ten years of operation within CMS.
- Offers the user a system that will be "plug and play" and provides the choice between all the options shown in item 2 of the list.

Having deduced the reasons of significance and requirements of the MTRS project, the chapters of this dissertation can be reviewed. This thesis is organized as follows –The second chapter gives a brief overview of the LHC and its concepts by explaining its phases, particularly HL-LHC and Run 3, and a brief description of its consecutive interconnected collider chains. The third chapter introduces the CMS sub-detectors along with primary importance upgrade; HL-LHC, and new demands and developments. Chapter 4 focuses on the description of the CMS detector control and safety systems and the reason why the temperature monitoring systems are quite essential for Si-based detec-

tors. A novel approach for temperature read-out is presented in Chapter 5. It highlights the steps of the MTRS project, how the new readout PCBs were designed, and their DAQ streams. The next chapter presents the data transmission via socket programming, Open Platform Communications Unified Architecture (OPC UA) communication protocol and its nomenclature, and how the server-client communication between Raspberry Pi (RPi) and the PCBs was implemented. Chapter 6 demonstrates the first test results of the MTRS by employing a variety of chillers used for High Granularity Calorimeter (HGCAL), ECAL, and Tracker before being installed on the CMS detector-off side. The conclusion of this work is drawn in the final chapter. It underlines the importance of cutting-edge solutions and outlines the attainable future of the MTRS project. A few general remarks on the achievement so far of the performance of the MTRS system conclude this dissertation.

2. LARGE HADRON COLLIDER

This chapter introduces the environment of this thesis. It will promisingly serve to understand the Large Hadron Collider (LHC) experiment which employs a temperature measuring system. Section-2.1. gives a broad overview of the particle accelerators along with the essential nomenclature so that readers can follow the discussion throughout the dissertation. Section-2.2. aims to outline the LHC and its phases as well as the future LHC upgrade –HL-LHC. Finally, the structure and working principle of the LHC is presented in Section-2.3.

2.1. Overview of Particle Accelerators

Technological progress has always been connected to the never-ending human quest to understand the Universe that surrounds us. Ever since the human understood that there is more in nature than the bare eye can see, microscopes evolved to electronic microscopes, and finally turned into particle detectors that allow us to observe matter to the level of subatomic particles. The particle accelerators have been developed to recreate the Universe's conditions during the first fractions of a second after the Big Bang. Therefore, they are built so physicists focusing on the field of high energy physics can observe the tiniest of subatomic particles.

The underlying physics theory of particle accelerators is based on an energy-mass equivalence that is Einstein's theory of relativity; is expressed with $E = m \cdot c^2$. Accelerated particles gain kinetic energy when the particles get closer to the speed of light with accelerators. Thereby, this energy transfers into a mass due to the relativistic effect, and at the end of the day, this results in a variety of scattered particles that have a bigger mass. Along with Einstein's theory, Rutherford's idea in which the positively charged particle source had more energy emitted from natural radioactive materials has been made it

possible to produce beams of particles. Thus, the necessity that is the development of the particle accelerators had stepped forward. (Myers, 2012).

The particle accelerators, defined as huge "microscopes", give a spatial resolution to the physicists to explore the new substructures. This spatial resolution is associated with the beam energy. According to the *de Broglie wave-particle duality* (De Broglie, 1924), the momenta of any particle has a corresponding wavelength. (*ETH – Institute for Theoretical Physics – Particle Physics Phenomenology 1 – HS 2010*, 2010).

The relation is given by

$$\lambda = \frac{h}{|\overrightarrow{p}|} \tag{2.1}$$

If the momentum (i.e., the energy of the particle) increases, the wavelength of the particle packet gets smaller; thus, subatomic particles located at the high-frequency region of the electromagnetic spectrum can be observed. Accessing higher energy provides a very good resolution for observation of the secondary particles that can be stable, unstable, charged, or neutral. For instance, considering the spatial resolutions at $|\overrightarrow{p}| = 1$ GeV/c and $|\overrightarrow{p}| = 10^3$ GeV/c are expressed in Equation 2.2 and Equation 2.3, we can observe protons and even quarks. (*ETH – Institute for Theoretical Physics – Particle Physics Phenomenology 1 – HS 2010*, 2010).

$$|\overrightarrow{p}| = 1 \text{ GeV/c} \rightarrow \lambda = 1,24 \cdot 10^{-15} \text{ m} \cong \text{ size of a proton} \tag{2.2}$$

$$|\overrightarrow{p}| = 10^3 \text{ GeV/c} \rightarrow \lambda = 1,24 \cdot 10^{-18} \text{ m} \cong \text{ size of quarks} \tag{2.3}$$

2.1.1. Energy in centre-of-momentum (COM) frame

The accelerators provide sufficient collision energy to the particles to collide particles with either a fixed target or another beam head-on. This energy is determined by a reference frame calculating the cumulative collision energy of a target particle and a projec-

tile particle. This frame is known as the center-of-mass (CM) or center-of-momentum frame (COM) in which the projectile and the target particles have the same magnitude but opposite momentum; p. It is critical for the emergence of secondary high-energy particles. The "Mandelstam variable" s (Mandelstam, 1958), represents the particles' total kinetic and rest energy, and $\sqrt{s}$ corresponds to the CM, calculating by the following formula;

$$s = \left(\sum_{i=1,2,\ldots} E_i \right)^2 - \left(\sum_{i=1,2,\ldots} p_i \right)^2 \cdot c^2 \tag{2.4}$$

(*PHYS3002 : NUCLEI AND PARTICLES Lecture Notes*, 2015).

Considering collision of two particles –the target and projectile particles –s that is invariant quantity, is defined by

$$s = \left(p_1^\mu + p_2^\mu\right)^2 \tag{2.5}$$

$$s = (E_1 - E_2)^2 - (\overrightarrow{p_1} - \overrightarrow{p_2})^2 \tag{2.6}$$

(*PHYS3002 : NUCLEI AND PARTICLES Lecture Notes*, 2015).

If the collision performs at an incident angle;θ, s is expressed as,

$$s = (m_1 \cdot c^2)^2 + (m_2 \cdot c^2)^2 + 2 \cdot (E_1 \cdot E_2 - 2 \cdot p_1 \cdot c \cdot p_2 \cdot c \cdot cos(\theta)) \tag{2.7}$$

(Cid-Vidal X. and Cid R., 2010; *PHYS3002 : NUCLEI AND PARTICLES Lecture Notes*, 2015).

The E_{CM} is calculated as following formula.

$$s = (m_1 \cdot c^2)^2 + (m_2 \cdot c^2)^2 + 2 \cdot (E_1 \cdot m_2 \cdot c^2) \tag{2.8}$$

In fixed target collision, four momentum of target and projectile target by Lorentz inva-

riant is $p_1^\mu = (E_1, \overrightarrow{p_1})$ and $p_2^\mu = \left(m_2, \overrightarrow{0}\right)$. The CM energy, $\sqrt{s}$ is

$$E_{CM} = \sqrt{s} = \sqrt{m_1^2 + m_2^2 + 2E_1 \cdot m_2} \tag{2.9}$$

$$\text{if } E_1 \gg m_i \; \sqrt{s} \cong \sqrt{2 \cdot E_1 \cdot m_2} \tag{2.10}$$

where m_2 is the mass of the target and m_1 is the mass of the projectile particle to be collided to the fixed target. Here, c is considered as natural unit (i.e $c = 1$) and the momentum of target, p_2 is taken as zero. (Cid-Vidal X. and Cid R., 2010)

Besides fixed target collision, the center-of-mass energy for head-on collision is defined by the following equation,

$$E_{CM} = \sqrt{s} = \sqrt{m_1^2 + m_2^2 + 2 \cdot (E_1 \cdot E_2 + |\overrightarrow{p_1}| \cdot |\overrightarrow{p_2}|)} \tag{2.11}$$

(Cid-Vidal X. and Cid R., 2010).

Recalling that, $\theta = 180^\circ$ is incident angle between two beams, due to head-on collision. if $E_1, E_2 \gg m_i$; $\sqrt{s} \cong \sqrt{4 \cdot E_1 \cdot E_2}$; thus, following equation is obtained as,

$$\sqrt{s} \cong 2 \cdot \sqrt{E_1 \cdot E_2} \tag{2.12}$$

(Cid-Vidal X. and Cid R., 2010).

If particles having the same momentum (like proton-proton) collide together, the center-of-mass energy for the symmetric beam is $2 \cdot E_{beam}$. For instance, the LHC is the symmetric collider that is potent to accelerate 7 GeV beams in clock and counterclockwise where the E_{CM} reaches 14 GeV.

2.1.2. A Performance Parameter: Luminosity

One of the things that determine the performance of an accelerator is luminosity. The luminosity is the measure of the number of collisions per surface unit and per unit time. The luminosity is stated as two different ways; instantaneous and integrated luminosity. The instantaneous luminosity is the rate of pile-up events in the accelerator and is defined by the formula below. (L. R. Evans & Bryant, 2008).

$$\dot{\mathscr{N}} = \sigma \times \mathscr{L} \tag{2.13}$$

Here, $\dot{\mathscr{N}}$ is number of collision in a certain time, σ is cross-sectional area of crossing beam, measured in cm^{-2} or *barn* [1], and $\mathscr{L}$ is luminosity. The geometry of two beams is

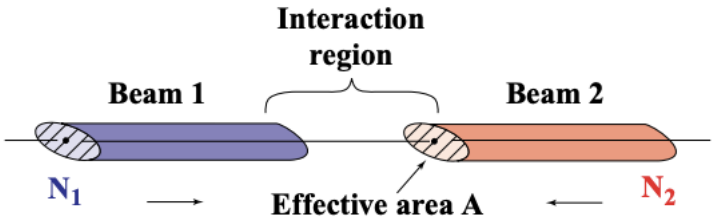


Figure 2.1: Instantaneous luminosity is calculated by taking the geometry of the bunches of protons and the parameters of the beam into consideration.
(*Large Hadron Collider (LHC) Lecture*, 2016).

shown in Figure-2.1, and instantaneous luminosity is expressed as a number of collisions per a cross-sectional area at a second. It is expressed as

$$\mathscr{L} = \frac{1}{\sigma} \cdot \frac{\triangle N}{\triangle t} \tag{2.14}$$

[1] The barn that is the metric unit corresponds to a cross-sectional area of a nucleus. A *barn* (shown as *b*) refers to $10^{-28}\ m^2$.

It is denoted in units of $cm^{-2} \cdot s^{-1}$.

$$\mathscr{L} = n \cdot \frac{N_1 \cdot N_2}{\sigma} \cdot f \tag{2.15}$$

(Cid-Vidal X. and Cid R., 2010).

where n means number of bunches, N_1 is number of particle inside the Beam-1 and N_2 is number of particle inside Beam-2, f is number of revolutions per seconds, so $\triangle N$ equals to $n \cdot N_1 \cdot N_2$.

Integrated luminosity is the sum of all luminosity occurred in within a certain time range.

$$\mathscr{L}_{int}(t_1 - t_0) = \int_{t_0}^{t_1} \mathscr{L}(\tau) \cdot d\tau \tag{2.16}$$

(Cid-Vidal X. and Cid R., 2010).

Increasing luminosity states that the bunches are required to be more intense and more focused than the current case in any accelerator (e.g., the LHC). To increase luminosity, the number of bunches (n) and the number of particles (generally protons are used) in a bunch (N_1 and N_2) have to be increased. Moreover, one increases the luminosity by decreasing the cross-sectional area at the interaction point of beams and the distance between successive bunches measured in time.

2.1.3. Acceleration Methods

Ever since 1930, various types of accelerators with ever-higher energies have been built and have been operating for servicing different purposes. Over time the level of maximum reached center-of-mass energy was increased from 100 keV to 10 TeV exponentially, and hence this has been opening the doors for new research and discoveries (Myers, 2012). When taken into consideration of discoveries in high energy physics, the mandate of particle accelerators is to accelerate charged particle beams at a speed close

to the speed of light, either for making them collide to a specific target or for providing collisions of (two) beams together.

To carry out the above-stated purposes, one needs a potential difference to speed up charged particles in the simplest form. The potential difference can be formed by connecting two metal plates to the poles of a DC source, and thus particles start to be accelerated under the influence of the electric field. These accelerators are called the simplest electrostatic accelerators. (Ogur & Yildiz, 2020-09-12).

In the progress of time the electrostatic accelerators like the Cockroft-Walton (COCKCROFT & WALTON, 1932), Van de Graff have been built, but the maximum energy reached with these accelerators is limited with the power supply. To address this issue, the accelerator design was switched from Direct Current (DC)-based to Alternating Current (AC)-based. The AC-based accelerators are also known as RF accelerators owing to operating under a certain resonance range. Providing energy to RF accelerators performs with the RF cavities. (Ogur & Yildiz, 2020-09-12).

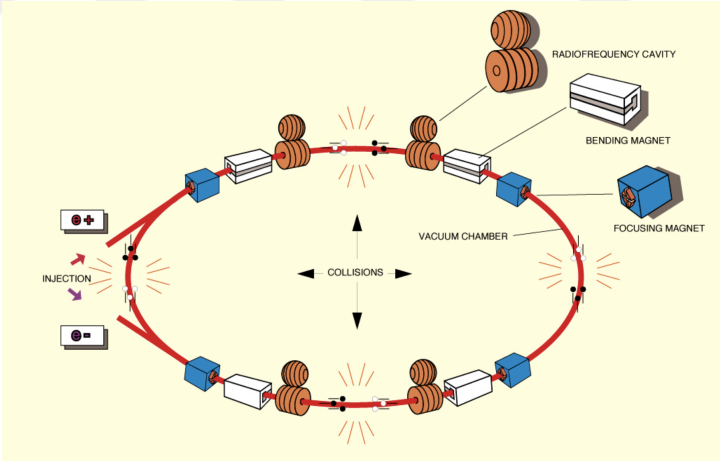


Figure 2.2: A circular accelerator with RF cavities, bending and focusing magnets. (Burnet, 2016).

Nowadays there are two main types of AC-based accelerator —Linear and Circular. The linear accelerators are based on the sequential drift tubes connecting an AC source

and an ion source. Two sequential drift tubes are connected to different poles of the AC source and oppositely charged each other. Thereby, an electric field is generated in the space between two drift tubes and accelerates the particles. Besides the linear accelerators, the circular accelerators accelerate charged particles using RF cavities to provide energy to the particles. They are bent and kept their path on an orbit using dipole magnets. Also, the particles are forced to pass from the RF cavities several times until reaching the final energy, as shown in Figure-2.3. (*PHYS3002 : NUCLEI AND PARTICLES Lecture Notes*, 2015).

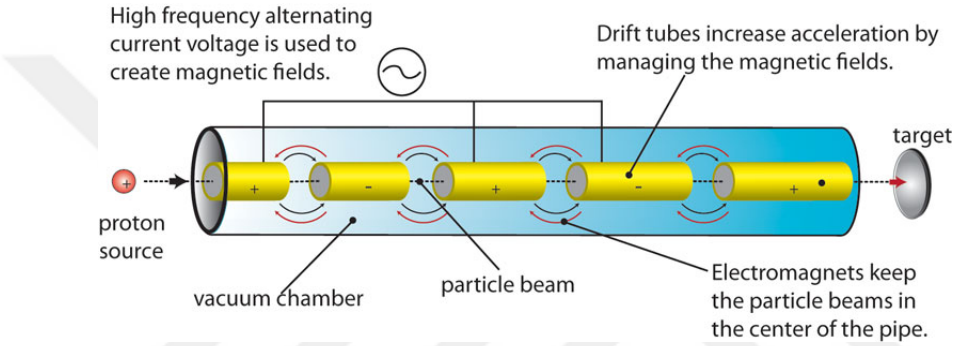


Figure 2.3: Design of a linear accelerator.
(*The Atomic Age, A Linda Hall Library Exhibition*, Unknown).

In today's accelerator physics, circular accelerators are employed more than linear accelerators around the world because the linear accelerators must have a tremendous length to reach the energy of the circular accelerator. Furthermore, the circular accelerators provide many collision chances because the particles circulate many times into the accelerator. (Ogur, 2020-09-12). The most commonly used circular accelerator is the synchrotron(Myers, 2012).

In the world, the largest and most advanced research accelerators are located at CERN. There is a total of nine linear and circular accelerators, and decelerators; Large Hadron Collider (LHC), Linear Accelerator (Linac), Proton Synchrotron (PS), Super Proton Synchrotron (SPS), Anti Decelerator (AD), Proton Synchrotron Booster (PSB), Isotope

Separator Online Device (ISOLDE), Low-energy Ion ring (LEIR), CERN Neutrinos to Gran Susso (CNGS), as shown in Figure- 2.4.

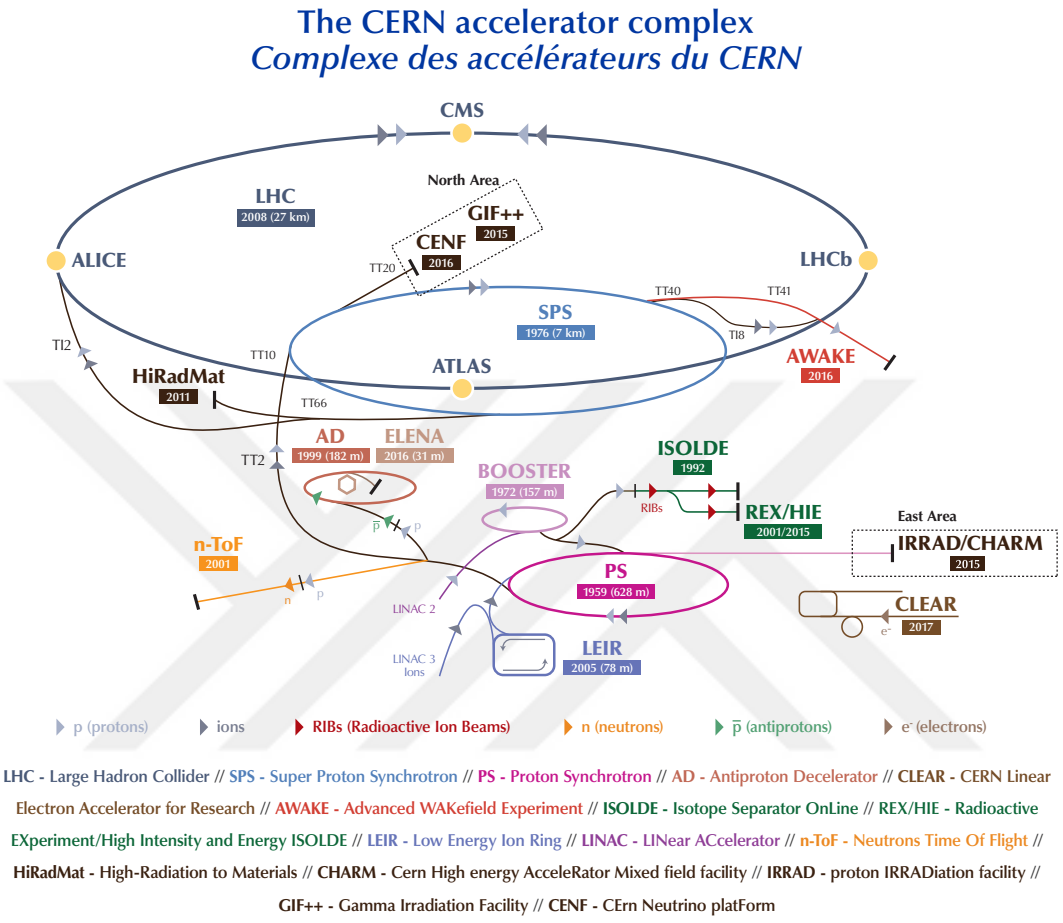


Figure 2.4: Accelerator complex at CERN.
(Mobs, 2018).

2.2. Overview of LHC and its Status

The LHC (O. S. Brüning et al., 2004) is the most powerful and the largest particle accelerator ever built up to now in the world. It is located on the Swiss-France border near Geneva. It is housed in an underground enormous donut having a 26.7 km circumference, and lying on average at 100 meters below the Earth's surface; the structure is

about 3 meters tall. LHC is a collider. Table 2.1 details the nominal design parameters of the LHC.

Table 2.1: The nominal operation parameters of the LHC ring. (O. S. Brüning et al., 2004).

Design Parameters	**Values**
Dipole operating temperature	1,9 K
Main RF System	400.8 MHz
Voltage of 400 MHz RF system at 7 TeV	16 MV
Number of magnets (dipoles, quadrupoles ... dodecapoles)	9300
Number of dipoles	1232
Number of quadrupoles	858
Number of RF cavities	8 per beam
Nominal energy, protons	7 TeV
Magnetic dipole field	8,33 T
Nominal energy, ions	2,76 TeV/nucleon
Minimum distance between bunches	$\sim$7 m
Bunch spacing	25 ns
Design Luminosity	$10^{34}\ cm^{-2} \cdot s^{-1}$
No. of bunches per proton beam	2808
No. of protons per bunch (at start)	$1,5 \cdot 10^{11}$

Physics searches that will be pursued and the technological capabilities of the accelerator constructors. Adequate energy has to be provided by the colliding beams to supply the particles under search with the required energy to be “released” from their confinement. Protons are the LHC’s main accelerated particles; this is because protons are extremely stable particles; the ones that are in the LHC beams are the same ones created after the Big Bang gradual cooling.

The LHC beams are not a continuous flux of protons; the beam consists of approximately 2808 proton bunches that move in opposite directions. They are accelerated in opposite directions till they reach 14 TeV center-of-mass energy and when they collide

they are at about the speed of light (0.999 999 991c). Colliding bunches are spaced at every 25 ns which means that we have 40 million bunch collisions per second. The bunch is a few centimeters long (measured in the direction of motion of the particles); every bunch has around 1.15×10^{11}charged particles. From two colliding bunches, we get, on the average 50 collision "pile-up" at every collision point. (L. Evans & Bryant, 2008).

Apart from proton-proton collisions, lead ion collisions are also created in the LHC collider, for different physics studies. The LHC collider started providing physics data in 2010 when the first 7 TeV collisions were recorded. During the LHC Run 2 (between 2015 and 2018), the E_{CM} was raised to 13 TeV, whilst beam intensity increased to 1.15×10^{11} protons per bunch, and at the end of Run 2 the integrated luminosity reached up to 189 fb^{-1}.

More details on LHC can be found in the given References-(L. Evans & Bryant, 2008; O. S. Brüning et al., 2004).

2.2.1. Upgrades and Schedule of LHC

In the LHC collider, the first proton-proton collision was performed at 900 GeV in 2009. After the first collisions, the first successful studies at LHC were carried out between 30 March 2010 and 13 February 2013 (which is called Run 1 or Phase 0). Physics data at 3.5 TeV per beam (total energy of 7 TeV for two beams) were collected and a total of 6 fb^{-1} luminosity was reached until the end of 2011. In 2012, scientists manage to increase both the center-of-mass energy at 4 TeV per beam and reach a total of about 23 fb^{-1} of luminosity. During this year, the Higgs boson was discovered; the discovery was verified by both the CMS (Collaboration et al., 2008) and the ATLAS experiments (Aad et al., 2008). Apart from p-p collisions, collisions of a proton with lead-ions initially took place in eearlier 2013 before the LHC machine shut down. Run 1 stage finished on

the 13th of February 2013 with the start of the LS1 stage. (O. Brüning & Rossi, 2019; Orfanelli, 2016). LS1 had a goal increasing to a nominal peak of luminosity at 10^{34}

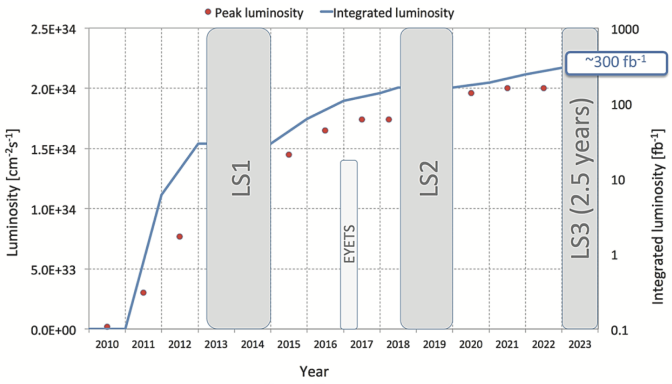


Figure 2.5: Instantaneous the LHC luminosity over 10 years with the evolution of possible peak luminosity at LHC.

(Rossi & Brüning, 2015).

$cm^2 \cdot s^{-1}$ and energy as well as preparing for all future upgrades. LHC went into this consolidation and maintenance period (LS1) until early 2015. After the accelerator and the subsequent detector upgrades, the LHC resumed operations on the 5th of April 2015 and reached the center-of-mass energy of 6.5 TeV per beam.(Orfanelli, 2016). Satisfactory luminosity was achieved ($\sim$ 190 fb^{-1}) for the first time, as shown in Figure 2.6. The Run 2 stage started in 2015 and was stopped for further upgrades at the end of 2018. At this date, LHC entered the LS2 period that will last until, probably the end of 2021.(O. Brüning & Rossi, 2019).

The LS2 period is very important because it will allow the LHC accelerator to prepare for the HL (High Luminosity)-LHC period, in which the luminosity will reach 10^{35} $cm^2 \cdot s^{-1}$; this is foreseen for 2028. Several installations of new instruments that withstand high luminosity and high radiation, and upgrades of current ones have already started.(Béjar Alonso et al., 2020).

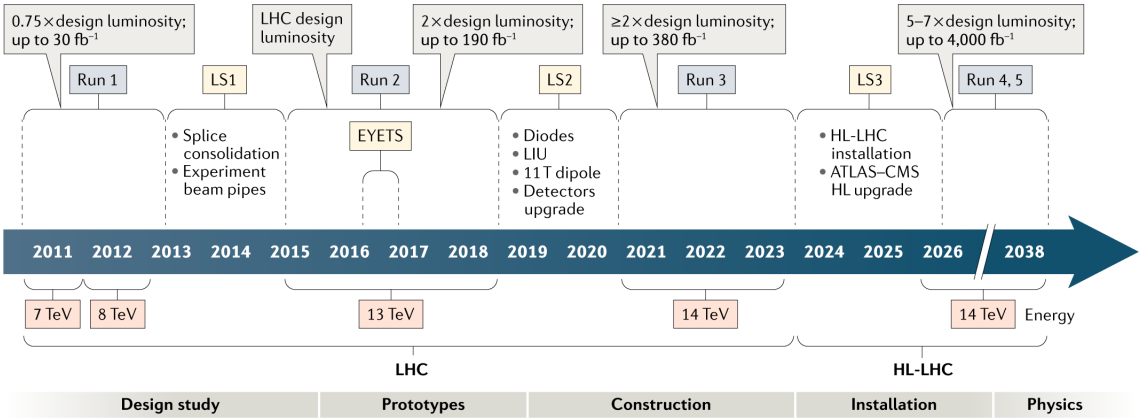


Figure 2.6: The schedule of LHC upgrades.
(O. Brüning & Rossi, 2019).

2.2.2. High Luminosity LHC (HL-LHC)

Increasing luminosity is paramount for observing rare events and further study particle physics questions. All studies depend on the amount of data because discoveries (or lack of) depend on statistics. To obtain more data, the number of events in LHC should increase. This means higher luminosity; the higher the luminosity, the more the data. This will allow us to further study physics phenomena. The construction and installation of radiation-hard electronics instrumentation for the HL-LHC accelerator will be carried out during the LS3 process which is scheduled from 2026 to the middle of 2028. Its objective is to increase the integrated luminosity by ten-fold and to achieve an increase of nominal (instantaneous luminosity) of a factor of five.(Béjar Alonso et al., 2020).

2.3. The Layout of LHC

2.3.1. Journey from Proton Source to Vacuum Chamber

In the LHC accelerator, protons or lead-ions are accelerated and collided. LHC performs proton-proton (or lead-lead) collisions to observe new “hidden” subatomic particles. Proton generation for collisions is carried out using hydrogen atoms. Having created

the protons using the proton source, bunches of protons are formed by grouping together protons. Thus the LHC beam is "created" by sending intermittently the bunches of protons to the beam-pipe. The gaps between successive bunches of protons are referred to as bunch space and are measured in units of time. Bunch spacing in LHC is 25 ns. The collision of two accelerated beams in the detector means that we have more than one proton (per beam) colliding with a proton from the opposite side. This event is called a "pile-up" event. Each time a bunch in one beam passes by a bunch in the other, multiple protons can interact with each other. Rarely more than one of these interactions gives an interesting hard scatter event. Other unimportant interactions still happen and some number of new particles are produced. At LHC, 1.15×10^{11} protons per beam and 2808 beams for each beam are produced, that is, $3 \cdot 10^{14}$ protons per beam. (O. S. Brüning et al., 2004).

The produced beams are injected into the vacuum chamber called a beam pipe. The vacuum chamber minimizes to prevent collision of protons and gas molecules with each other so that the beam pipes are kept at ultra-vacuum, P$\sim 10^{-10}$ mbar, is shown in Figure-2.7. The beams inside the beam pipe begin to accelerate by supplying 90 kV. Quadrupole magnets are used to both accelerate with the effect of an electromagnetic field and provide protons travel in a focused manner without scattering in the beam pipe. (O. S. Brüning et al., 2004).

2.3.2. Accelerator Complex at CERN

In the CERN site (O. S. Brüning et al., 2004), "older" and more recent accelerators, all the way up to LHC are connected like chain links combining their different features to achieve various functions. For getting the beam in LHC, the first starting point is the Linac 2 (Linear Accelerator-2). With the helping of RF cavities, Linac 2 loads the cylindrical conductors that are consecutively placed, positively and negatively in order. The particles are accelerated under the influence of the electric field created by the RF

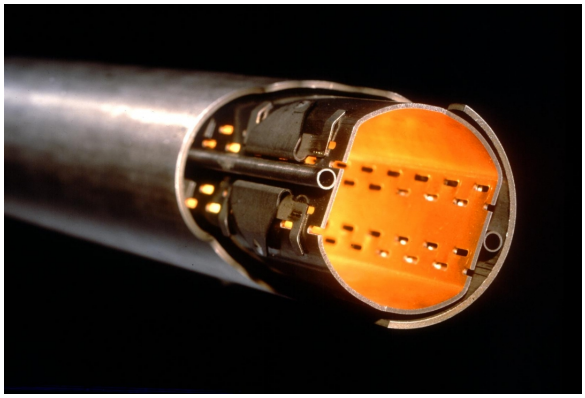


Figure 2.7: The cross section of LHC ultra-high vacuum pipe.
(Kahle, Steerenberg, & Pandolfi, 2017).

cavity along with the spaces between the consecutive conductors; one conductor pushes the particle into space and the other conductor pulls the particle from the space between conductors. Proton bunches are injected and accelerated in Linac 2, one end of which is connected to the proton source. In Linac 2, the accelerated protons reach 50 MeV and their mass increases by 5% too.

Then the PSB takes over from the Linac 2 as the second element of the accelerator chain. The PSB, which is a circular accelerator, boosts the energies of particles up to 1.4 GeV. Protons that are accelerated from the PSB, or heavy ions, whose energy is raised from the LEIR, are injected into the PS. It contains 277 conventional magnets (functioning at room temperature) and 40 dipole magnets to bend the path of the particle. It accelerates the particle bunches up to 25 GeV for a 628 meters circumference. The bunches of protons that gain 25 GeV energy are injected into SPS, the second-largest accelerator of CERN, built before LHC. The SPS accelerates the particles until getting 450 GeV by using 1317 conventional magnets and 744 dipole magnets with a circumference of about 7 km, and then the bunches of protons are ready for acceleration and collision in the LHC.

Besides the acceleration of protons, Linac 3 was built to accelerate lead ions and heavy ions for quark-gluon plasma research. The Linac 3 accelerator used for specific purposes is the starting point of the chain, like LINAC-2, to speed up ions. To accelerate the ions more easily, they are injected into Linac-3 following being stripped from their electrons and accelerated in a focused manner using quadrupole magnets. Afterward, when the ions have reached about 4.5 MeV energy they are injected into the LEIR ring and accelerated until getting 72 MeV. As soon as they leave the LEIR, they are prepared to be accelerated in LHC by following the same path as the protons leaving from the Linac 2 travel. After gaining 5.9 GeV energy per nucleon thanks to PS, they are delivered the LHC from SPS at 177 GeV for each nucleon. Lead-ion bunches are then accelerated up to 1.38 TeV per nucleon in the LHC.

More details about accelerator complex at CERN can be seen in References (O. S. Brüning et al., 2004; L. Evans & Bryant, 2008).

2.3.3. Beam Collimation and Arc Layout at LHC

LHC ring (O. S. Brüning et al., 2004) comprises eight 0.545 km long straight segments and eight arcs which of each is 2.45 km, as shown in Figure-2.8. Each arc includes 23 cells which are formed superconducting “lattice” magnets. Lattice magnets are used to bend trajectories of particles and longitudinally align them inside the vacuum tube. They enclose the beam pipe to tighten and steer particles and are employed in different ways; as quadrupole, dipole, and sextupole magnets. LHC has 1232 dipole magnets, each 15 m long, operating at 8.3 T (100 000 times the Earth’s magnetic field) for bending bunches. It has included 154 dipole magnets in each arc. Quadrupole magnets squeeze particles in the vacuum chamber in a horizontal way using properties of four poles placed symmetrically. They consist of two types in lattice structure; F type and Q type, as can be seen in Figure 2.9.

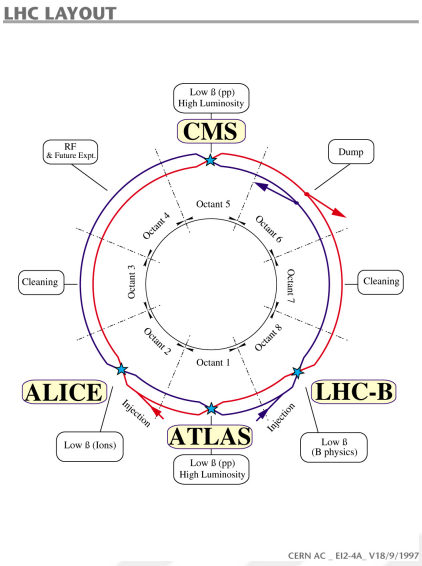


Figure 2.8: Arc layout of the LHC.
(Caron, 1997).

F type of quadrupole magnets focuses beam horizontally, whilst Q type provides beam to focus vertically. We can make an analogy of operation of concave and convex lenses with working of F and Q type magnets together, is shown in Figure-2.10. Their magnetic fields cancel out, in case of using F and Q type of magnets back to back to focus beam both horizontally and vertically. Therefore, focusing can be achieved by providing enough space between them. In lattice structure, FODO lattice is commonly used; consisting of focusing magnet, nothing (is generally used bending magnets such as “dipole”), defocusing magnet, another bending magnet as well as multipole magnets.

While beams are coming close to detectors, protons in bunches must be squeezed to achieve collisions easily and precisely, so they have to be focused. For this purpose, the inner triplet system is used. It consists of three quadrupole magnets. Insertion systems involve eight inner triplets, two of which are at each of the four collision points (ATLAS, A Large Ion Collider Experiment (ALICE) (Aamodt et al., 2008), CMS, and Large Hadron Collider beauty (LHCb) (Alves Jr et al., 2008)). More so, superconducting magnets are used inside the detectors themselves to bend trajectories of emerged

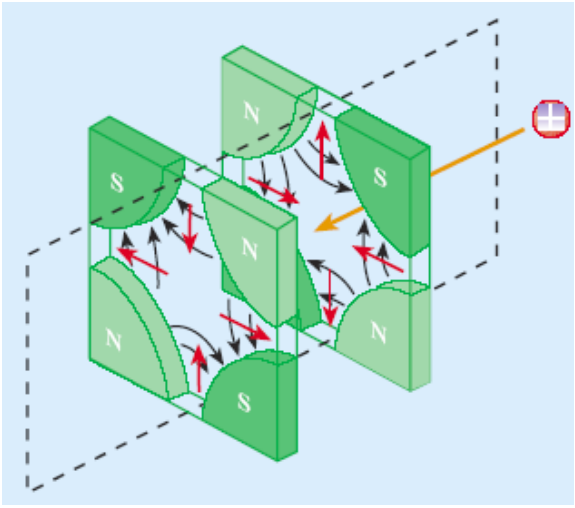


Figure 2.9: F and Q type quadrupole magnets.
(Cid-Vidal X. and Cid R., 2010).

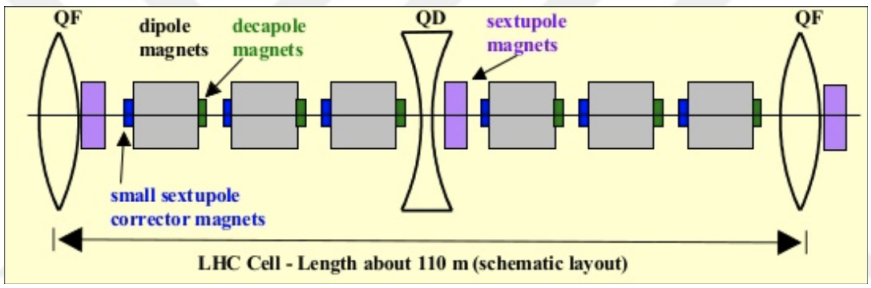


Figure 2.10: The structure of each arc cell at the LHC. Dipole magnets aims to keep the beams inside the ring and quadrupole magnets focus them in both directions.
(Wenninger, n.d.).

particles so that their momentum can be measured. On this subject, see the description of the CMS magnet system. After crossing the beams, the process of splitting them from each other is achieved through dipole magnets again.

A more detailed description of arc layout and beam collimation can be presented in References (O. S. Brüning et al., 2004; L. Evans & Bryant, 2008).

3. COMPACT MUON SOLENOID (CMS)

The CMS (Collaboration et al., 2008) is one of the two general-purpose particle detector experiments at LHC. The experiment enables us to observe highly massive particles and perform precise measurements of the SM. Besides the SM studies, it also carries out other physics studies such as extra dimension, dark matter, SUSY, etc. CMS detector is located at Interaction Point (IP) 5 of the LHC ring, around Cessy, France. It is operated in a cavern, 100 m underground. Having 14000 tonnes weight, 15 meters high, and 21 meters long, these properties give it a relatively compact structure.

It keeps the most powerful solenoid superconducting magnet ever made inside the detector with a magnetic field of 3.8 T and has muon chambers to detect muons precisely. It is called CMS - Compact Muon Selonoid by having these properties. The detector consists of sublayers: a tracking system (known as a tracker), electromagnetic calorimeter and hadronic calorimeter, superconducting magnet, and muon system as seen in Figure 3.1.

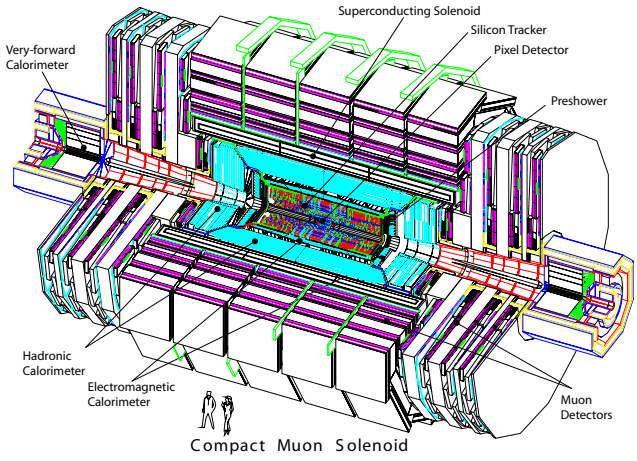


Figure 3.1: Labelled schema of the CMS detector. (Drollinger, 2006).

The CMS detector was built on the surface with separate 15 slices. Then these slices were downed to a cavern and assembled slice by slice in the cavern. The CMS cavern consists of two caverns; an experimental cavern and an underground cavern. CMS detector is situated in the experimental cavern called Underground Experimental Cavern (UXC), while Underground Cavern Experiment (USC) procures installation some services like powering, electronic readouts, controlling, and monitoring to the sub-detectors.

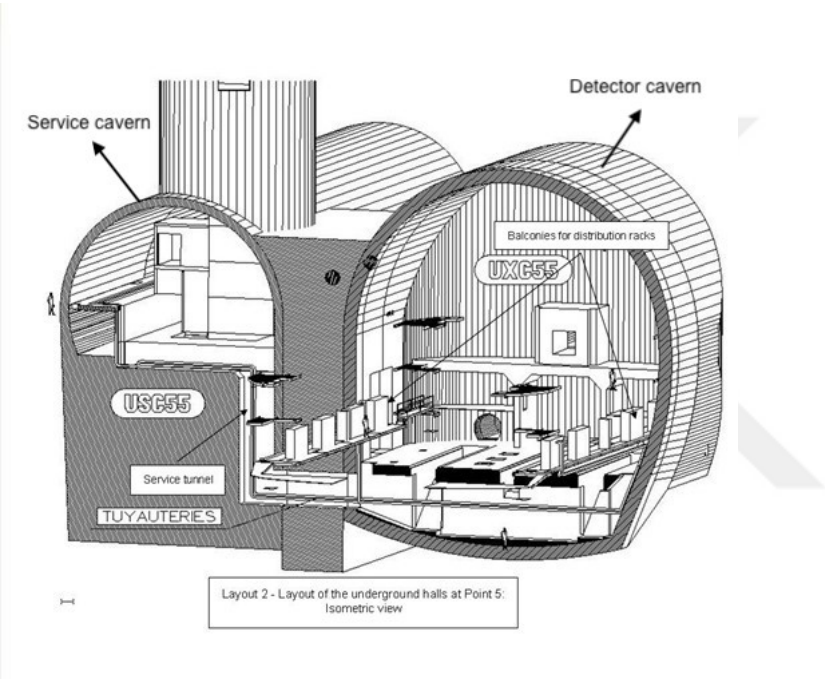


Figure 3.2: CMS cavern consists of UXC (experimental cavern) and USC (underground cavern). (Focardi, 2008).

A more detailed description on CMS detector and experiment can be found in (Collaboration et al., 2008).

3.1. Structure of CMS Detector

CMS detector was designed utilizing two different coordinate systems: nominal interaction point and "pseudorapidity". The orientation of the nominal collision coordinate system follows beam direction and the LHC plane, which is also known as the $x-y$ plane. The direction of two accelerated counter-rotating proton beams inside the LHC is called longitudinal and z-axis of CMS coordinate, being perpendicular to the LHC plane. The negative z-axis is along the clockwise beam direction while the positive z-axis points counterclockwise beam direction. The x-axis is the horizontal axis of the LHC plane and is inward to the center of the interaction point, while the y-axis is pointing vertically upward to the LHC plane. $+x$-axis is called the near side of the detector, while $-x$ refers to the far side of the detector. (Orfanelli, 2016, p. 24).

Another coordinate system is "pseudorapidity" which is used by barrel sub-detectors. Azimuthal angle, ϕ is measured concerning for x-axis on LHC plane, whilst polar angle is measured from z-axis, which is also referred to as beam axis as presented in Figure-3.3. Thereby, pseudorapidity is defined as $\eta = \ln(\tan\left(\frac{\theta}{2}\right))$. (Orfanelli, 2016, p. 25).

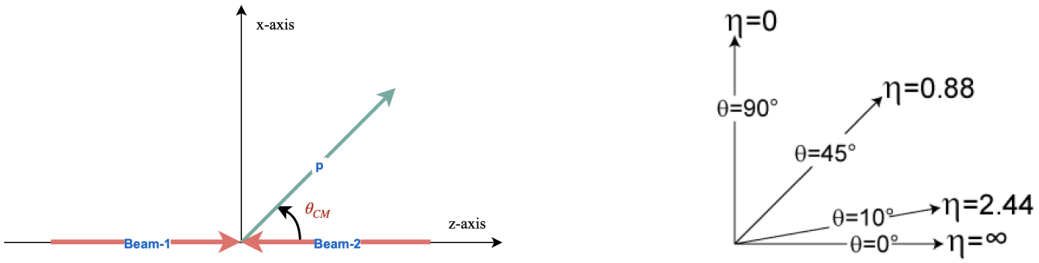


Figure 3.3: (a) Illustration of the longitudinal scattering angle θ_{CM} is presented (left) and (b) a variety of pseudurapidity corresponding to different values of θ_{CM} is given (right).
(*ETH – Institute for Theoretical Physics – Particle Physics Phenomenology 1 – HS 2010*, 2010).

The CMS detector comprises sub-detectors built-in layers just like other major detectors of the LHC. Each sub-detector was designed in a sequence with different properties and

functionalities so that it can detect various emerging particles by scattering from the heart of the collision. The subsystems measure the energy and momentum of particles to attain the above-mentioned purpose.

The subsystems of the CMS detector were hermetically and cylindrically built. The detector carries a cylindrical barrel part and two facing endcap parts. Almost many particles emerging from inelastic collisions can be observed thanks to this order of the detector. The layers of CMS detectors are consecutively surrounded by the tracker, electromagnetic calorimeter, hadronic calorimeter, superconducting magnet, and muon detector systems, shown in Figure 3.4. Indeed, layers of the detectors can be defined as innermost, intermediate, and lastly, outermost layer either.

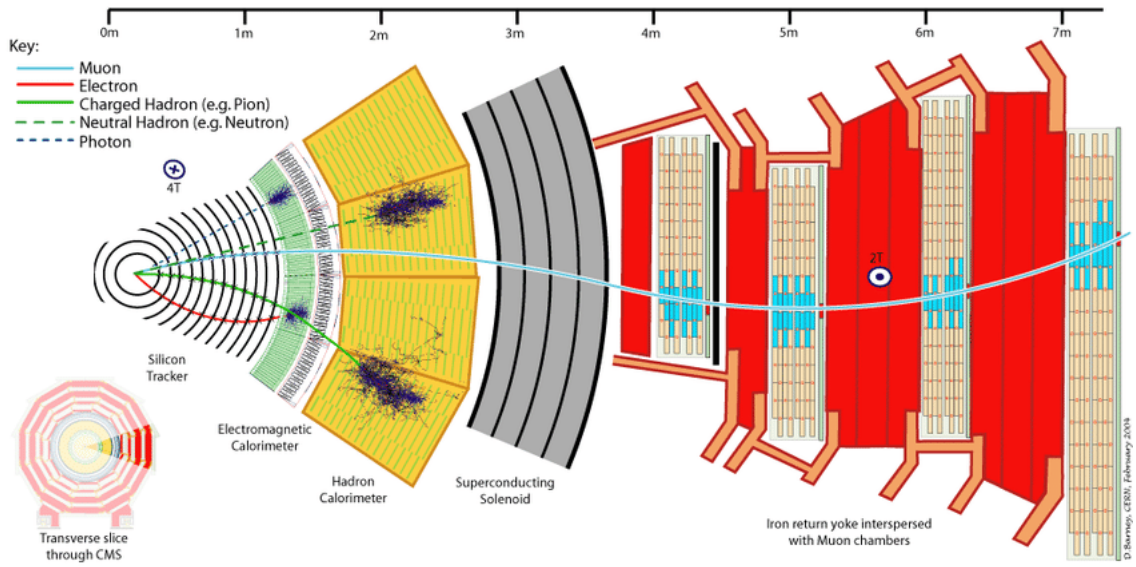


Figure 3.4: Sublayers of CMS detector with different signatures of the particles. (Murnane, 2014).

The innermost layer has a completely silicon-made tracker system to get information about the trajectory of particles arising from the interaction point. Intermediate layers are composed of calorimeters, electromagnetic and hadronic calorimeters to absorb and measure the energy of particles. Following calorimeters, a superconducting magnet, be-

ing the magnetic field of 3.8 T, is used to bend the path of particles Bending the trajectories of the particles allows us to measure the radius of this curvature bent. Thus, the momenta of the particles can be calculated using a strong magnet, which carries 41.7 MAmpere-turns and made up of Niobium-Titanium (NbTi). (*The CMS magnet project: Technical Design Report*, 1997). The outermost layer is designed to detect muons that have more penetrating than other particles. It holds a muon detector system which is integrated with an iron return "yoke" (Layter, 1997).

A more detailed information on layout of CMS detector can be followed in References-(Collaboration et al., 2008).

3.2. Tracker

After the collision, the particles scattered from the interaction point firstly pass through the tracker layer (Karimäki et al., 1997) entirely made of silicon. It is designed to record paths of particles curved by a magnetic field such that it can measure precisely the momenta of particles above 0.5 GeV/c. Additionally, its mandate is to find the primary vertex and specify secondary vertices positions as well as determine whether particles are charged. Trajectories of particles can be reconstructed and tracked precisely in that the tracking systems ensure us to determine the positions of particles. Thereby, the first layer of the CMS detector was called tracker. In the CMS detector, the tracker was made using lightweight materials to avoid interference with their paths, allowing us to measure the particles accurately. .

The all-silicon-made tracking system of the detector covers a total area of about 200 m^2. It was made of entirely silicon sensors. Because it is placed to the closest part to the beam pipe, the tracker encounters a very high flow of particles, around 1000 charged particles per 25 ns collision. Being the closest place to the collision point leads to operating in very harsh environmental conditions; thus, materials employed for the

tracker must be very resistant to high radiation. Besides working under high radiation, the cooling system of the tracker is a crucial factor to decrease radiation effects and keep the lifetime of detector modules as well as electronics. It was designed to operate at -20°C by a mono-phase liquid cooling system with C_6F_{14}.

Tracker is composed of pixel and strip parts. The pixel layer of the tracker systems located at the heart of the detector is encircled by strip layers and contains 66 million pixels with a total area of 1 m^2. Silicon pixel detector consists of three concentric cylindrical barrel layers (BPIX) situated at a radius of 4.4 cm, 7.3 cm, and 10.2 cm, and two endcap disks (FPIX) at each side, located from 6 to 15 cm in radius. Charged particles leaving from silicon pixel detector follow their paths over silicon strip detector consisting of four subsystems with ten layers; four-layer tracker inner barrel (TIB) and six-layer tracker outer barrel (TOB). On each side of, the tracker inner barrel layers are put in two inner

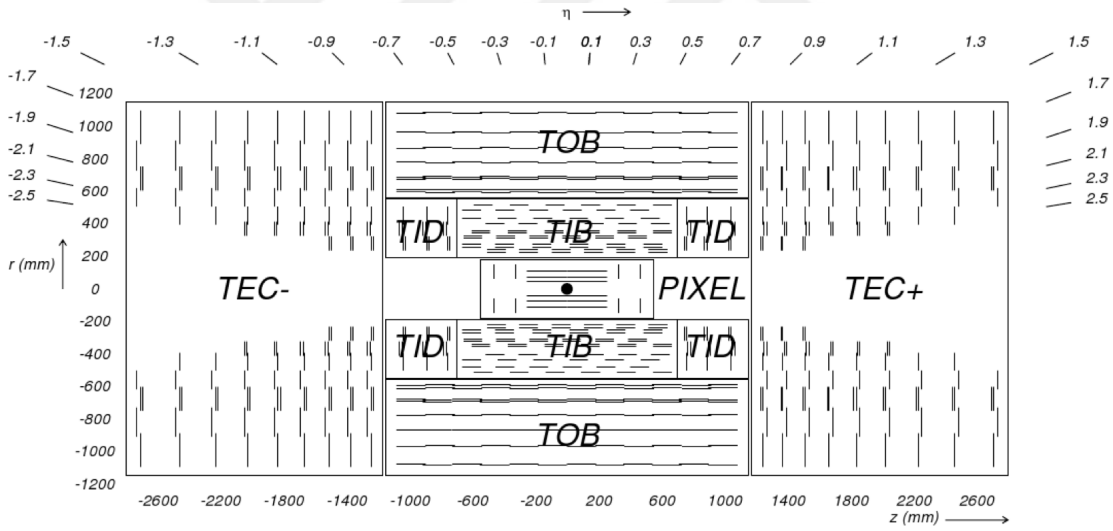


Figure 3.5: Schematic view of CMS Tracker in r-z plane.
(TDR, 2006).

disks (TID) consisting of three disks, and the tracker outer barrel contains two endcaps (TEC) with nine layers, as illustrated in Figure 3.6. Silicon strip detector contains about 9.6 million active elements and has a total area of 198 m^2. As shown in Figure 3.5, the

silicon tracking system of the detector is a length of 5.8 m and a diameter of 2.4 m by covering the pseudorapidity range up to $|\eta| < 2.4$.

For more details about CMS tracker, the given reference-(Karimäki et al., 1997) can be followed.

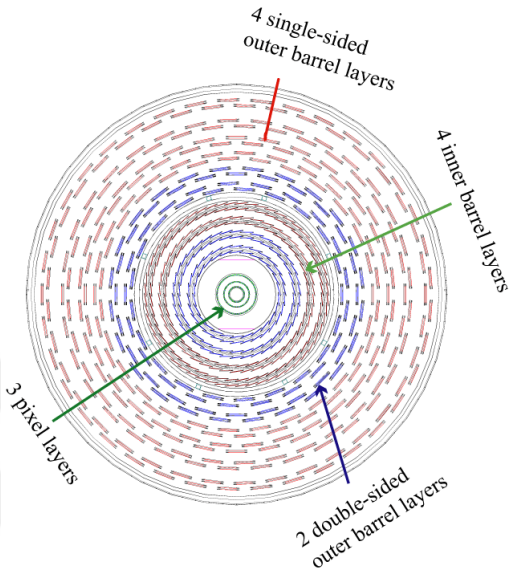


Figure 3.6: The barrel part of CMS Tracker in xy plane.
(Luciano, 2017).

3.3. Electromagnetic Calorimeter (ECAL)

Particles passing through the tracker meet with an electromagnetic calorimeter (ECAL) to precisely measure their energies. Unlike the tracker, the calorimeters of the detector were developed to interact with particles; the reason is that they can absorb their energies. In electromagnetic interaction, ECAL measures the energies of electrons and photons and covers up to $|\eta| = 3$. (collaboration et al., 1997). It was made of lead tungstate (PbW04) scintillator crystals resisting high radiation doses and ensuring a fast response time and short radiation length, X_0[1]. Lead tungstate allows producing fast light

[1] The radiation length, denoted by X_0, refers to the energy loss of a substance whose electrons electromagnetically interact with high energy particles. X_0 is expressed as the average

pulses when the particles passing through ECAL. Therefore, it needs highly sensitive photodetectors. Silicon avalanche photodiodes and vacuum photodiodes were constructed with crystals to detect light inside both barrel and endcaps of ECAL.(collaboration et al., 1997).

The electromagnetic calorimeter comprises a barrel having 61200 lead tungstate crystals and two endcaps with 7324 crystals on each side, as can be seen in Figure-3.7. The barrel crystal of ECAL (EB) has a depth of 23 cm, corresponding to 25.8 X_0, whereas the length of the endcap part (EE) is 22 cm, associated with 24.7 X_0. EB is located at a distance of 1.6 m from the interaction point, covering by $\mid \eta \mid < 1.479$. Endcaps of ECAL are assembled at a length of 3.25 m from beamline and covers the pseudorapidity range from 1.653 to 1.479. In addition, a finer-granularity pre-shower detector (ES) was constructed in front of EE to get a better resolution and detect the difference between high-energy photons and low-energy photons. The pre-shower section of ECAL is made up of Pb and covers range $1.653 < \mid \eta \mid < 2.6$. (collaboration et al., 1997).

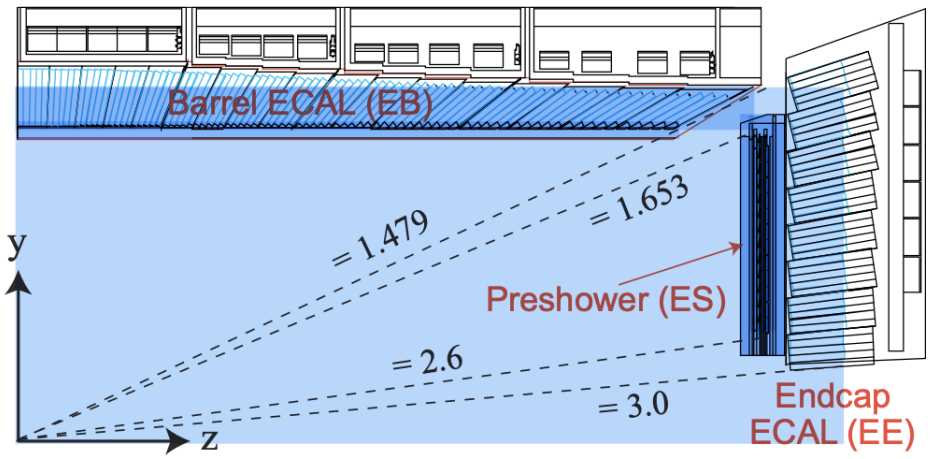


Figure 3.7: The ECAL sublayer of CMS detector.
(TDR, 2006).

minimum length to decrease the energy by factor 1/e by Bremsstrahlung (Eidelman et al., 2004).

3.4. Hadronic Calorimeter (HCAL)

Following energy measurement of electrons and photons, other particles emerging are directly flying to the Hadronic Calorimeter (HCAL) layer of the detector without interacting on previous layers; it is so-called "hadrons" which are made of quarks and gluons such as protons, kaons, pions, and neutrons. The energies of these particles are required to measure in this layer. For this purpose, HCAL is aimed to measure the energy of hadrons and assembled by surrounding the ECAL. Contrary to the ECAL, it is not a homogenous calorimeter. It is a "sampling" calorimeter allowing us to determine the particle's position, arrival time, and energy. To perform these measurements, alternating layers of "absorber" made up of brass plates and of fluorescent "scintillator" tiles placed into trays are used. Scintillator material generates light pulses when hadrons interact with the layers. Thus these pulses are collected using optical fibers, and then they are sent to electronics read-out parts providing to amplify pulses using photodiodes. Once hadrons meet the surface of dense absorber (which is also called as "shower"), secondary particles emerge. To measure their energies, the amount of materials required is around one meter. However, the "compact" feature of the CMS detector needs to be kept. That's why HCAL consists of the barrel, endcap, and forward parts as well. ("The CMS hadron calorimeter project: Technical Design Report", 1997).

The barrel part comprises Hadronic Barrel (HB), positioned inside the magnetic coil and Hadronic Outer (HO) sections. It is located in the range of $\mid \eta \mid < 1.4$, as shown in Figure 3.8. Indeed, HB covers the majority of HCAL with 36 barrel "wedges", each weight of 26 tonnes. Moreover, HB is integrated by HO, consisting of a few layers of scintillators outside of the magnet. The layers of the HO do not allow energy leakage, undetected by the hadronic barrel. The HCAL layer is also defined as "hermetic" calorimeter to capture every particle occurring from collisions. Therefore, it includes hadronic forward and endcap calorimeters to achieve this feat in addition to the barrel part. ("The

CMS hadron calorimeter project: Technical Design Report", 1997).

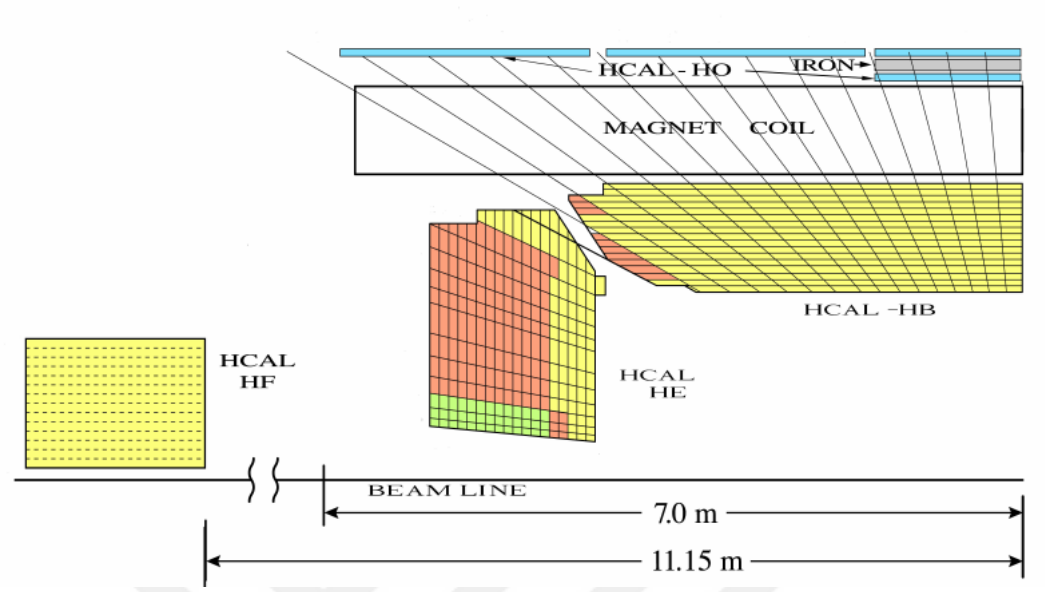


Figure 3.8: A schematic view of the HCAL.
(TDR, 2006).

Hadronic endcap calorimeters are located at both ends of the magnet, covering a range from $1.3 <| \eta |< 3.0$. Likewise, hadronic endcap calorimeters involve 36 "wedges", thereby performing energy measurement of particles flying up to the end of the coil. To collect numerous particles scattering from the heart of the detector at shallow angles concerning for z-axis (which can be defined as beamline), another layer was designed as a part of HCAL; hadronic forward calorimeter covering range $3.0 <| \eta |< 5.0$. The energies of myriad particles scattered are absorbed by the HF colorimeter made from a steel absorber with quartz fibers. So, the myriad particles generate much more luminosity. For this reason, it requires utilizing special materials to mitigate the high amount of radiation doses considering other layers of HCAL. To provide radiation tolerance, photomultipliers are employed for reading quartz fibers that emit Cherenkov light when they meet with the relativistic charged particles.("The CMS hadron calorimeter project: Technical Design Report", 1997).

3.5. Muon System

Muons that are monocharged particles have more momentum and more energy than other scattered particles. The calorimeters of the detector do not have sufficient magnetic fields to bend trajectories of muons. They can not be halted by any calorimeters of the detector owing to having the characteristics mentioned above. Thereby, by penetrating several detector layers, they fly up to the outermost layer of the detector; muon systems.(Layter, 1997).

The muon system is assembled around the magnetic coil as the detector's outermost layer to detect the muons. Muon system composes three different types of gaseous detectors for detection, identification, and momentum measurement of the muons; Cathode Strip Chambers (CSC), Drift Tubes (DT), and Resistive Plate Chambers (RPC) detectors. The system consists of 1400 muon chambers in total; 250 DTs, 540 CSCs, and 610 RPCs. The DT and CSC allow tracking the paths of muons and triggering, while 610 RPCs aim to form a different trigger system such that it decides on whether acquired muon data are kept. (Layter, 1997). In addition to identification and muon measurements, the muon system also includes four iron return yoke plates around magnetic coils to prevent arrivals of any leaking hadrons to muon stations. Iron return yokes are mounted as interleaved with four muon stations on the barrel part of the muon systems, as seen in Figure 3.9.(Layter, 1997).

Similar to other sub-layers, the muon system consists of concentric cylindrical barrel region and endcaps disks with four muon stations; for barrel (MB1, . . . , MB4) and endcaps (ME1, . . . , ME4). Each barrel station deploys drift tubes covering $| \eta | < 1.2$ inside the magnet yoke. The DTs are made up of 12 layers and perform trajectory measurements of muons. The CSCs with six layers are situated in each station of endcaps, where the magnetic field is not uniform, and the rate of the muon and neutron-induced background rate is high, covering a range from $0.9 < | \eta | < 2.4$. (Layter, 1997).

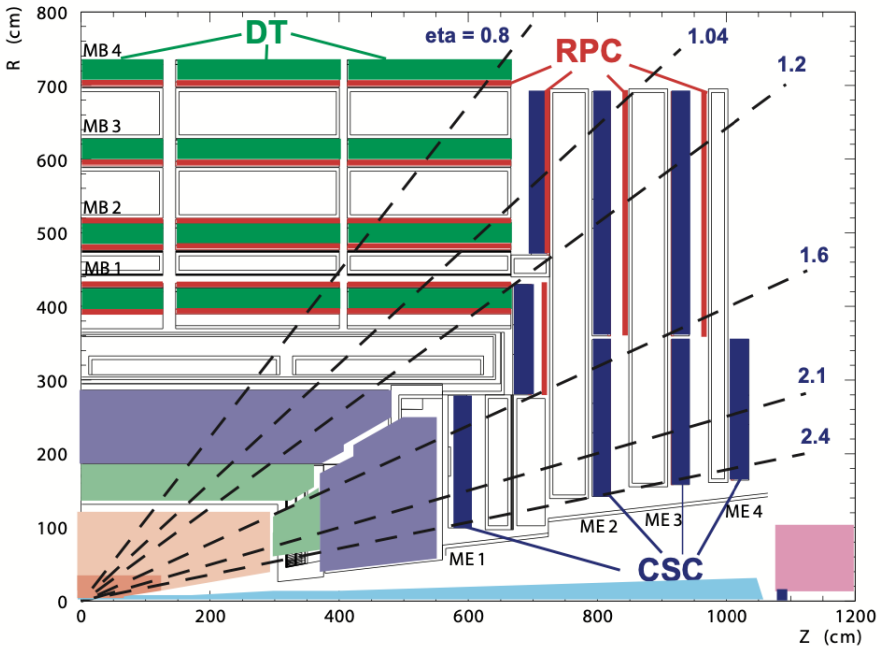


Figure 3.9: The muon chamber with its three gaseous detectors. (TDR, 2006).

The third type of muon detector is RPCs covering the range up to $\mid \eta \mid < 1.6$ on the layout of the CMS detector. They are deployed both barrel and endcaps part of the muon system. The RPCs are a fast gaseous detector, composing a highly plastic-resistant material and separated by a gas volume. Their purpose is to ensure good spatial and timing resolution with just one nanosecond to determine whether worth muon data are kept. (Layter, 1997).

3.6. Trigger and DAQ System

When beams meet head-on inside the CMS detector, nearly one billion proton-proton collisions occur every second. The rate of raw data generated is approximately 40 Tbps at 40 million times collisions. It is beyond the possibility of recording and reading out data from all events, notably energetic and head-on collisions. Therefore, a “trigger” system must be designed to address the events at high luminosity and interaction rates.

The trigger and DAQ system works based on a decision-making system such that it decides whether the events are interesting and substantial. Additionally, another purpose of the system is to reduce the event rate to a few hundred so that highly significant data collected from collisions for further variety of physics analysis can be read-out and stored on large-scale computer clusters. To achieve these feats, the trigger and DAQ system consists of two levels; Level 1 trigger (L1) and High-level trigger (HLT), as shown in Figure 3.10. (Cittolin, Rácz, & Sphicas, 2002).

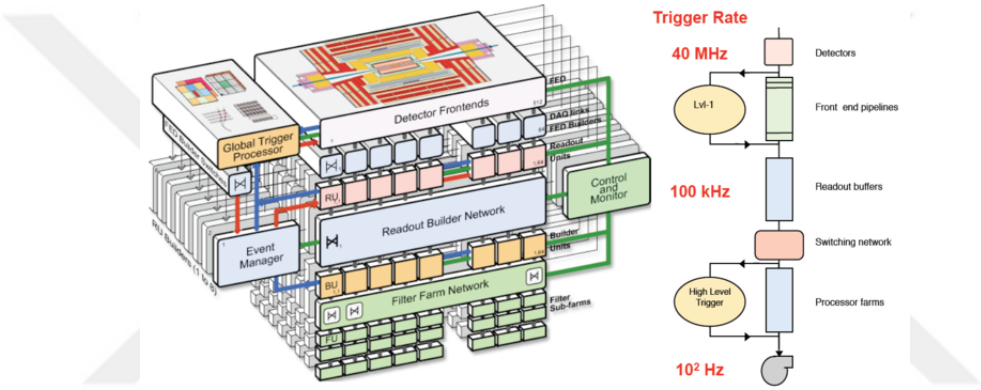


Figure 3.10: CMS triggering and DAQ system.
(Halyo, Hunt, Jindal, LeGresley, & Lujan, 2013).

The L1 trigger system is composed of programmable custom processors and front-end electronics as can be seen in Figure 3.11. They are very heterogeneous in the way of buffer management, functionality, and details about the read-out process. The goal of the L1 trigger is to perform a maximum event rate to reduce 100 kHz and decide whether data is accepted and stored. While the decision-making mechanism on the L1 trigger takes place within $3.2\mu s$, reduced granularity and reduced-resolution data from the muon and calorimetry systems are used and kept in a pipeline. The latency of the decision

results from a selection of local, regional, and global trigger components; meanwhile, it concerns the readiness of the sub-detectors and DAQ. After reducing the rate of data accepted from the L1 to 100 kHz, the data are transferred to industrial processors holding one thousand multicores. The processors operate the HLT to make decisions on the data; thus, the HLT reduces event rate with interesting signature to 100 Hz from 100 kHz. This decision varies from 10 ms to 1 s. Ultimately, the selection of events is stored on the grid of computers distributed in global computer infrastructure for further data analysis. (Cittolin et al., 2002).

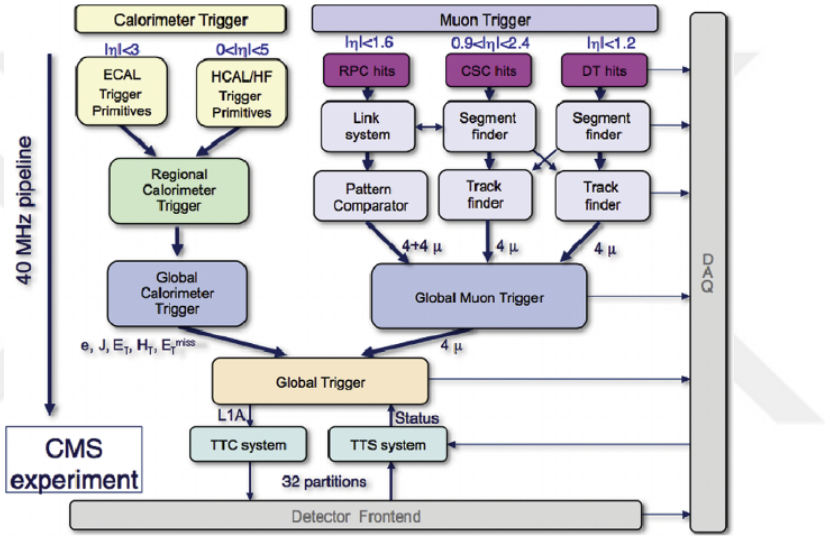


Figure 3.11: Data flow in L1 triggering system of the CMS detector. (Jeitler, 2013).

3.7. HL-LHC Upgrade of CMS

Detectors and accelerators have been ever upgraded by making massive improvements on machines, electronics systems, etc., for taking place more collisions providing to be analyzed more data. Following Run 3, the LHC machine will be upgraded, which is also called HL-LHC. Its mandate is to increase luminosity by a factor of 10 to store a more extensive dataset. It will be performed more collisions such that the HL-LHC will incre-

ase the average number of collisions 40–60 to 140–200. The HL-LHC experiment will allow observing unprecedented events. Thereby, the CMS detector needs improvement to be operated in a harsher radiation environment due to high luminosity and coping with the aging effect. All sub-detectors and off-detector sides have been preparing for the HL-LHC upgrade of CMS. (Tsirou, 2020-12-05).

3.7.1. Upgrade of CMS Tracker

The tracker system of the CMS detector will be completely renewed to achieve the goals, which are to resist solid radiation hardness and to carry out a high data rate and selection of events with exciting signatures. The inner part of the tracker has exposed much more radiation because of being the closest region to the interaction point, so it must withstand radiation levels up to $2.3 \cdot 10^{16}$ neq/cm^2 and an accumulated ionizing dose of 2 MGy. Therefore, the front-end electronics part of the tracker will be upgraded concerning readout, cooling, and power system without ever altering its structure. The high granularity will ensure a selection of significant events.(*The Phase-2 Upgrade of the CMS Tracker*, 2017).

3.7.2. Upgrade of CMS Calorimeters

Likewise, CMS calorimeters will undergo an upgrade to work under the ionizing high radiation doses are brought by HL-LHC. Endcaps of ECAL and HCAL will be exposed to radiation doses of more than $1.5 \cdot 10^{15}$ neq/cm^2 due to being close to the beamline (*The Phase-2 Upgrade of the CMS Barrel Calorimeters*, 2017). This high radiation level will damage ECAL crystals, on-detector cooling circuits, and motherboards, and HCAL photodetectors, and tile response. That's why a new endcap calorimeter that will maintain high granularity has been designed in such a way to take the place of two endcaps (EE and HE); High Granularity Calorimeter (HGCAL). It is made up of two different tradition-tolerant materials; silicon for high radiation environment and plastic scintilla-

tor tiles for less radiation harsh region. As an absorber, the ECAL endcap will deploy tungsten, while the HCAL endcap will be designed using lead. The HGCAL provides extremely high readout and trigger granularity and will be cooled to around -35° C to mitigate the effects of radiation damage. Providing high triggering granularity and timing resolution, high performance on particle identification, detection, and triggering are foreseen even if around 200 pile-up events occur during HL-LHC. (*The Phase-2 Upgrade of the CMS Endcap Calorimeter*, 2017).

3.7.3. Upgrade of Muon System

For Phase 2 and HL-LHC, the muon system must undergo maintenance on existing systems in the endcaps. A new muon system that will deal with challenges regarding high radiation has been designed; GEM detector. Additional redundant trigger systems and measurement points will be carried out by the GEM detector such that precise muon tracking and identification are provided in the critical forward region. It will be assembled in part $1.6 <| \eta |< 2$ during LS2 to remove background triggers while resuming high trigger efficiency and measure cosmic ray muons. Throughout HL-LHC, further improvements and enhancement will occur with the second GEM station and new RPCs modules, aiming to bear a high rate of particle flows up to a few kHz/cm by integrating triggering and tracking properties. (*The Phase-2 Upgrade of the CMS Muon Detectors*, 2017).

3.7.4. Upgrade of the Trigger and DAQ system

Upgrade of the trigger and data acquisition system L1 trigger upgrade will exploit FPGAs in a new electronics system, taking advantage of the high-bandwidth optical transmission and more complex algorithms for the data rate reduction. The upgraded trigger rate will increase from 100 kHz of the LHC to 750 kHz of the HL-LHC. (*The Phase-2 Upgrade of the CMS DAQ Interim Technical Design Report*, 2017).

4. CONCEPTS OF THE CMS MONITORING SYSTEM

This chapter aims to explain the concepts and the development reasons underlying the thesis that is a novel temperature monitoring system. Section-4.1., first of all, describes the importance of temperature and the necessities of the temperature monitoring for Si-based LHC detectors. Then Section-4.2. briefly presents the CMS detector readout and monitoring system. In Section-4.3. and Section-4.4., what DCS and DSS are, the reason why they are used for, and also their working principles are described. Following that, the aim of Section-4.5. is to explain how the signals are acquired and how to handle any abnormalities throughout readout and monitoring procedures. Ultimately, the functionalities of the cold detector system for which the thesis project is developed are discussed in Section-4.6..

4.1. Temperature Monitoring System for Silicon Detectors

In this section, all information and details on silicon detectors and the significance of temperature monitoring were obtained from the private discussion with Andromachi Tsirou, and presented to the readers.

The silicon technology has been considered in the design of the LHC detectors dating back to 1996. The silicon material steps forward due to its radiation tolerance. For this reason, it is used in all big experiments of LHC which are CMS, ATLAS, LHCb and ALICE. Actually, as a material, silicon may not be regarded as radiation hard material, yet it can operate and bear up to a certain level of radiation. Thereby, the CMS's inner part, i.e. the Tracker, is also made of the silicon. (Tsirou, 2020-12-05).

As the silicon technology advances, the LHC detectors have deployed and utilised silicon more often in their tracking system as well as in some parts of calorimeters like

in the case of the CMS HGCAL. However, Si detectors are meant to be used in the temperature-controlled and monitored conditions since the Si depletion voltage rises with the radiation dose. Furthermore, there is a maximum bias voltage which can be applied to Si detector without provoking breakdown. All in all, if the operating voltage with increase of irradiation is not adequate to deplete the detector, the signal from the neutral region will be lost. (Tsirou, 2020-12-05).

The impact of the radiation on material stems strongly from the temperature, T. There are also some annealing effects, where the damage can be recovered with time or which can lead to an increase in the depletion voltage with time. The latter effect, which known as "reverse annealing", can be avoided if the detector is operated at lower temperatures. Indeed, the low operating temperature is beneficial since it reduces the leakage current and the heat generation. In contrast, if the cooling system cannot compensate for the self-heating of the sensor, the current and temperature will increase in an uncontrolled way causing the detector to become unstable. This phenomenon, known as "thermal run-away", is a positive feedback loop where the leakage current increases as the temperature. (Tsirou, 2020-12-05).

Lately, there has been a remarkable increase in the luminosity of the LHC. As a matter of fact that this also increases the irradiation which causes the sub-detectors to be operated at even lower temperatures. Table 4.1 tabulates the operating temperature values of the Si-based LHC detectors used in the past, and includes the current and future upgrade plans. For instance, the operating temperature of the CMS detector changed from $-10°$C to $-20°$C over the last decade. The trend suggests that there might be a considerable temperature drop in the operation temperature of the LHC detectors in return of an increase in luminosity. (Tsirou, 2020-12-05).

The choice of the operation temperature is a crucial parameter of the detector design requiring a combined effort of the Si-detector experts, the cooling system engineers

Table 4.1: Si-sensor operating temperatures of the multi-purpose LHC detectors. (Tsirou, 2020-12-05)

	Past	Present	Future
ATLAS	-70° C.	-10° C.	-25° C.
CMS	-10° C.	-20° C.	-30° C.

as well as the detector mechanics. Due to the tight layering of the LHC detectors, the Si-detectors are in the neighbourhood of other non-Si detectors which are operated at different temperatures. To illustrate, during the last two years of operation, the CMS Si-Tracker has been running at -20° C, while the Barrel ECAL has been holding over at -17° C. For this reason, the temperature measurement has to be conducted at several parts of the Si-detector even at its periphery and services. The measured temperature values are either used to interlock or just to monitor the system. The interlocking refers to setting the Si-detector in the safest state concerning the bias voltage, whereas the monitoring means following the temperature evolution and possibly taking a decision on the detector bias voltage. The interlock systems are the integrated systems composed of the sensors (in this case the temperature sensors) and actuators acting on the detector power. The required system resolution depends on its application. Each detector has made its own choices but in general terms, there is a certain cost for each interlock channel that is to be considered together with the actuators attached to. (Tsirou, 2020-12-05). All in all, apart from being part of the LHC detector infrastructure, the control and monitor of the Si-detector temperature are necessary during the preparation, evaluation, and integration of the new systems.

4.2. CMS Detector Readout and Monitoring System

In the light of all systems mentioned above, the LHC detectors consist of two major systems which are DSS and DCS which the latter brings the temperature values into play. The aim of the DSS is to guarantee the safety operations and the hardware can interlock

the system. On the other hand, the DCS is in charge of the control of the cold and dry systems. To illuminate, if the CMS DCS realises an unusual output from the HGCAL monitoring system, it sends an alarm to the CMS DSS which, in return, interlocks all systems. As conclusion, we can assert that the DCS is an established additional software layer on the DSS. (Barney, n.d.).

4.3. CMS Detector Control System

The high luminosity occurs when the beams are collided head-on. However, the luminosity may degraded due to the accompanying scattered particles which are also crucial while carrying out the particle analysis of the acquired detector data. For this reason, the front-end electronics and the detector modules are deployed. These systems are also to control the required bias voltage, the required excitation current and to power these modules and circuits. For this reason, a distinct DCS has been developed for each detector along with the common DCS of the CMS. Any fundamental LHC detectors have sub-detector control systems that were designed for each layer. The CMS has the sub-detector control systems for the Tracker DCS, HGCAL DCS, etc. Each sub-detector control systems have a connection to the main DCS. This means that the main CMS DCS is a dependent system, whilst sub-DCSs act as standalone systems, as seen in Figure 4.1. *(A. Tsirou, P. G. Verdini (personal communication, December. 10, 2020).)*

The main purpose of the DCS is to foresee any safety system operations and to avoid automatic mechanisms occurring in any hazardous actions. Also, it copes with the issues releasing the alert notifications both on the detector-on and detector-off sides. As a consequence, it has to serve without any interruption in order to ensure the safe and efficient detector operations. The DCS operates under lower reaction thresholds. It may come up against dangerous situations such as high temperatures, high voltages, gas or water leaks, power cuts and so on. Thus, it hands over the reins to the DSS which per-

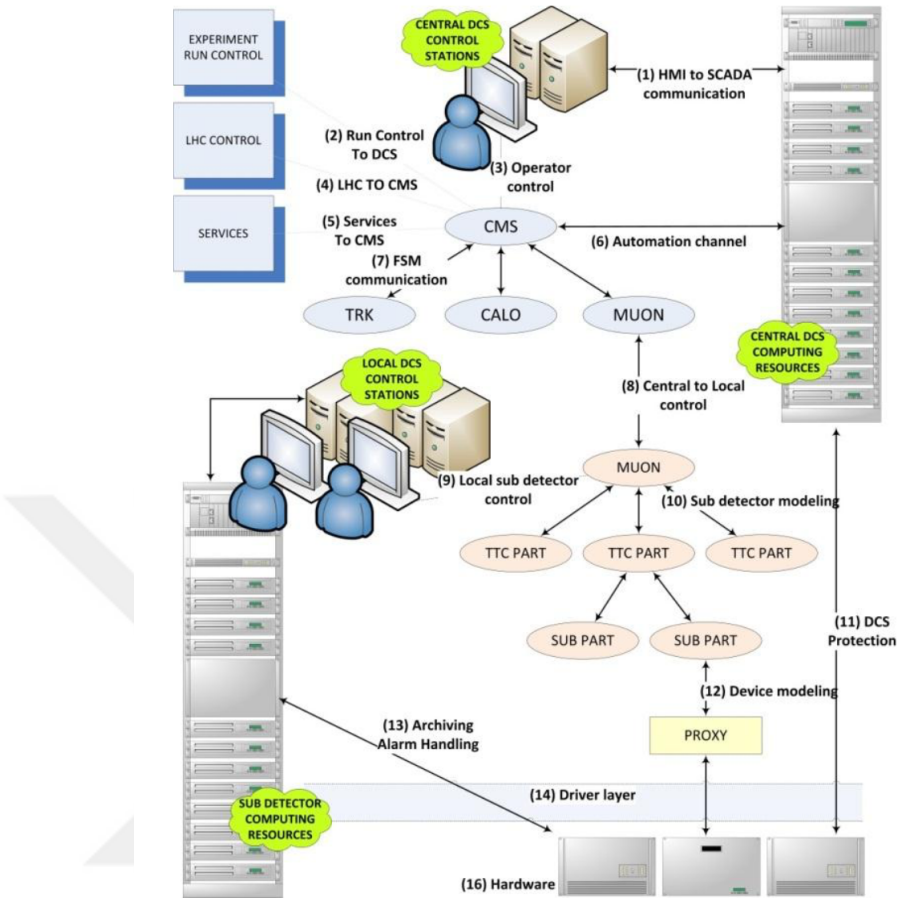


Figure 4.1: A schematic view of main CMS DCS with its sub-DCS.
(Bauer et al., 2012).

forms further safety operations. The reason why DSS takes safety responsibilities from the DCS in some particular cases is that the DSS gets into action when the radical decisions concerning safety are required since it has more granular hardware. Moreover, the DCS remains on operation under some conditions such as when a hardware runs near the operation temperature limits. Actually, this might not affect the modules and front-end electronics neither abruptly nor directly. Nevertheless, it may reduce the lifetime of the detector. Because, if the control is transferred to the DSS, then the DSS will immediately cut the power of the modules, that is worse than the ageing effect. Alternatively,

the DCS might set values of the voltage until the normal operation conditions are met (Chatrchyan et al., 2008).

4.4. CMS Detector Safety System

The DSS of any LHC detector is set up for retaining its operation until the safest condition possible of the main DSS is reached. As stated previously, the CMS detector consists of sub-detectors; hence, it has its own main DSS, whilst each subdetector holds its standalone detector safety system. In a similar procedure as for DCS, each DSS is hierarchically in connection with the main DSS. The reason why running hierarchically is that a sub-detector runs under different parameter values than other sub-detectors in terms of the temperature, voltage, current, or humidity. Therefore, all sub-detectors need to be controlled and monitored as well as interlocked under an extremely harsh operating environment via their own DCS and DSS.

The DSS receives sensor inputs coming from a detector; thus provides information and overall status concerning the subsystems to its DCS. Taken into consideration the requirements of each sub-detector, the operation logic of DSS has been designed in order to resume its lifetime. To clarify this point, the HGCAL DSS has been designed as a standalone system since it will independently run without any sub-safety or control system, as shown in Figure 4.2. Furthermore, it will be integrated as a slave to the main CMS DSS. As well as the connection to the main CMS DSS, the HGCAL DSS is also a slave to the CMS Cold DSS because it is one of the main cold CMS detectors which are the Tracker, MIP Timing Detector (MTD), HGCAL, and partially ECAL (ECAL operates in 10° C.). The HGCAL DSS will operate below -30° C which is achieved with the CO_2 cooling. the HGCAL DSS will needs to integrate both the CMS DSS and the CMS Cold DSS via interlock lines in order to provide the working conditions that can be dry or cold, Therefore, its lifetime can be guaranteed to last 10 years (Chatrchyan et al.,

2008).

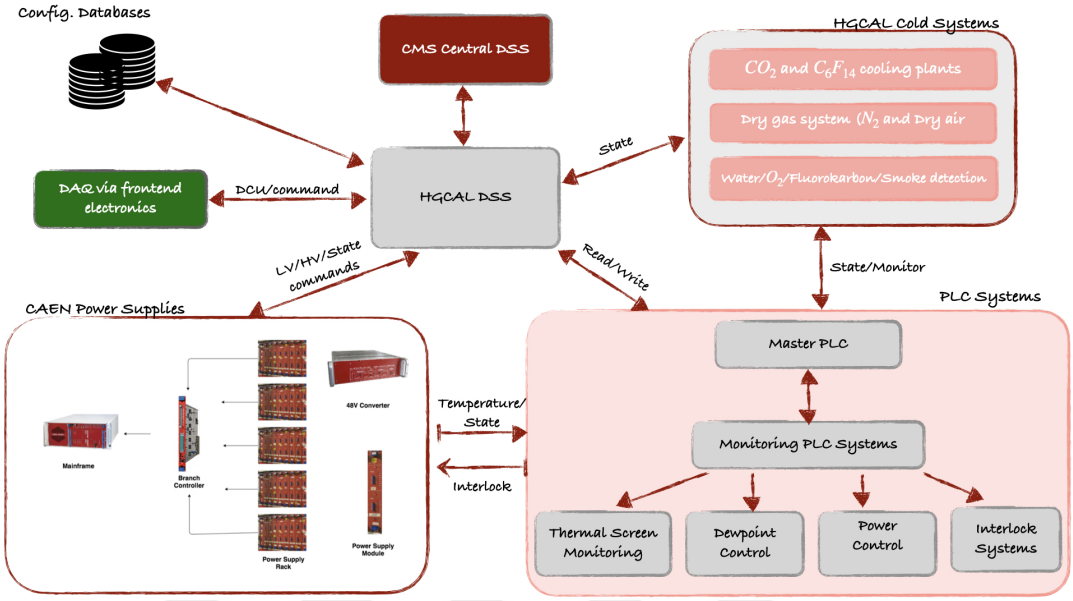


Figure 4.2: Overview of HGCAL Detector Safety System.
(Karimeh, Wassef, Chammoun, Maroun, Shvetsov, Ivan, Tsirou, Andromachi, & Verdini, Piero Giorgio, 2020).

4.5. CMS Detector Readout System

Over the past two decades, the CMS subsystem control has been depending upon a certain procedure. In this procedure, the signals coming from multiple sensors attached to the subsystems are conveyed to the “PLC” industrial automation system to determine the overall status of the sub-detectors. Subsequently, the states are fed into each sub-DCS and sub-DSS using the standard OPC-UA server. The key aspect of this procedure is how the signals are acquired and how the abnormalities are monitored to ensure a safe environment. The safe environment refers to that the inside, periphery and outside of the sub-detector are kept cold and dry. To achieve that, the most crucial environmental parameter in a Si-based sub-detector is the temperature. To sum up, one has to monitor the temperature at the three locations: firstly inside, secondly at the periphery, and lastly

outside of the sub-detector where latter corresponds to the power supplies, mechanical cooling pipes etc. (Barney, n.d.).

An illuminating example of the temperature readout inside a sub-detector is the HGCAL readout system. The temperature monitoring will be performed on the inside the HGCAL and off the sub-detector side. The temperature will be measured through the Gigabit Transceiver-Slow Control Adaptor (GBT-SCA) ASIC front-end electronics. Then the data will be digitised and extracted by the DAQ part of the HGCAL. This part will transmit all temperature data to the HGCAL DCS using again the standard industrial Open Platform Communication (OPC) protocol. (Barney, n.d.).

Another temperature readout part is that externally produced signals in the cable chains and on mechanical pipes are read via MTRS. Hence, the sensor signals are sent to the HGCAL DCS. Therefore, the control of power supplies (set on/off in exceptional states), monitoring states and quantities such as voltage, current, temperature, the humidity will be made via the OPC UA server connected to the WinCC Open Architecture (WinCC OA) which is a standard industrial data acquisition and control program (Siemens, n.d.).

4.6. CMS Cold Detector System

As it has been mentioned earlier, CMS sub-detectors have to run under conditions, which are cold and dry environments, in order to maintain their lifetimes. These working conditions are monitored and controlled by a cold detector system such that it feeds into CMS DSS as a slave.

A cold detector consists of three main systems which are the cooling, dry gas and detection systems, which are all serve different functionalities. The cooling system works in two ways –the evaporative CO_2 and the C_6F_{14} cooling plants aiming to keep sub-detectors below the zero temperature. In addition to the cooling system, the cold detector also deploys a dry gas system, which is based on using dry air and the N_2 separation

plant. Finally, the CMS cold detector has the detection system to detect the water, O_2, fluorocarbon as well as smoke leakages. (Tsirou & Verdini, 2020-10-23).

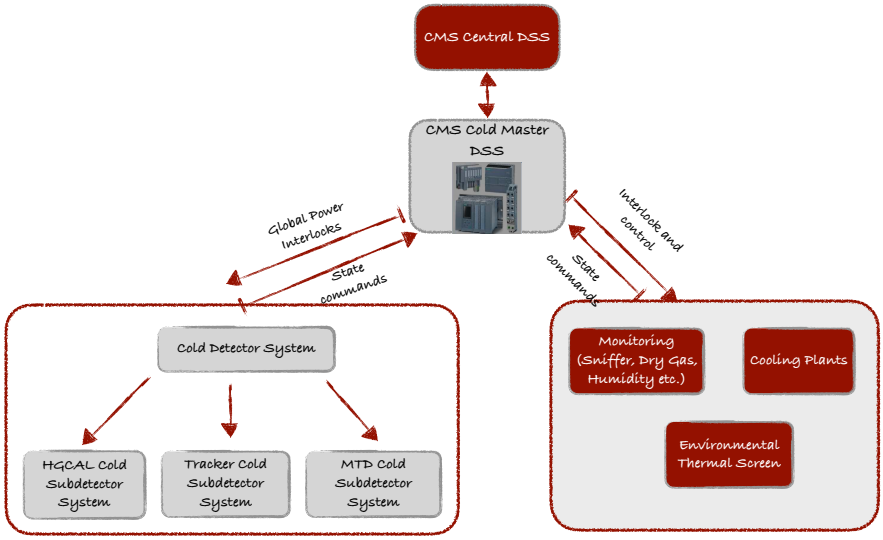


Figure 4.3: CMS Cold Detector Safety System.

The CMS cold detector system was designed for major CMS cold sub-detectors –the HGCAL, Tracker and MTD as well as ECAL partially. CMS cold detector system has individual cold sub-detector systems functioning in a standalone manner. The reason lies behind is that they commissioned and installed at different times. Fortunately, each cold sub-detector was designed with the same kind of infrastructure and policy. As a result, the cold sub-detectors have been servicing their sub-detectors can be monitored by a single CMS cold monitoring processor, and in case of any failure, the processor can send a report to the master CMS cold detector. (Tsirou & Verdini, 2020-10-23).

The temperature measurement is great of importance for the CMS cooling system throughout Phase-II and HL-LHC along with humidity, dewpoint measurements. For this reason, a number of hardwired RTD sensors will be situated onto the cooling pipelines of the cold sub-detectors mentioned above. The CMS cold detector system will be controlled by standard PLCs, which are the foci of the following chapters.

5. MASSIVE TEMPERATURE READOUT SYSTEM

The temperature that is the most crucial parameter in the cooling systems is measured by temperature sensors embedded in the readout chips of Si-based sub-detectors of CMS (Tracker, HGCAL, MTD). Apart from the fact that we have to monitor temperature around the periphery of the detector and detector-off side. Therefore, it is demanded more monitoring RTDs rather than the temperature sensors embedded in the readout chips for the environment of Si-based subdetector. These monitoring and control procedures are traditionally carried through PLC-based systems. It is a well-known fact that PLCs are remarkably robust systems for data acquisition, monitoring, and controlling processes.

Notwithstanding that, the PLC-based systems known as commercial off-the-shelf (COTS) electronics are not cost-effective products as the number of channels to be monitored increases. Considering increasing the number of channels, the cost per channel which is read by PLC is 50 CHF (Tsirou, 2020-12-05). Also, considering the fact that the cost as well as occupied space for temperature readout and monitoring, this issue was driven us to address with a reliable solution when the sensors will be strictly used for monitoring, therefore connecting them to a PLC system.

In this optimization problem, our objective functions which are the cost and the occupied space should be minimized utilizing cutting-edge technologies. Along with the substantial importance of embedded systems and the Internet of Things (IoT), we proposed an embedded-based and cost-effective novel development for temperature monitoring which is named as Massive Temperature Readout System (MTRS).

Prior to commencing the development of MTRS, the temperature sensor is required to determine. In view of the fact that the temperature sensors should be radiation-hard, reliable, compatible with detector conditions as well as engageable into DSS and DCS, it was concluded that RTD 4-wired temperature sensor was the optimum preference.

We, therefore, have not been making any calibration and it does not even indicate any degradation. Another point worth mentioning for the choice of RTD is that they are very tiny, always available, and affordable COTS products and also operate at as low as -200 °C to 850 °C (Tsirou, 2020-12-05). Moreover, it furnishes high measurement accuracy with the compensation of all series resistance due to engaging each other with lead connectors.

In pursuit of the selection phase of the RTD sensor, in order to conduct the MTRS study, the following steps were taken as presented in Figure-5.1;

- Evaluation and testing of LTC2984 chips with a microcontroller developed by Analog Device,
- Designed, read, and tested the Stage-I of MTRS readout cards
- Redesigned and tested the Stage-II of the MTRS readout cards to handle the issues arisen.



Figure 5.1: The development steps of the MTRS project.

5.1. Evaluation of the LTC2984

To commence developing the temperature readout system, the first step can be envisaged as evaluating the performance of the LTC2984 chip in Figure-5.2 because of the fact that one will be designed a readout electronic card through these chips. The key point here is that the DCS or DSS requires digital sensor inputs for controlling or monitoring process;

for that matter, we required a converter for analog sensor measurements in order to convert them as digital outputs. This conversion and digital measurement system were accomplished thanks to incredible features of this chip, which are referred the following sections.

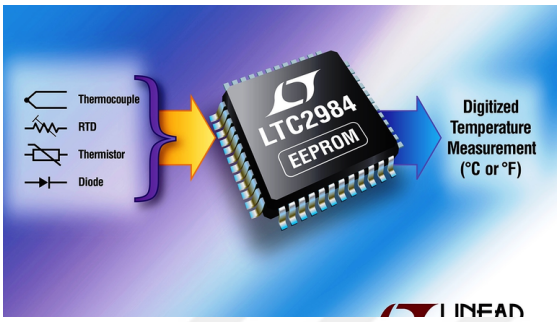


Figure 5.2: The LTC2984 chip measuring various temperature sensors with high accuracy. (Electronics, n.d.).

5.1.1. Overview of the LTC2984 Chip

The LTC2984 (Device, n.d.-b) is recognized as being among the most widely used chip in temperature measurement, produced by the Analog Device. It was designed to measure the following temperature sensors –RTDs, thermocouples, diodes, and thermistors.

Firstly, bearing in mind that we look into its structure, the chip includes 20 channels for wiring sensor connections and their configurations. Furthermore, it has buffers to preserve itself from all signals coming externally; hence it does not require external buffer circuitry. Besides, the LTC2984 chip consists of switches and active circuitry in order to detect faults and linearize data.

As a matter of having the active circuitry, it prevents sensor burn-out and short-circuits on-chip. It conducts the measurement of all virtually (type B, E, J, K, N, S, R, T) and custom thermocouples by providing thermocouple cold junction compensation and also

measures negative thermocouples voltages. Aside from operating with thermocouples fact that it is also compatible with resistor-based temperature sensors such as RTD sensors and thermistors. It allows measuring most RTD types such as PT50, PT100, PT200, and PT1000 with a variety of wired types (2-, 3-, and 4- wired). In this project, the

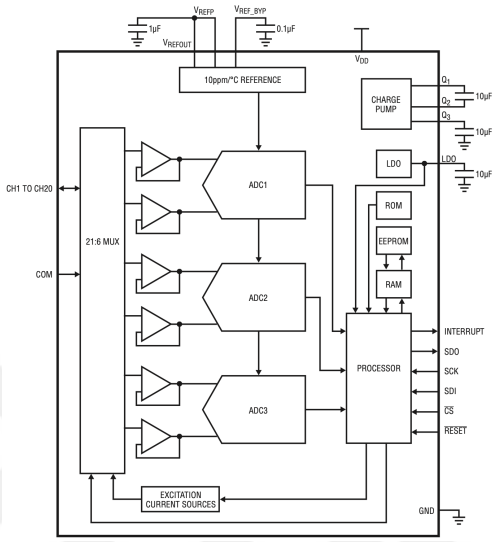


Figure 5.3: Blok diagram of the LTC2984 chip.
(Device, n.d.-b, p. 11)

primary eligibility cause of the LTC2984 is that it provides conversion analog sensor input to a digital output on account of including three 24 bits Analog-to-Digital Converter (ADC), as shown in Figure 5.3. Furthermore, considering that we will build a reliable readout system, this particular apparatus was decided the best choice for this study owing to the accuracy of 0.1 ° C and resolution of 0.001 ° C.

What is equally important is that the LTC2984 chip has the potential to prevent restoring configuration data and custom coefficients to memory. Therefore, it can be concluded that we do not have to configure the chip every time it runs by reason of containing EEPROM in itself. All in all, we can draw a conclusion that the LTC2984 chip option is the best way of measuring our RTD 4-wired sensors.

More detailed information about LTC2984 chip can be presented in References-(Device,

n.d.-b).

5.1.2. Testing the LTC2984 with the DC2420 Kit

Following the conducted research about the properties of the chip, our steps proceeded by testing the chip with a DC2420 starter kit, which is a temperature measurement system produced by Analog Device.

The DC2420 kit (Device, n.d.-a) aims to make easier the usage of LTC2984 and consists of three boards including Linduino, DC2399 (includes LTC2984 chip), and DC2210 (enable to connect sensors like breadboard). The readout kit allows communication between sensors to the computer. Considering the fact that we probe inside the DC2420 kit in detail; the Linduino board has two inputs; one of them provides communication to the PC via USB cable and the other input is plugged into the DC2420 board with 14 conductor ribbon cables. What's more, the DC2420 board is directly connected to the DC2210 daughter board. The readout circuit for configuration and testing was therefore installed as it is presented in the Figure-5.4.

Prior to commencing the configuration, the DC2399 housing the LTC2984 chip was equipped with six RTD sensors as well as 1000 Ω sense resistor (tied to Channel-2). All employed RTDs were selected as standard PT-1000/100 (DIN EN 60751). Apart from this, considering that the readout wires from inside the detector will be, on average, 100 m long; that's why the 4-wired RTD was preferred to be read out this type of RTD such that we can compensate errors arising from the different lengths. All in all, the five RTD 4-wired PT-1000 sensors were connected to Channel-4, 7, 10, 13, and 16 on the board respectively and RTD 4-wired PT-100 was wired to Channel-19 on the DC2210 board as in Figure- 5.5.

Also, taking into account the parasitic thermocouple effects that might arise due to the connection between RTDs and the instrument, we read the sensor under the excitation

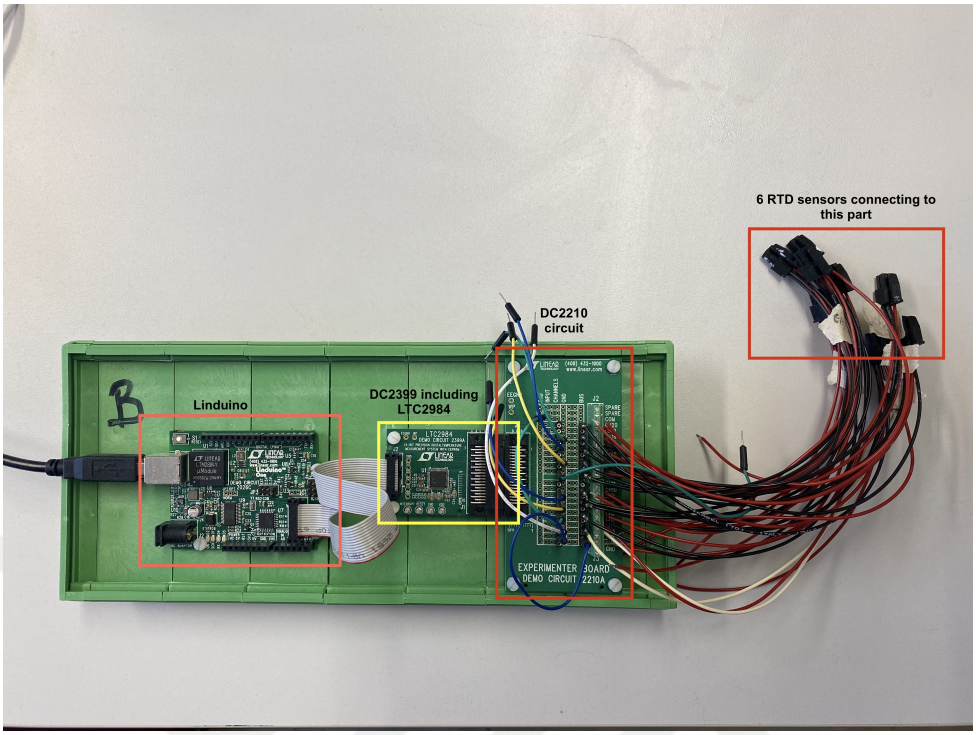


Figure 5.4: The DC2420 evaluation kit comprises of Linduino, DC2399 circuit including LTC2984 chip and DC2210 circuit for connection of six RTD sensors.

current rotation mode in order to eliminate these effects. In addition, this mode can not merely enhance the reading accuracy of the RTDs but also allow allows us to use more channels.

By setting the first of the configuration, the next step is to specify an excitation current value in order to avoid faults such that voltage dropping across the resistor will be a maximum of 1 V (Device, n.d.-b). That's why we opted for the excitation current of 100 µA by reason of setting sense resistor as 1000 Ω. Afterward, the RTD standard was assigned to "European" owing to preferring the standard DIN EN 60751 PT-1000/100 RTDs.

Having adjusted working mode as sharing/rotation excitation mode, the first wire of all four-wire RTDs was attached to the sense resistor on Channel-2 since each sensor

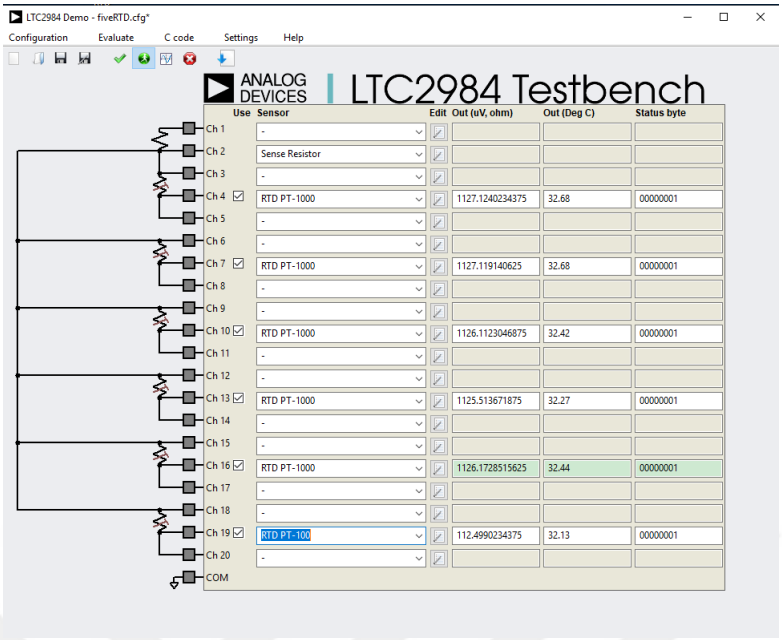


Figure 5.5: Configuration of five RTD PT-1000 and a RTD PT-100 sensors tied to LTC2984 board.

requires a sense resistor. Subsequently, all sensors are swapped to Channel-2 on the standard QuikEval GUI program. The reason why the choice of the QuikEval program is to make a verification for functionalities of the boards beforehand developing of the firmware, as shown in Figure- 5.6.

It is essential to point out that, the maximum number of the connected sensor on the DC2210 board was effectively optimized by means of sharing a common sense resistor for all connected RTDs. Because, if an RTD were separately connected with a sense resistor, one input of the sense resistor would have shared a wire of the four-wire RTD and this would have taken five pins on the board per sensor. Thus, we could have attached solely four RTD 4-wired sensors using 20 channels of the board. From what has been presented, one might conclude that the sharing/rotating excitation mode allowed us to make use of more channels by common resistor instead of six sense resistors.

Having established the configuration shown in Figure-5.5, evaluation of the readout was

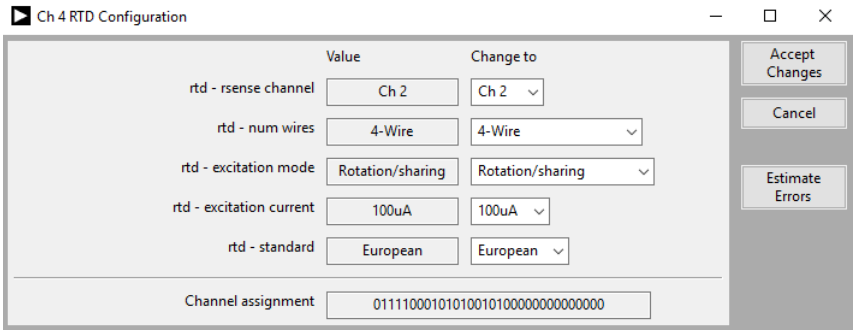


Figure 5.6: Configuration of a RTD sensor tied to Channel-4 is performed using QuikEval software.

carried out by the program written in C. The program was embedded to DC2026 Linduino which communicates with DC2420 over Serial Peripheral Interface (SPI) protocol and the QuikEval software enables visualization of the temperatures measured by the attached RTD sensors on an interface as in Figure- 5.5. Consequently, the LTC2984 chip was evaluated and six RTD sensors were substantiated using 20 channels on-chip.

5.2. The First Stage of the MTRS

Having determined a maximum number of the 4-wired PT1000/PT100 sensor which will be able to employ for a chip, the next step is to design and develop a massive channel readout system. For this view, the first stage of the MTRS (MTRS-I) was carried out over the following steps;

- The first step in this development is to design a 3U sized Eurocard due to utilizing this type of racks in the detector-off side and the fact that the 3U sized cards will be situated into these racks after production. These cards were designed by housing convenient four LTC2984 chips given the fact that a VME connector allows us to accommodate merely 24 RTD sensors,
- Subsequent to the design, the produced the first stage of the MTRS card was read and performed DAQ by developing a C-based program on Raspberry Pi,

- Finally, resolving all the issues concerning servicing them and verifying the performance of DAQ.

5.3. The Readout Card Design of MTRS-I

Once the maximum number of sensors attached to the LTC2984 has been functionally verified, the next stage is to design a readout circuit. Both PCB layout as can be seen in Figure-5.7, and schematic drawing of the readout circuit were performed using Altium Designer. The card includes two VME connectors; the first VME connector (J1) serves a connection of 24 4-wired RTD sensors to the readout card, whereas the second VME connector (J2) is exploited for communication between the readout card and Raspberry Pi 4 over ribbon cables.

The pins of J2 are in connection with board selection pins, chip selection pins as well as SPI communication inputs such as Master Input Slave Output (MISO), Master Output Slave Input (MOSI), and Clock (CLK). As a matter of fact that, a VME DIN41612 connector consists of 96 pins, and hence it allows us to tie just 24 sensors because the preferred RTD sensor has four wires. As a consequence, the card can accommodate only four LTC2984 chips.

Furthermore, four LTC2984 chips were attached to the design so that these chips fulfill digital temperature measurement as noted earlier. Accompanied by the chips, ceramics capacitors were drawn and function as a filter in order to compensate for the voltage regulations.

Apart from that, two integrated circuits (ICs) were added to specify which board and chip should be selected. The SN74HC688PWT IC along with an 8-input switch aims to select the board, while the SN74ACT32D IC works for chip selection. Once putting the electronic instrumentations, the PCB card was designed under the conditions of Eurocard (3U sized) with the size of rack units in mind. Thereby, the first PCB design

of the MTRS was completed.

A more detailed description about the Stage 2 of the MTRS board can be found in Appendix-2. EDA-04119-V1-0 Schematic View and (Tsirou, Tekis, & Verdini, 2019).

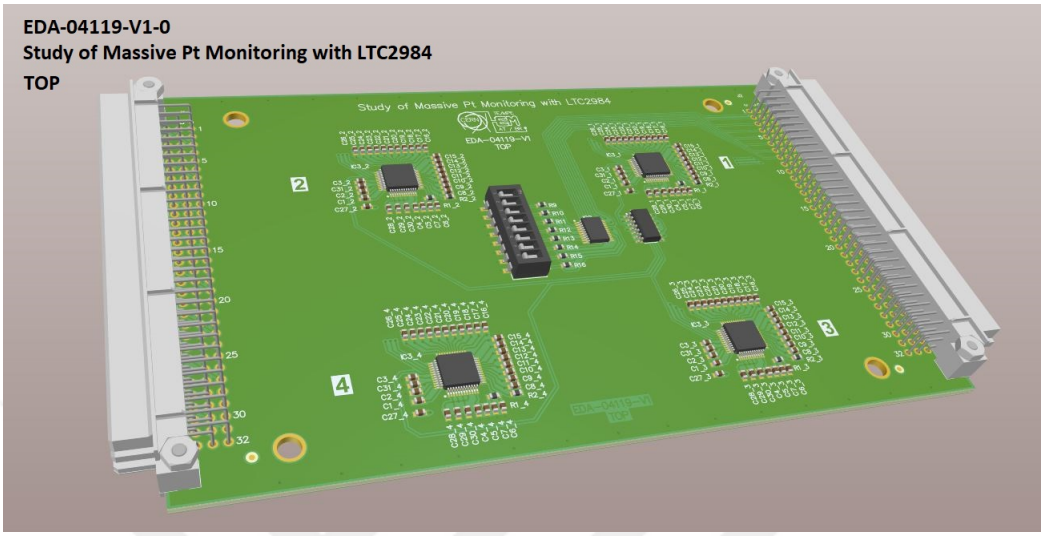


Figure 5.7: The first stage of the MTRS board.

5.4. The DAQ of the MTRS-I

The readout of the MTRS board can be achieved either with a microcontroller or microprocessor. The most crucial point here is that the sensor values acquired from the board have to be transferred to DCS or DSS of any cold detector. Thereby, we required a server for data transmission. Keeping in mind that we need enough memory space to develop a socket server/client and OPC server, it was decided to use Raspberry Pi 4B+, which is not a microcontroller, is a System-on-Chip (SoC); hence it makes deploying a server possible on itself. Hereby, the data acquisition and transmission of the MTRS project was achieved by Raspberry Pi 4 B+ which is in charge of operating as a controller, and was performed by following the steps as showed in Figure-5.8.

As looking into how the data is acquired by RPi, the designed and produced PCB board has two connectors as input; one of them is connected to 24 sensors, and the other side is

attached to RPi via a ribbon cable for providing SPI communication as well as selecting which board and chip will be read out at that time.

For getting sensor data from the chips, the readout program was written in C on RPi using both bcm2835 and wiringPi library in order to perform SPI communication. The pins on RPi corresponding to one of the SPI libraries used (bcm2835 or wiringPi) are set up and bcm2835 or wiringPi SPI functions are called. Following these, the selection of board and chip to be read out is made by setting as low. Having selected the board and chip, configuring channels corresponding to each RTD tied to the LTC2984 is enabled by programming into RAM of the chip with a 32-bit channel assignment word. The word consists of information related to RTD and sense resistor, such as RTD type, sense resistor channel pointer, sensor configuration, excitation current, RTD curve, and custom RTD data pointer. Thus, the channels for each chip on the selected board are configured.

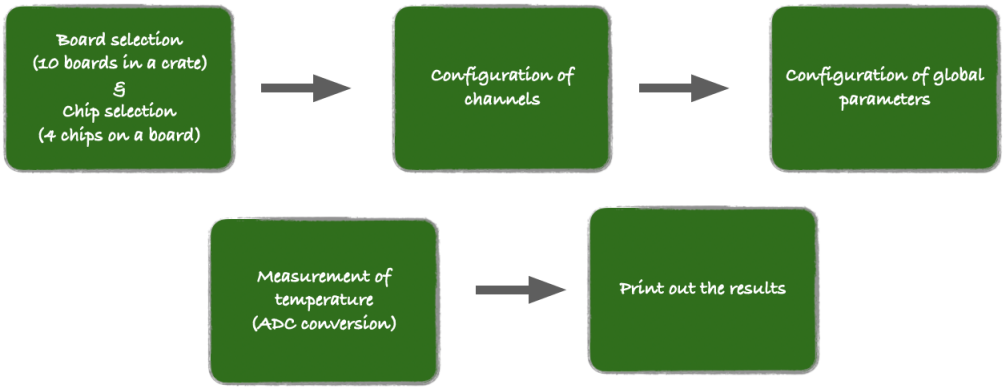


Figure 5.8: The block diagram of temperature sensors readout procedure for MTRS Stage 1.

The RTD type for configuration is defined as the first five bits of the channel assignment word that is to say from B31 to B27 and the five inputs are assigned as seen in Figure-5.9. In the figure, nine different types of RTD can be determined as linearization coefficients (RTD types PT-10, PT-50, PT-100, PT-200, PT-500, PT-1000), NI-120 with selectable common curves ($\alpha = 0.003850$, $\alpha = 0.003911$, $\alpha = 0.003916$, and

(1) RTD TYPE					
B31	B30	B29	B28	B27	RTD TYPE
0	1	0	1	0	RTD PT-10
0	1	0	1	1	RTD PT-50
0	1	1	0	0	RTD PT-100
0	1	1	0	1	RTD PT-200
0	1	1	1	0	RTD PT-500
0	1	1	1	1	RTD PT-1000
1	0	0	0	0	RTD 1000 (α = 0.00375)
1	0	0	0	1	RTD NI-120
1	0	0	1	0	RTD Custom

Figure 5.9: The five MSBs of the channel assignment word are set as RTD types configuration. (Device, n.d.-b, p. 33).

$\alpha = 0.003926$) and RTD custom (Device, n.d.-b, p. 35). Since the measurements of temperature will be performed with RTD PT-1000 sensors in the project, RTD type is chosen as RTD PT-100, and that's why the first five bits are assigned as `01111` in binary representation.

5.4.1. Configuration of the Sense Resistor

A sense resistor is tied to each chip because it allows determining the temperature of the sensor using a look-up table for RTDs or solving Steinhart-Hart equations for the thermistors. For RTD measurements, a R_{sense} resistor is required to perform measurement radiometrically and differentially.(Device, n.d.-b). The sense resistor channel pointer part of the channel assignment word shows where the R_{sense} resistor is connected to for the RTD. It was connected between CH-1 to CH-2 for each chip-on-board and bits from B26 to B22 are set as `00010` in binary representation.

5.4.2. Configuration of the RTD Sensor

In the sensor configuration field of the word, RTD properties (like 2-, 3-, or 4-wires) can be specified between B21 to B18 bits on the word. B21 and B20 bits indicate properties of RTD while other pins represent excitation current source type (defining as rotation/no

rotation) and sense resistor type (defining as sharing/not-sharing). (Device, n.d.-b). On the chip, these bits are defined as `1010` which are corresponding to 4 wires PT-1000 sensors excitation current rotation and sharing resistor used.

The next part of the word is to control excitation current using pins from B17 and B14. The excitation current enables us to prevent thermocouple parasitic effects which may be arisen from physical connections between RTDs and electronic instrumentation for measurement. It can also eliminate soft and hard faults. To prevent these problems, an appropriate excitation current is chosen so that the maximum voltage drop value corresponding to the used R_{sense} or sensor is 1 V(Device, n.d.-b, p. 35). For instance, when $R_{sense} = 10\,\text{k}\Omega$ and type of RTD is chosen PT-1000, maximum excitation current value has to be 0.1 mA such that maximum value of V_{drop} is provided as 1 V.

That's why the excitation current value depends on the max voltage drop and R_{sense} to be used. In the project, R_{sense} and the excitation current was selected as $1\,\text{k}\Omega$ and 100 μA respectively so that it is less than the maximum value when the voltage drop value is calculated as 0,1 V. Therefore, the field for the excitation current is assigned as `0101` according to Table 5.1.

Following defining the excitation current field of the word, B13 and B12 are allocated to assign RTD curves. There are a couple of tolerance standards that determine a grade or a class to get the better accuracy value of platinum RTD. Two types of standards are mostly used in the industry: American and European types. American type is also known as ASTM E1137 and generally used in North America, whilst European type is also called as DIN or IEC and the most used type is DIN IEC60751 by selecting the worldwide wide. The LTC2984 chip allows us to assign six types of RTD curves: American, European, Japanese, ITS 90, RTD1000-375, and NI-120. Regarding selected the RTD curve, Callendar-Van Dusen constants are determined and so the temperature value is calculated using these constants. For the MTRS project, RTD measurement is

Table 5.1: The excitation current values corresponding to RTD wire types.
(Device, n.d.-b, p. 35)

Excitation Current				
B17	**B16**	**B15**	**B14**	**Current Value**
0	0	0	0	Reserved
0	0	0	1	5 μA
0	0	1	0	10 μA
0	0	1	1	25 μA
0	1	0	0	50 μA
0	1	0	1	100 μA
0	1	1	0	250 μA
0	1	1	1	500 μA
1	0	0	0	1 mA

carried out using the European RTD curve type because it is widely used in the world. B13 and B12 are set as 00 for the European curve as seen in Figure-5.10. (Device, n.d.-b, p. 35).

Table 34. RTD Curves: RT = R0 • (1 + a • T + b • T^2 + (T – 100°C) • c • T^3) for T < 0°C, RT = R0 • (1 + a • T + b • T^2) for T > 0°C

(5) CURVE						
B13	B12	CURVE	ALPHA	a	b	c
0	0	European Curve	0.00385	3.908300E-03	–5.775000E-07	–4.183000E-12
0	1	American	0.003911	3.969200E-03	–5.849500E-07	–4.232500E-12
1	0	Japanese	0.003916	3.973900E-03	–5.870000E-07	–4.400000E-12
1	1	ITS-90	0.003926	3.984800E-03	–5.870000E-07	–4.000000E-12
X	X	RTD1000-375	0.00375	3.810200E-03	–6.018880E-07	–6.000000E-12
X	X	*NI-120	N/A	N/A	N/A	N/A

Figure 5.10: Bits B13 and B12 are assigned as the RTD curve and are the corresponding *Callendar-Van Dusen* constants.
(Device, n.d.-b, p. 35).

The rest of the bits in the channel assignment are set in place with a custom RTD data pointer with 12 bits. If custom RTDs are used for the measurement, specific data defined by the user are stored in the on-chip RAM. The custom RTD is not used in the project. Instead, The measurements are made by RTD PT-1000 4-wire sensors, thus this field is completely assigned as all zeros of 12 bits. Having assigned all bits, 32 bits

0x78A94000 of channel configuration data is obtained and are mapped into the RAM locations corresponding to R_{sense}. Besides the configuring channel, the selected R_{sense} is also required to be configured.

Channel assignment data for sense resistor is allocated by two parts; sensor type and sense resistor value. Since sensor type is a sense resistor, 11101 is assigned to this field as a 5-bit word as it is seen in the Table- 5.2. The rest of the bits indicates a sense resistor value. In the project, the channel assignment data for R_{sense} is 0xE80FA000. This means that 1 kΩ of sense resistor is tied to each LTC chip and the rest of the bits, 27 bits from B26 to B0, are mapped as shown in Table- 5.3.

Table 5.2: The most significant 5 bits of the sense resistor channel assignment word consisting of 32 bits.
(Device, n.d.-b, p. 37).

B31	**B30**	**B29**	**B28**	**B27**	**Sensor Type**
1	1	1	0	1	Sense Resistor

Table 5.3: Sense resistor value (1 kΩ) representation with binary notation.
(Device, n.d.-b, p. 49).

Sense Resistor Value (1 kΩ)													
B26		**B25**	**B24**	**B23**	**B22**	**B21**	**B20**	**B19**	**B18**	**B17**	**B16**	**B15**	**B14**
0		0	0	0	0	0	0	1	1	1	1	1	0
B13	**B12**	**B11**	**B10**	**B9**	**B8**	**B7**	**B6**	**B5**	**B4**	**B3**	**B2**	**B1**	**B0**
1	0	0	0	0	0	0	0	0	0	0	0	0	0

As a result, channel assignments for both R_{sense} and all used RTDs are defined. After this configuration, if supplemental information is desired to be defined, the LTC2984 chip has another register into memory regarding this configuration. Two different registers into RAM provide to configure global parameters and extra MUX delay. The global parameter configuration aims to define the notch frequency of the digital filters as well as the format of temperature measurement (° C or ° F). The global parameters configuration is performed with the local configuration register into 0x0F0 of the memory location. (Device, n.d.-b, p. 64,65).

The notch frequency is set at 50/60 Hz rejection as default (i.e. 75 dB rejection with 1 ms MUX delay). However, in particular, a different frequency value can be desired to be defined. In the case of operating at higher 60 Hz rejection, `0x01` value is written into `0x0F0` address of global parameter register. If the digital filters run at a higher 50 Hz rejection, `0x02` value is required to write into the same memory location. Concerning representation of temperature results, the default unit is determined as °C by setting bit `0` into memory location `0x0F0` yet the LTC2984 chip also gives reporting in °F by writing 1 to B2 of memory location `0x0F0`.(Device, n.d.-b, p. 64,65). In our global configuration, the chips have been operated under 50/60 Hz rejection and the results are reported in °C. Thus, data is written into memory location `0x0F0` as it is seen in the Figure- 5.11.

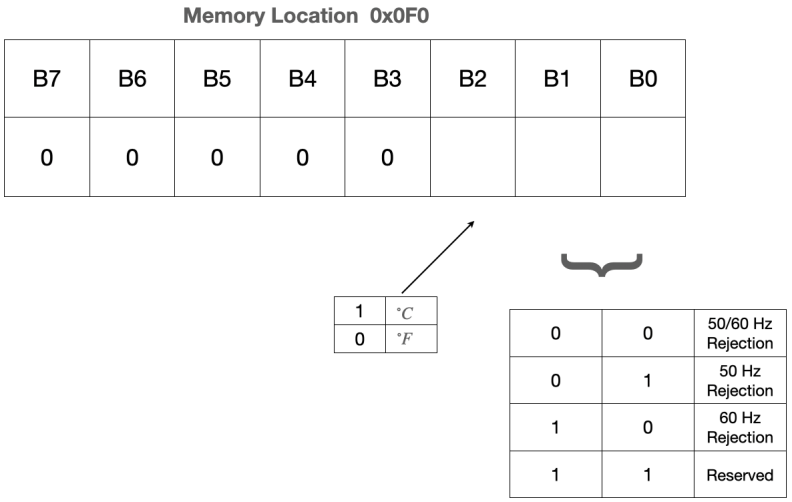


Figure 5.11: The global configuration register of the LTC2984 chip is used for defining the notch frequency and temperature format.
(Device, n.d.-b, p. 65).

Apart from global parameter configuration, if excessive RC time constants appear on external sensor circuits consisting of large bypass capacitors used for RTD and thermistor, the rise of the setting time between MUX switching and excitation current source might be done. This delay can be configured by writing a determined value into the

0x0FF address of the MUX configuration delay register onto the RAM. The delay is calculated by multiplying the value by 100 μA; for example, if the value written into memory is 0x0FF = 255, the maximum extra MUX delay is obtained 25.5 ms (i.e., 255*100). (Device, n.d.-b, p. 64,65). For the MTRS project, we don't need to add the extra MUX delay since not used external sensor circuits cause the presence of excessive RC time constants in this case. We, therefore, assigned 0 to memory location 0x0FF.

Once channel assignment words are written corresponding to channels, an analog to digital conversion is initiated on the specified channels for RTDs and R_{sense} channel by writing 1 to B7 and 0 to B6 into memory location 0x000 (aka COMMAND STATUS REGISTER address). B7 indicates START pin, while B6 serves as DONE bit for the conversion. These bits are assigned as 10 to start conversion. Bit B5 is selected 0 as default. Bits from B4 to B0 states the input channels. The binary values of used channels are set to this bits—from B4 to B0.

After assigning START pin as HIGH and DONE bits going LOW, INTERRUPT pin is set to LOW so the conversion is initiated. During conversion, an accomplishment of the writing process into memory location 0x0000 depends upon the sensor configurations and lasts around two or three 82 ms cycles. While waiting for the process, reading data from the 0x0000 address of RAM must be 0x40 such that conversion can be completed. Otherwise, we have to wait for writing a command into the memory until getting 0x40. INTERRUPT pin goes to HIGH, START pin, and DONE pin toggles as 01 at end of the conversion.

As concerning the MTRS project, six RTD sensors are tied to CH4, CH7, CH10, CH13, CH16, and CH19 channels corresponding to 0x04, 0x07, 0x0A, 0x0D, 0x10 and 0x13 in hex representation. When the conversion is started, the 0x80 starting command is added by channel commands above respectively, thus channel selected commands which are 0x84, 0x87, 0x8A, 0x8D, 0x90, and 0x93 respectively, are mapped to

memory location `0x0000`. After conversion, data obtained from memory is `0x40` means that B7 and B6 are `0` and `1` respectively and the rest of the pins are entirely `0` because we don't specify channels for ADC conversion anymore and START pin going `0`, DONE pin assigning as `1`.

For more detailed information on LTC2984 chip, you may follow its datasheet in (Device, n.d.-b).

6. THE FIRST RESULTS OF THE MTRS

This chapter presents results and readout challanges of MTRS Stage 1 and proposed solutions. Section-6.1. shows the first results of MTRS boards and explains the readout problems and the reasons why the problems are arisen. In Section-6.2., a variety of solutions for the communication problem are proposed. Finally, by selecting the best approach as a solution the second design of MTRS board is explained in Seection-6.3. to readers.

6.1. Results and Challenges of the MTRS Stage 1

As pointed out in Chapter-5, communication between RPi and read-out boards was performed by SPI protocol throughout the first production of the MTRS (CERN EDMS EDA-04119-V1-0). It must be born in mind at this point that the boards were communicating directly with a processor (Raspberry Pi 4B+). During getting read-out streams from boards, we encountered problems which were sensor faults ("missing" temperature sensors) as shown in Figure-6.1. However, we were able to get sensor data streams from the same chip accurately. In other words, the sensor data could be sometimes obtained accurately as presented in Figure-6.2b while sometimes getting bad data from sensors as can be seen in Figure-6.2a. In short, the system couldn't work properly.

6.2. Proposed Solutions for the Stage 1 Boards

With the aim of finding the crux of the problem, the SPI lines were monitored via oscilloscope, and high-frequency noises on the chip select line of SPI were observed. These high-frequency noises on the RPi kills the *chip-select* functions (and subsequently, the readout). To address this issue, although we designed diverse filter circuits working as externally, the noises could not be eliminated. Consequently, communication with bo-

```
              CHIP SELECT#1
  Temperature of PT#1 = 27.955078
  Temperature of PT#2 = 27.961914
  Temperature of PT#3 = 27.947266
  Temperature of PT#4 = 0.000000
INVALID READING !!!!!!
  Temperature of PT#5 = 27.795898
  Temperature of PT#6 = 27.980469
```

(a) Reading five RTD sensors correctly except for the fourth sensor from chip-1 onto the first board.

```
              CHIP SELECT#1
Temperature of PT#1 = 27.971680
Temperature of PT#2 = 27.984375
Temperature of PT#3 = 27.962891
Temperature of PT#4 = 28.084961
Temperature of PT#5 = 27.826172
Temperature of PT#6 = 28.045898
```

(b) Reading all sensors accurately from chip-1 placed onto the first MTRS board.

Figure 6.1: Sensors values from chip-1 at different times.

```
              CHIP SELECT#4
Temperature of PT#1 = 27.732422
Temperature of PT#2 = 29.485352
Temperature of PT#3 = 27.500000
Temperature of PT#4 = -999.000000
- SENSOR HARD FALURE
- SENSOR_ABOVE
Temperature of PT#5 = -999.000000
- SENSOR HARD FALURE
- SENSOR_ABOVE
Temperature of PT#6 = -999.000000
- SENSOR HARD FALURE
- SENSOR ABOVE
```

(a) Reading three RTDs correctly except for the last three RTD sensors from Chip-4.

```
Chip Number 4
  Temperature of PT#1 = 26.993164
  Temperature of PT#2 = 26.901367
  Temperature of PT#3 = 27.031250
  Temperature of PT#4 = 27.351562
  Temperature of PT#5 = 26.914062
  Temperature of PT#6 = 26.867188
```

(b) Reading all sensors from Chip-4.

Figure 6.2: RTD values reading from Chip-4 located onto the first version of MTRS board.

ards could not be provided consistently.

The second approach dealing with the communication problem was to write time-delayed read-out program. The program managed to remain stable communication between five temperature cards and a RPi. However, it has obviously performed this achievement using time delays that have to be "calculated". Also, the delays have to be set under certain conditions because the system has to make deployment of diverse size and position systems impossible. Therefore, this solution could not be preferred.

Another proposed more practical solution for this challenging problem is that Arduino Nano was connected to each board. In this system, read-out operation was done by connecting Arduino Nano per board over SPI protocol. In point of fact, the system has run perfectly without facing any communication problem. This system was tested as

stated below.

In Figure-6.3, the first version of the MTRS board was connected to Arduino from one input and was tied to 24 RTD sensors from the second input. The sensors were installed around the two pipes coming from the chiller for the ECAL. When one/two Arduino were connected to the MTRS board, any communication errors were not observed, as seen in Figure-6.4.

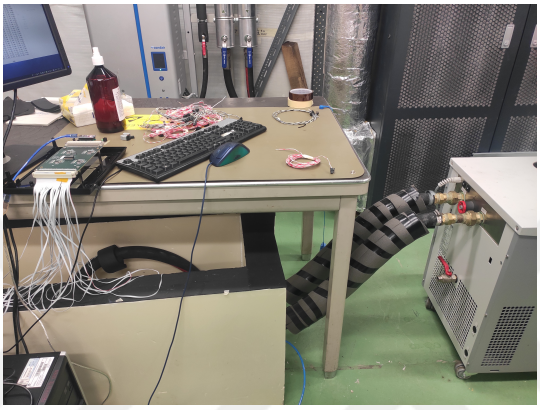


Figure 6.3: It is the first version of MTRS board which were connected Arduino to the first VME input and tied chiller via sensors to its second VME input.

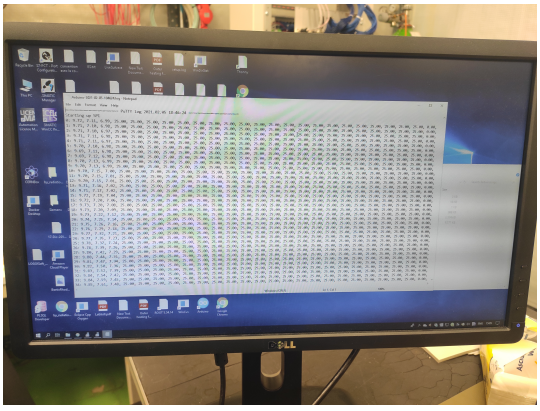


Figure 6.4: The temperatures reading with Arduino connecting the a single MTRS board.

Nevertheless, in this scheme, we need to employ Arduino Nano for each board, and the Arduino Nano doesn't allow us to develop the OPC UA server. That's why it was

a necessity of a microcomputer including System on Chip (SoC) for further processes such as data control and monitoring instead of using a microcontroller. For this reason, a new solution was developed.

It was considered as a new approach that is based on the attachment of one Arduino Nano to one card since the scheme worked perfectly. Considering that we have to use RPi for the development of the OPC UA server, the Arduino Nano, however, offers no direct Ethernet connectivity with RPi. For this reason, it was decided that the data stream flow between RPi and Arduino Nano will be performed with Modbus, which is a very debugged and standard communication protocol, commonly available for connecting industrial electronic devices (Tsirou, 2020-12-05). Using the "standard" Arduino Modbus library, the Arduino Nano can send data to the RPi using serial communication over RS485 with Remote Terminal Unit protocol.

In this readout scheme, the reason why RS485 was chosen is that it acts as a filter between the Arduino and the Raspberry Pi 4B+. Thus, the direct access of the Raspberry Pi 4B+ to the temperature chips is removed. We developed an adaptor mini board to test the proposed approach as presented in Figure-6.5. The adaptor board consists of a ATMEGA328P, RS485 to TTL circuit and Modbus inputs. This adaptor board is connected to the first MTRS boards. Then, ATMEGA328P placed onto the adaptor board can read the sensor data by selecting chips over SPI protocol and also selecting boards using I^2C. The RPi communicates with ATMEGA328P via RS485 to TTL IC over Modbus protocol and then RS485 to TTL IC gets data from ATMEGA328P over UART protocol as shown in Figure-6.6. The scheme works with Modbus as a master to RS485 Modbus interface.

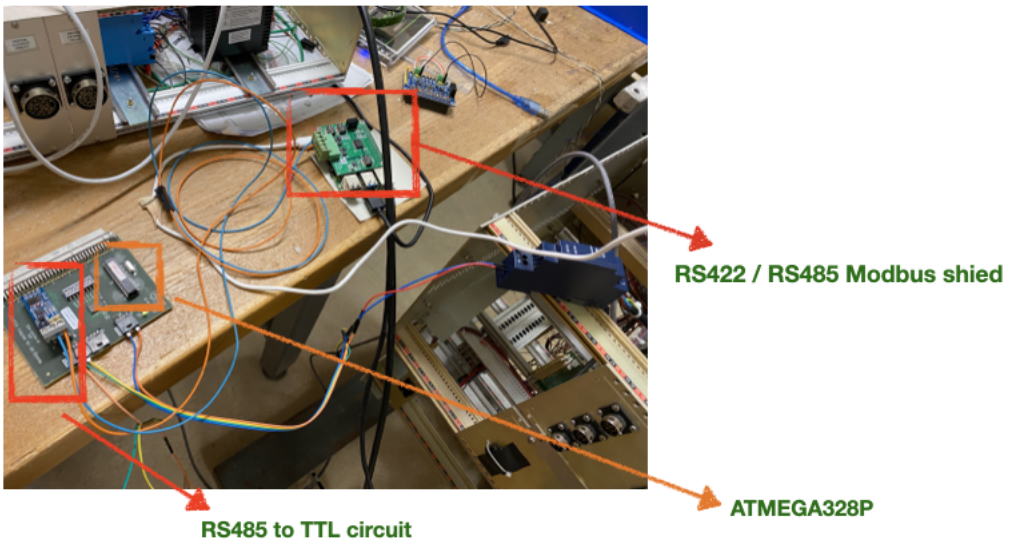


Figure 6.5: Adaptor Board including RS485 and ATMEGA328P is connected to RS422/RS485 Modbus shield onto Raspberry Pi 4B+.

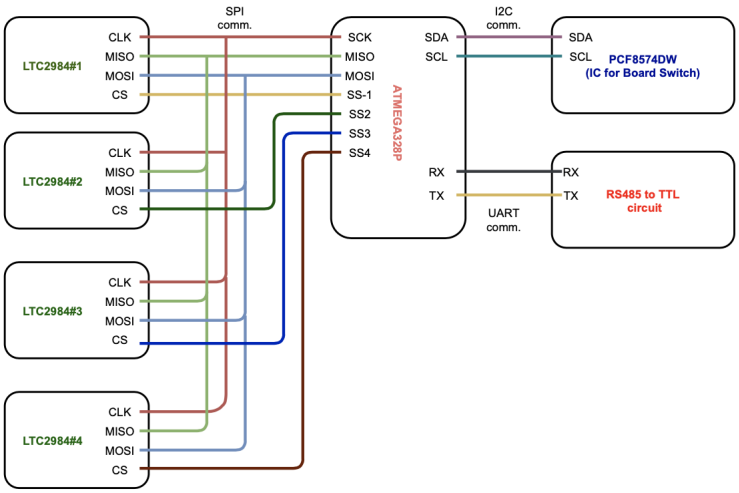


Figure 6.6: Three different communication protocols were used with Atmega328P.

6.3. The Second Version of the MTRS Boards

Having found the best solution, it is decided to insert just the ATMEGA328P chip (and its clock for timestamp) and the RS485 chip on the temperature card itself. This is a much more compact and powerful design that eliminates can function standalone.

Moreover, we are not even constrained by only one “mechanical crate”.

In the PLC structure, each PLC has a certain number of crates which are objects transmitting data to the PLC as shown in Figure-6.7. Each crate contains up to eight modules that are of various types and every module has a certain number of channels. Different modules have different number of channels. The channel is the quantum of information, providing a “value” with an “id”, a “type” and “flags” related to the “monitored value”. The module also provides “flags” for general diagnostics. The PLC does not provide a real timestamp but a “heartbeats” which can be translated to a timestamp and should be considered as such. In the same way, for the developed temperature monitoring we can

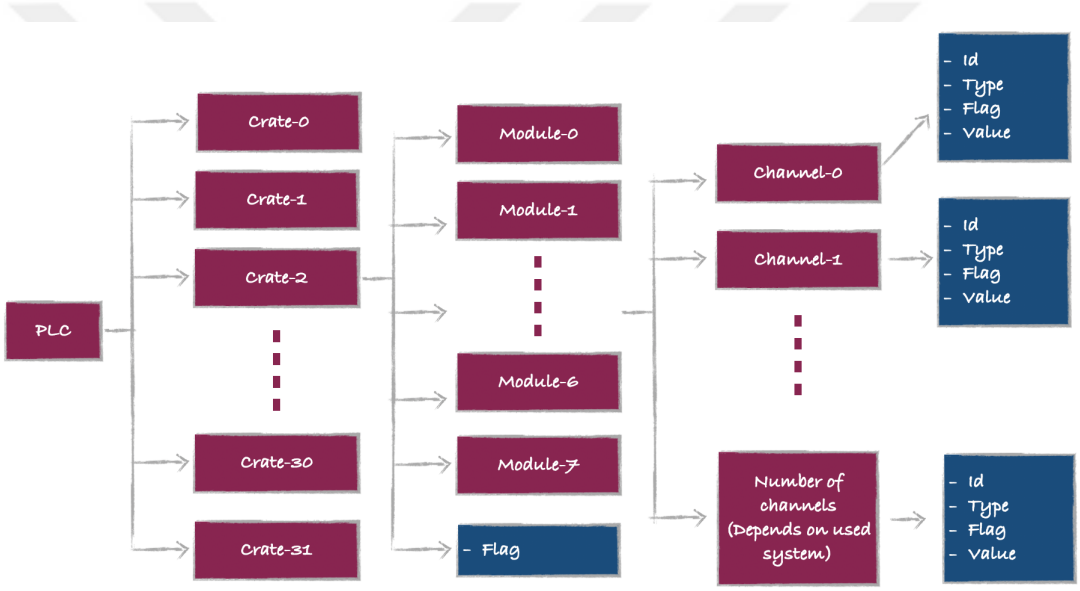


Figure 6.7: PLC structure consists of 32 crates and each crates has 8 modules. Each module associates with a number of channels (depends upon the system) and each channel gets data with some information–id, type, flag.

have a structure that starts with the RPi 4B+ as can be seen in Figure-6.8. the RPi that transfers data via an OPC UA protocol is equivalent to the PLC. The *RPi* is consisting of a certain number of boards which are the temperature monitoring boards each equipped with one Arduino. With developed MTRS, we will test 32 readout boards per RPi because maximum 32 crates can be connected to PLC. This is to say that in this scheme,

the board is equivalent to a crate of the PLC system. Each readout board consists of four chips that are equivalent to the modules. Each chip reads data over six channels and each channel provides "value" with an *id*, a *type* and *flags* related to the monitored sensor. Each chip gives us the flags for general diagnostics. Furthermore, each board provides us a *timestamp*.

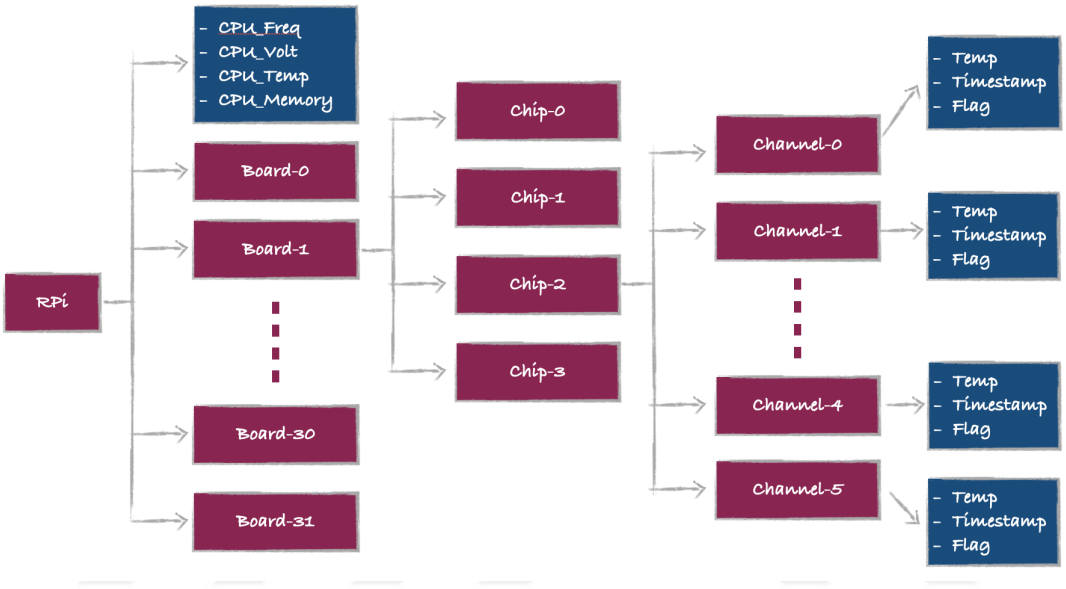


Figure 6.8: An overview of MTRS structure.

Depending on the requirements of the new approach:

- The ATMEGA UART communicates via an "RS485 to TTL" circuit that works as Modbus slave in order to send data to any Modbus master receiving hardware, thus providing the minimal readout system, as it is seen in the Figure-6.9
- The RS485 bus is employed to communicate to a Modbus master that can also run a TCP socket server. This intermediary partner can be any low cost, low power computer like a RPi or a Beagle Bone. The number of boards to interconnect can be up to 32 (for reasons of the load on the bus) so the communication partner acts like a concentrator. The communication partner can then connect to any TCP

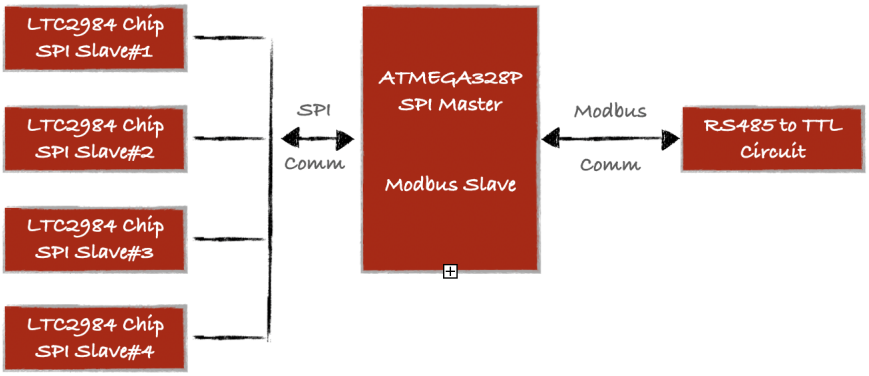


Figure 6.9: Board connectivity with minimal implementation (adaptor board).

socket client and the data can be further handled. The communication between the server and the client is performed over Ethernet, as can be seen in the Figure-6.10 below.

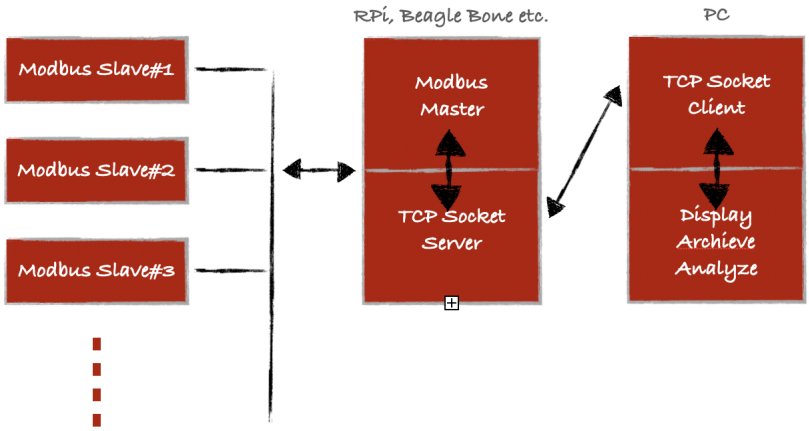


Figure 6.10: The limited implementation of the MTRS.

- The intermediary partner can run an OPC UA server which allows for connecting to any OPC UA client and deeveloping a OPC UA server. Most SCADA systems (and certainly the CERN-wise SCADA) have OPC clients that provide for the seamless integration of the data to the SCADA system, as seen in Figure-6.11

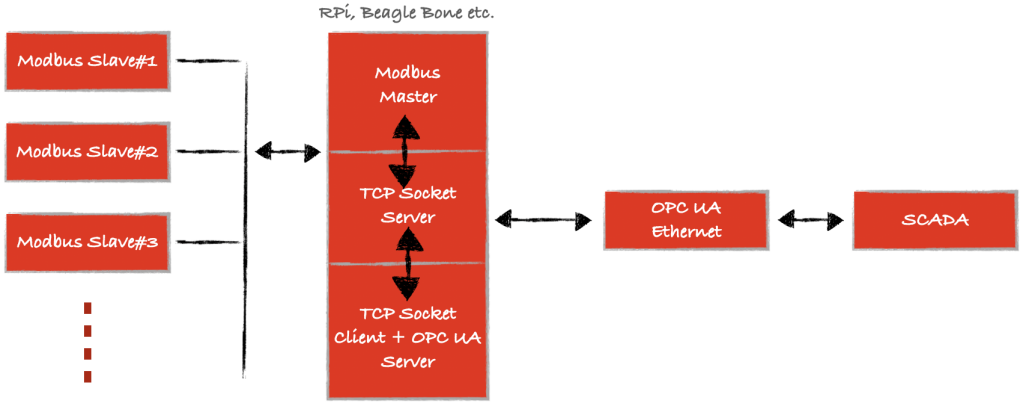


Figure 6.11: The rich implementation of the MTRS with intermediary partner.

- When it is important that the data is available at a PLC (DSS) level and not at the DCS level then the intermediary partner can be connected to a PLC Modbus communication unit (i.e. the CP341 for Siemens S7), as can be seen in the Figure-6.12 below.

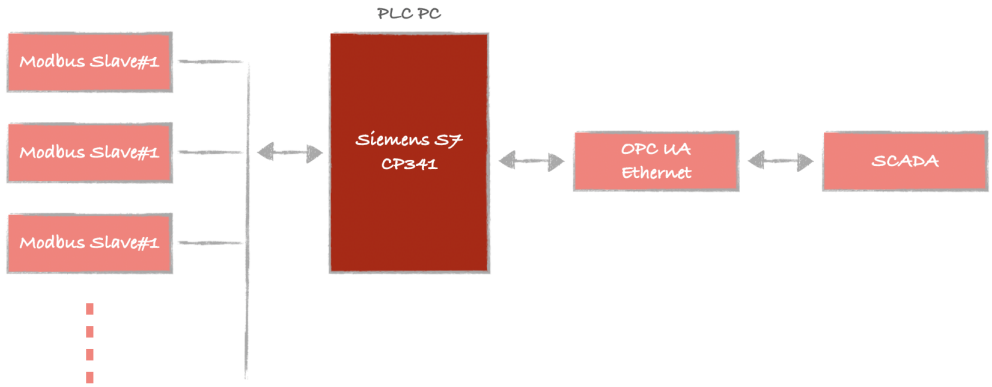


Figure 6.12: PLC system communicates its slaves over Modbus protocol.

All in all, within in this mind, the Stage 2 of the MTRS boards was redesigned in Altium using above-mentioned structure similar to PLC structure and the new approach. The design of the second version of board is available as EDMS document (EDA-04119-V2.0) (Tsirou, Tekis, & Verdini, 2020), as presented in Figure-6.13. Each board conditions up to 24 RTD sensors using four LTC2984 chips. An ATMEGA328P-U microcontrol-

ler is used for selecting and addressing the LTC2984 chips. The data is read over the ATMEGA SPI bus. The ATMEGA I^2C bus is used for reading the status of the board switches and the ATMEGA UART is employed to communicate the information to the outside world but also to initiate the transfer of data to RPi over RS485 protocol, as can be seen in Figure 6.6.

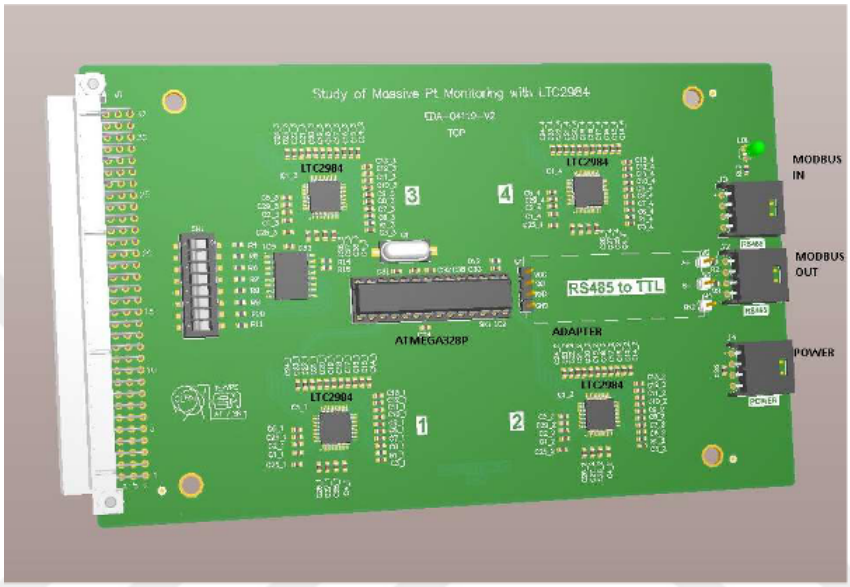


Figure 6.13: The Stage 2 of the MTRS board.

A more detailed description about the Stage 2 of the MTRS board can be found in Appendix-3. EDA-04119-V2-0 Schematic View and (Tsirou et al., 2020).

7. DATA TRANSMISSION: RPi to DCS

Having provided DAQ of the MTRS by a program developed in C, sensors data and their flags need to be sent to the OPC UA server such that it can publish them to OPC UA clients, i.e., CMS sub-detector control systems. Because OPC UA was developed using Python and executing on Raspberry Pi, we need an interface to flow out data from the C-based program to the OPC UA server. Thus, it was decided to develop a socket interface that defines the communication functions for an API TCP/IP network. Since the socket allows it to be developed in any language, a server that was developed in C sends the data to a client written in Python onto the OPC UA server. The socket client's main task is to send requests to receive and read data and then share them with the OPC UA server, while the socket server aims to transmit the sensors data to the socket client. The socket was created utilizing TCP protocol to ensure reliable convey between socket server and socket client in this work as shown in Figure-7.1.

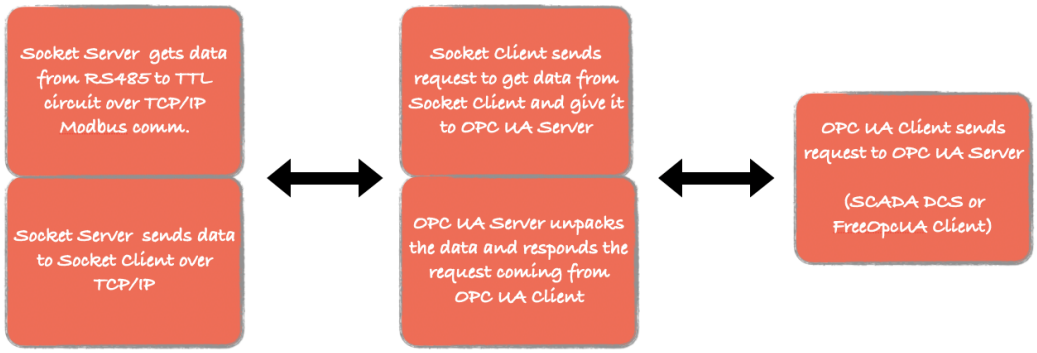


Figure 7.1: The sensor data flow from the boards to the DCS by developing socket server/client and OPC UA server/client.

7.1. Overview of Socket Programming

Inter-process communication over a network can be performed through the Internet. This is so-called socket programming. Internet-based socket programming is also known as network socket or the Internet socket since it uses Internet protocols to enable communication over the Internet. Therefore, two endpoints (also known as sockets) require a specific IP address and a port for the installation. The port is pertaining to an IP address of a device and depends upon a type of protocol chosen for the communication. Defining a particular process or application executing on a computer or a machine needs a special identification, that's why the ports concerning the used protocols play a vital role in determining a unique server. The IP addresses do not permit the installation of a particular server or process because a computer/machine owns an individual IP address but more than a server can be set up on a computer. Thus, the ports composed of the IP address and the protocol provide unique identification to servers/processes. (Kalita, 2014).

A port of a socket is created with 16-bit integer numbers. Some ports specified between 0 and 1024 are reserved for the proprietary network applications such as FTP 21/TCP, telnet 23/TCP, login 513/TCP, SMTP 25/TCP, or HTTP 80/TCP, User Datagram Protocol (UDP). Thus it has to be defined the port from after 1024 when we desire to utilize except for the well-known ports stated above. In Internet-based communication, the socket programming employs the Transport Layer Protocols, namely Transmission Control Protocol and User Datagram Protocol of Transmission Control Process/Internet Protocol (TCP/IP) stack. The protocols always interact with the ports such that received data are paired with defined applications or processes. This port has to be defined that the client meets with the server. (Kalita, 2014).

By developing socket programming, one of the Internet software stacks has to be selected under required features. The TCP protocol is based on a connection-oriented service.

This is to say; data exchanges are provided after a link between the client and the server is launched by the TCP protocol. The TCP connection enables a virtual pipe between the hosts (socket-server and socket-client). This pipe is established by sending a connection request from the client and accepting it by the server. After establishing the pipe, the server sends out the information bytes to the client over the network (which is the Internet); the socket client receives the bytes in the order sent. The client sends the acknowledgment via the TCP protocol when the bytes arrive at the client. Otherwise, the server waits for the acknowledgment. Although the TCP-based communication takes time due to waiting for acknowledgment, this is highly reliable (Coner, 1995).

Apart from the TCP protocol, the communication between the two endpoints can be carried out with the UDP protocol. The UDP does not provide the connection while exchanging data between the client-server, and data are directly sent to or receive from the hosts. The data packages can get lost during inter-process communication owing to the use of a connectionless protocol. That's why it is not reliable, yet it is faster than the TCP since it does not wait for an acknowledgment.

7.2. Development of the Socket Programming

The socket programming can be implemented in a variety of ways because it depends upon the socket family, socket type, and protocol. While we were developing the socket server program, we followed the steps explained below;

- Creating a server socket,
- Binding the address to the server socket,
- Setting up a listener and start to listen to the requests coming from the client,
- Accepting it and connect to the client,
- Sending/receiving data to/from the client.

The server socket needs to use a domain (socket family), socket type (TCP or UDP), and protocol for bi-directional communication. AF_INET6 (IPv6 protocol) which is the commonly used version is opted for the domain, while socket type is selected $SOCK_STREAM$ for TCP due to being more reliable (Stevens, Rudoff, & Fenner, 2003). The protocol is defined as the Internet protocol, too. Hence, the socket of the server is set up by initializing the parameters above. Afterward, the installed server is bound with the address information which is the hostname and specified port number. In addition, the server can be bound to the localhost. Having bound the address to the server, a listener function is defined for the number of clients that will be listened to. The server passes the quiet/passive mode until the client makes a connection. When the client sends a connection request, the listener accepts the request and then data communication is started. For installation of the socket client, we followed the ways stated below;

- Creating socket client,
- Making a connection request,
- To send/receive data from socket server.

Creating the client is the same as the installation of the socket server. The same parameters have to be defined while creating the socket client. Following this, connect() function provides a TCP server connection to send a request to the socket server. As soon as the socket server accepts it, the communication is enabled and data exchanging is started.

7.3. The OPC UA for the MTRS

Along with the development of the socket programming developed for sending the data digitized with a C-based program to Python script, the client sends a request to the socket server programmed in C to obtain the digitized sensor data. Received data from each cold sub-detectors via the client are required to publish to the corresponding

sub-detector control system and general detector safety system. The DCS and DSS are operated by the industrial PLCs performing controlling, monitoring, and interlock processes. Therefore, these operations are implemented on WinCC OA software that the software communicates between machines using industrial factory OPC UA protocol. With the MTRS project, obtained temperature values are monitored via a Graphical User Interface (GUI) developing in WinCC OA, and also the software can send alarms to the other machines where any exceptional cases may appear. For this purpose, a new server was designed to transmit the data with DCS over OPC UA protocol by enabling communication infrastructures and dynamical data exchange with industrial PLCs.

7.4. Overview of the OPC UA

OPC UA (Unified Architecture) is an Machine-to-Machine (M2M) communication protocol for connecting and exchanging data with different automation incubators and devices using the same interface. This communication protocol first appeared in 1996 under the name of OLE for process control. Then OPC protocol, special PLC protocols which are MODBUS, PROFIBUS, CANBUS, etc. For integrating its protocols into Human Interface (HMI)/SCADA systems, it was introduced to the market in 1996 as an interface that performs reading and writing operations according to the device. However, since OPC (Ole for Process Control) only works on Windows-based machines, this protocol has started to be called open platform communication as a platform-independent communication protocol to be compatible with every operating system. (Foundation, n.d.-a).

Thus, the OPC standard allows data exchange between two different systems without the need for an extra application. In other words, OPC allows the development of a human-machine interface (HMI) between client-server or server-server, rather than just a communication protocol, which means that from the end (defined as hardware) where

the data is received, the point where the data is processed and saved (can be said as the software part). Provides hardware-software compatibility. After the development of the features of OPC, the new generation OPC UA emerged system came up in 2008, which has all the features of the classic OPC and allows industrial systems to communicate on a common platform. (Foundation, n.d.-a).

OPC UA protocol, which has a service-based architecture, is a system that provides data exchange between two endpoints. This protocol provides a human-machine interface for communication between two endpoints such that the client sends a request from the server to acquire the data whilst the server becoming the source of the information replies to the requests within the OPC UA protocol. OPC UA client and server software can be built using different software languages such as C / C++, .NET, JAVA, and even low-cost embedded systems like Raspberry Pi 3B +, Beaglebone, etc. (García, Irisarri, Pérez, Marcos, & Estévez, 2017). It also allows development by using the standard Ethernet network. This process is implemented with three varieties of open-source OPC UA implementations; namely, open62541(Foundation, n.d.-f), freeOpcUa (for C++)(Foundation, n.d.-e), and freeOpcUa (for Python)(Foundation, n.d.-b).

During the data communication process, the server creates an address space with nodes, and variables associated with these nodes are declared. The client requests the value of the variable in the request from the server, which OPC UA allows the client to access the variables of wealth, and thus the data exchange begins. Creating address space and nodes in the server part is relevant to the information model of OPC UA consisting of different models for different operations.

Combining all the functions of classical OPC, OPC UA has a multi-layered structure, which provides OPC UA with platform independence, security, flexibility, functional equivalence, and comprehensive information modeling features. The functional equivalence feature aims to bring all COM OPC classic features to OPC UA and usability. With

its platform independence feature, it allows data exchange in embedded micro-controls, cloud-based servers, general-purpose PCs, and PLCs, while at the same time providing server-client development in different operating systems such as Microsoft, MAC OS, Linux, and Android, etc. Moreover, when a new feature is desired to be added to the system, it provides a flexible feature by adding a new feature without affecting the existing application. It is a very secure platform for transmitting data securely with encryption, authentication, and auditing features. In addition, it can effectively convert data into information with OOP-based multi-level structural modeling. (Foundation, n.d.-g).

7.5. Specifications of OPC UA

The structure of OPC UA consists of its base services and an information model as can be seen from Figure 7.2. Information models build on this infrastructure, and a couple of different functions that are defining alarms & conditions, data accessibility, and accessing historical data are performed with information models. These functions are also called OPC UA specifications. The specifications operate under IEC 62541 standards. To define the data accessibility function, OPC UA Data Access (DA) part works and provides to form and reveal the data. OPC UA Alarm & Conditions (AC) are used to give an alarm when the operating conditions exceed the limits and to monitor the environment such as temperature, humidity, or high/low power status. In addition, historical information and status in the past are ensured by OPC UA Historical Access (HA). Lastly, OPC UA Programs (Prog) on the top of infrastructure determines to start, supervising, and monitoring the implemented programs. (Mahnke, Leitner, & Damm, 2009)

7.5.1. OPC UA Data Access Specification

OPC UA DA , which is one of the essential OPC UA specifications, provides to acquire data from the machines such as PLC/controllers and indicates them on interfaces like

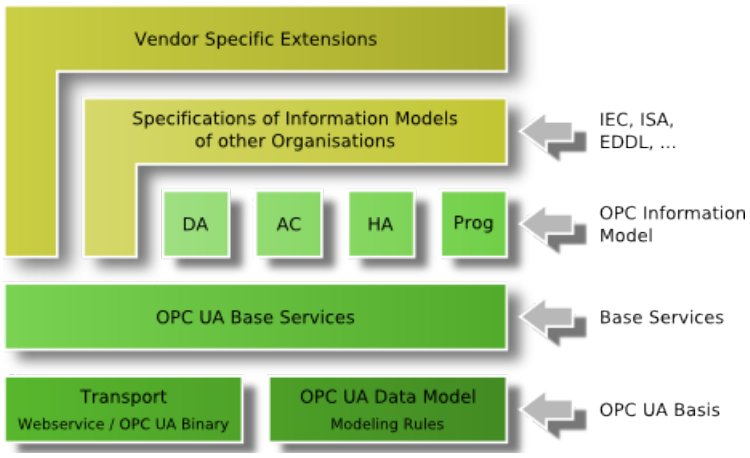


Figure 7.2: The OPC UA structure that composed variety layers. (Automation, n.d.-c).

HMIs, SCADA systems. The data transmission, which is the most significant property of the OPC UA DA, is fulfilled ceaselessly. It can be said that the data acquisition via OPC UA DA is based on client-server standards. Having sent a request by the client for desired data including a value and timestamp, a server responds to the client with the desired data; therefore this exchange is performed with a couple of capabilities of the OPC UA DA specification. (Foundation, n.d.-d).

Its specification primarily consists of five capabilities; discovery, browsing, read, write, and subscription. The discovery functionality aims to find out available OPC UA devices on a specified network. With the browsing features, an address space of a server is queried to get the available nodes. Read functionality of the OPC UA DA allows reading the nodes and giving the value, timestamp, and quality of the node in a single call, while the feature of writing the values to these nodes, accessing success/failure code within the single call. Lastly, the subscription performs the OPC UA DA to ask a server for monitoring the nodes and also to send a notification to the client, having changed the value of the node. (Foundation, n.d.-d).

7.5.2. OPC UA Alarm and Conditions (AC) Specification

OPC UA AC, which is one of the encapsulated functionalities of the OPC Classic, fundamentally depends on OPC UA Alarm & Event (AE). It is used to give an alarm to the end-users or clients in case exceeding the limit of the conditions. The responsibility is primarily based on processing the alarms and events received from the OPC UA AC server. In performing the processes, there are a couple of functions of OPC UA AC; namely receiving the alarm, receiving audit events, responding to alarms, and filter. The receiving alarms method aims to deliver alarms produced by the OPC UA AC server to a client such that it can represent the alarms on the screen for monitoring. Within the receiving audit events function, audit events created by the OPC UA AC server; i.e login, logout, accessing records and giving comments to the records, etc. are sent to the client. The goal of responding to alarm events function is that the client receiving the alarms enables us to acknowledge, to put the comment, to postpone, and to reply to the alarms. In addition to the above-mentioned capabilities of the OPC UA AC, the functionality of filtering aims the client to permit filtering of the events (Foundation, n.d.-c).

7.5.3. OPC UA Historical Access (HA) Specification

The specification of the OPC UA HA intends to receive data from PLC or other controllers as well as OPC DA Servers. Having obtained the data, it purposes to analyze and process historical events of the data. Fulfillment of these tasks is done by the capabilities of the OPC UA HA, namely read, write, and subscription methods. Read function is capable of getting the history of all created nodes. It defines the parameters such as start or end date but also determines the statistical events i.e average, max, min, etc. One of the goals of OPC UA HA is to update the data recorded in the database by some requests defining the actions such as delete, update, and create historical events. Moreover, the OPC UA HA introduces the functionality of subscription so that it monitors the nodes and delivers the notifications to the client when changing the values of the nodes (*OPC*

Historical Data Access, n.d.).

7.5.4. OPC UA Program Specifications

Program specification is intended to run, manipulate, and evaluate the program by utilizing a state machine. As it is well-known that a method or function, which is defined and compiled by the server, is called by the client and delivers the response to the client. However, programs are developed to handle them when coming up against a more complicated, long-running, and stateful set of processes. In other words, the programs are utilized for executing and controlling the batch processes. Controlling functionalities (which are to compile, run, and stop) of the programs are performed by the client, executed in the server. Having invoked the programs by the client, it responds to the client using Events. Though, it requires deploying the Finite State Machine (FSM) information model to manage whether the program is running or suspended to return to the client. The FSM is used as a base of operations to model Programs (Mahnke et al., 2009, p. 118).

7.6. Information Model of OPC UA

All the information models in OPC UA are designed within a framework ensured by the base information model. The information models aim to create objects and to define their properties, boundaries, and methods. The base information model primarily specifies entry points, base types, built-in but extensible types, and server objects. The entry pointers indicate the data of the OPC UA server into its address space used by the clients to cross through the instances and the types of the server. Another responsibility of the information model is to define base types that create a root for a particular type of hierarchy. It also allows to built extensible types such as object types and data types of the OPC UA server. Besides, the information model is designed to initiate the server object that gives diagnostic information (Mahnke et al., 2009, p. 81).

7.6.1. Address Space

The modeling of OPC UA is designed as an object-oriented model which is called the address space model. The OPC UA Server has an individual address space composed of a set of objects, and each of the elements in the object model is indicated as a node (Mahnke et al., 2009, p. 77). The nodes are characterized by the Attributes and are associated with the References as shown in Figure 7.3. Each node depends on a NodeClass which presents a particular element of the Object Model. Since the nodes consist of Attributes and References, the NodeClass comprises them in the same way. To define the Address Space, the nodes have to be integrated into NodeClass and be interconnected with other nodes via References. There are eight NodeClass in an Address Space; view, object, variable, method, ObjectType, DataType, ReferenceType and VariableType. (Automation, n.d.-a).

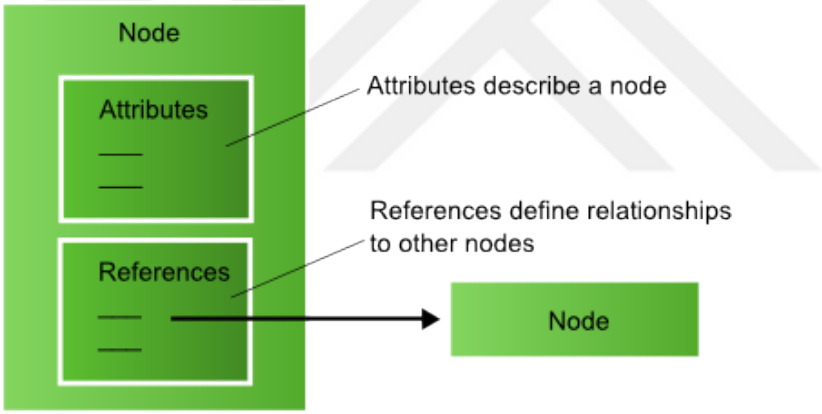


Figure 7.3: The node model of OPC UA within the framework of address space model. (Automation, n.d.-a).

In addition, each node in the Address Space is specialized by an id (which is called NodeId). Therefore, the NodeId allows to recognize to and map with the OPC UA client. The NodeId structure consists of namespaceIndex, identifierType and identifier. The namespaceIndex is a numeric value identifying the namespace. The namespace is specified by Unique Resource Identifier (URI), and it is in charge of naming authority

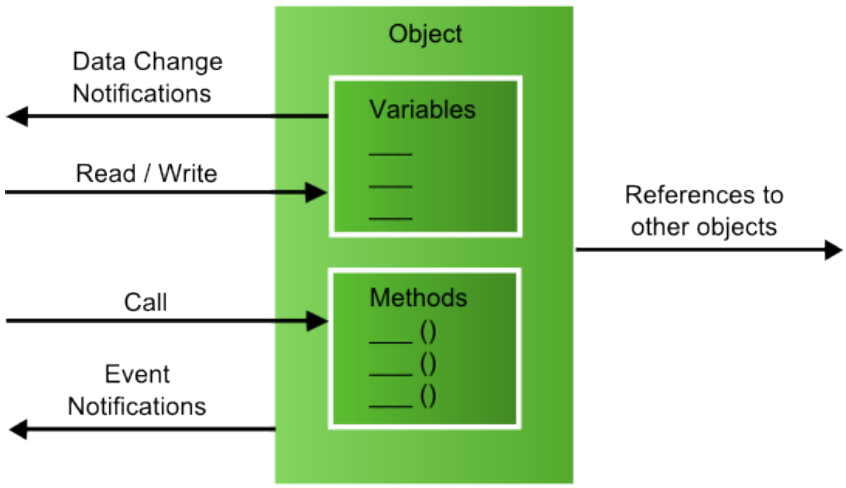


Figure 7.4: The object model of OPC UA.
(Automation, n.d.-a).

and assigning the identifier to the NodeId. The identifierType determines the type, format, and range of NodeId, and the type can be NUMERIC, STRING, GUID (Globally Unique Identifier), and OPAQUE. Besides, identifier provides unique identifier in the namespace (Automation, n.d.-b).

For more details on OPC UA, the given references above, notably in References- (Mahnke et al., 2009) can be followed.

7.7. Development of OPC UA Server and Client

In this work, OPC UA Server's requirement emerged from data transferring between RPi and CERN-wise WinCC OA Siemens SCADA for monitoring and controlling the temperature readout system. Raspberry Pi 4B+ connecting to the readout boards through a flat cable sends a signal to get data from the boards over SPI communication protocol. The Raspberry Pi 4B+ running as a master receives 24 temperature data per board acting as a slave. The data are packed by OPC UA Server executing on the Raspberry Pi 4B+ and sent to the OPC UA Client that is WinCC OA SCADA.

The OPC UA API can be implemented in different languages such as C++, Python, Java. However, it is impossible to develop the OPC UA Server on a microcontroller such as Arduino, STM32, etc. It requires a System on Chip (SoC), that's why it is developed onto Raspberry Pi 4B+, which provides to use the FreeOpcUa tools open-source OPC UA stack. The FreeOpcUa tool allows using C++ and Python for developing OPC UA server and client. Additionally, it ensures us a GPL Python GUI client to visualize the data in a panel.

The OPC UA server is developed in Python using the FreeOpcUa python-opcua package. The FreeOpcUa package and the libraries were installed on the Raspberry Pi 4B+ using the commands here. OPC UA works under the standard network protocols that it always has to authenticate and encrypt the data. Therefore, the 'cryptography' package was installed on the Raspberry Pi and imported its function in the Python script. Having installed the required packages, the server is created with previously specified port 4840 and the host's IP address.

Following this, an object per crate to be used is created named "Create-1", "Crate-2", "Crate-3" and so on. Because of having 32 boards per crate, the object consists of 20 variables called "Board-1", "Board-2", etc. Each board consists of 4 chips; four variables ("Chip-1", "Chip-2", and so on) are defined to each "Board" variable. Afterward, since a chip has a temperature value and timestamp, variables named "Temperature" and "Timestamp" are created under "Chip" and the sensor values received and unpacked from the socket-client are assigned to "Temperature" variables.

Having created the structure of the OPC UA server, the server starts to listen to port 4840. In the OPC UA Client python script, the nodes' IDs are assigned to be represented in a panel. Thus, the nodes, objects, and variables can be represented in both FreeOpcUa Graphical User Interface (GUI) OPC UA Client and WinCC OA Siemens SCADA, as shown in Figure 7.5.

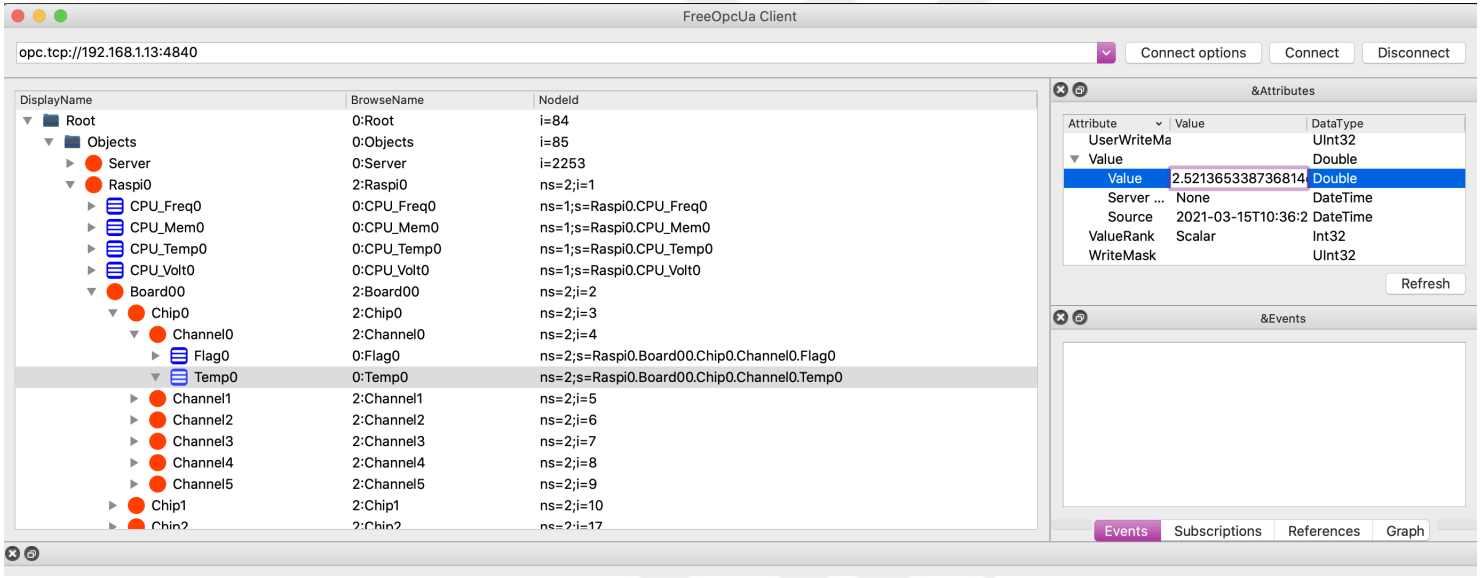


Figure 7.5: FreeOpcUa GUI OPC UA Client with its nodes, objects, and variables.

8. CONCLUSION

Effective temperature monitoring is a critical part of the CMS detector control unit to ensure quality and a reliable environment for the silicon-based sub-detectors. As a consequence of the increase of silicon detectors, which are very radiation-tolerant, they have to be operated under temperature control and monitoring because Si depletion voltage rises with the amount of radiation dose.

However, there is a limit of the maximum depletion voltage without arisen any breakdown. It is a significant thing that the temperature of the detector environment conduces to damage on the surface of the Si-based sub-layers of the detector. This is called the reverse annealing effect, which is resulted from the rise of depletion voltage over time. To mitigate or remove the revealing effect, the detector has to be run under very low temperatures, which ensures to reduce the leakage current and heat generation. Unless the cooling system can balance the self-heating of the sensors, current and temperature will increase in an uncontrolled way and cause thermal run-away.

With the increase of the number of collisions due to Upgrade 2 and HL-LHC experiments, existing luminosity will increase. On entirely or partially Si-based sub-layers of CMS detector, depletion voltage will be increased due to high luminosity. Thereby, we need to monitor the temperature to provide the operation at low-temperature degrees.

The temperature monitoring has been taken place using PLC so far. Though, PLC-based systems for monitoring are not cost-effective and take up big space on the off-detector side. This thesis focuses on the design and development of a new temperature monitoring system to tackle the above-mentioned issues.

Throughout developing new MTRS, the milestones of this work have been;

- The LTC2984 chip is tested and evaluated using the DC2420 kit. We decided to

use six sensors per the LTC2984 chip by optimizing the channels of the chip.

- Designed a dedicated temperature sensor PCB card consisting of 4 LTC2984 chips for monitoring four-wire PT1000/100 RTD sensors. Each card can monitor up to 24 RTD sensors, is powered at 5 V and 150 mA, and can function standalone or be part of a group.
- Handled some noise and communication issues arisen on the cards by re-designing PCB cards.
- The cards are tested in four different communication protocols;
  - Standalone for only a single card over Modbus,
  - One or more cards using an intermediary processor and TCP/IP Client-Server protocol,
  - Running an OPC-UA server on the intermediary processor additionally and accessing SCADA systems as clients,
  - PLC specific- Running Modbus communication using a Modbus CP, which is common in PLC hardware, thus integrating the temperature data in the PLC generated ones (which are used for DCS).
- The price and the installation overhead, hardware, and software, make the boards a desirable alternative to the current PLC-centric solutions for massive RTD sensor-based monitoring of CMS sub-detectors.

9. TÜRKÇE GENİŞLETİLMİŞ ÖZET

Bu bölüm İngilizce olarak yazılmış tezin bütün bölümlerini kapsayan ürkçe olarak yazılmış genişletilmiş bir özet olarak okuyuculara sunulmuştur. Bu kısım Giriş, LHC ve Parçacık Hızlandırıcıları, Kompakt Müon Solenoid, CMS'in Detektör Kontrol ve Güvenlik Sistemleri, Çok Kanallı Sıcaklık Sensörlerini Okuma Sistemi, MTRS Aşama 1'nin Sonuçları ve Getirdiği Problemler, RPi'den DCS'e Veri Akışı ve son olarak Sonuç bölümü olarak alt başlıklara ayrılmıştır.

9.1. Giriş

Dünya'nın önde gelen parçacık ve hızlandırıcı fizik laboratuvarı olan Avrupa Nükleer Araştırma Merkezi (CERN), atom altı parçacıkları ve bunların etkileşimlerini açıklayan Standart Model (SM)'in ötesindeki fizik, SM'deki her parçacığın bir çifti olduğunu varsayan Süpersimetri (SUSY) ile ilgili çığır açan keşifler üzerine araştırmalar yürütmektedir. Dünya'nın en büyük hızlandırıcısı olan Büyük Hadron Çarpıştırıcısı (BHÇ), en son teknolojili deneyleriyle, Uzun Kapatma aşamaları (hem LHC hem de dedektörleri için bakım aşamaları olan) dahil olmak üzere 12 yıldır çalışmaktadır. Son zamanlarda, LHC, 14 TeV kütle merkezi enerjisine ve $2 \cdot 10^{-34}\ cm^{-2} \cdot s^{-1}$ anlık parlaklık değerine ulaşmak amacıyla yaklaşmakta olan 3. Çalışma (aynı zamanda Aşama 2 olarak da bilinir) için devam eden Uzun Kapatma 2 (LS2) aşamasındadır. Run 3'ün ardından, anlık parlaklığın iki hatta üçkat artırılacağı LS3 aşamasına geçecektir. Bu nedenle LHC ve dedektörleri hem Run 3 hem de High Luminosity-LHC fazları için iyileştirilmektedir.

Şu anda, Kompakt Muon Solenoid deneyi, hızlandırıcının CMS'ye 2028'den başlayarak 10 yıllık çalışma boyunca yaklaşık 2500 fb'lik ek bir entegre parlaklık sağlayacağı Yükseltme 2 evresine hazırlanıyor. 10 yıllık çalışma olan HL-LHC projesi, potansiyel fizik keşiflerini artırmak için parlaklığı LHC'nin tasarım değerinin 10 katı kadar

arttırmayı hedeflemektedir.

Yüksek radyasyonlu ortamla başa çıkmak için alt dedektörlerin iyileştirilmesi aşağıdakileri gerektirmektedir.

- CMS İzleyici ve uç kalorimetreleri, İzleyici Pixel dedektörünün değiştirilmesiyle başlayarak tamamen değiştirilecektir.
- Namlu ECAL detektörün yerleştirildiği oyuk çiğ noktasının altındaki sıcaklıklarda çalışacaktır. Başka bir deyişle oyuk çiğlenme noktası 130◦C iken 100◦C'de çalışacaktır.
- Ayrıca, varil kalorimetreleri ve müon sistemlerinin büyük elektronik revizyonu ve pekiştirilmesi gerçekleştirilecektir.

Beklenen yüksek yığılmanın üstesinden gelmek şunları gerektirecektir:

- Elektroniklerden verilerin elde edilmesi için okuma çözünürlük düzeyinin iyileştirilmesi,
- 30 ps hassas zamanlama dedektörlerini kullanarak, yeni teknikler yığın etkisinin azaltılması,

Alt dedektörler ve sistem yükseltmeleri ile birlikte "çevresel" alt dedektörlerin sıcaklık, çiğlenme noktası, radyasyon, diğer gazların izleri ve kuruyan gazın bileşimi gibi parametrelerinin okunması, izlenmesi ve kontrol edilmesi için de yeni ön uç elektroniklerinin geliştirilmesi gerekiyor. Bu parametreler dedektörün çalışması ve servisleri için oldukça önemli olduğu kadar alt dedektörlerin değerlendirilmesi, testi ve montaj aşamaları için de aynı derecede önemlidir. Bu tezde, tüm Si tabanlı alt dedektör -İzleyici, HGCAL- geliştirmelerinde son derece önemli olan bir sıcaklık izleme sistemi tartışılacaktır, çünkü veri akışındaki ve ışınlamadaki artış sadece bağımsız sıcaklık izlemenin önemini etkilediği için değil aynı zamanda alt dedektörlerini ve hatta destekleyici sistemlerini de (soğutma, kuru gaz, Si-dedektör depolama kabinleri) etkilemektedir.

Faz 1 CMS Si tabanlı alt dedektörlerde, iki sıcaklık sensörü teknolojisi kullanılarak detaylı sıcaklık izleme sistemi ile izlenmektedir:

İzleyici katmanının okuma elektroniğinin sıcaklığını izlemek gömülü termistör sensörler DAQ akışı aracılığıyla verileri Detektör Kontrol Birimi'ne iletir. Ve rezistif sıcaklık dedektörü (RTD) sensörleri detektörün stratejik olarak önemli olan bölümlerine ve detektör servislerine bağlanır ki bu sistem PLC tabanlı kontrol edilen Detektör Safety Sistem (DSS) ile ilişiktir.

Aynı işlevsellik PLC tabanlı sistemlerde dedektör sahasının dışındaki birkaç CMS İzleyici tesisine eşlik etmektedir. Ancak sensör tabanlı izleme için bu vazgeçilmez endüstriyel aracını olan PLC'lerin kullanılması, optimum bir yöntem değildir. Maliyet, kanal başına 50 CHF'nin üzerindedir, bu da 100'den fazla sensörden oluşabilen bir sistem için önemli bir maliyet anlamına gelir. PLC, daha kalıcı uygulamalar için tercih edilir ve önemli donanım gereksinimlerine sahiptir; bu da alan gereksinimlerine dönüşür. Bir PLC aracılığıyla izlenen veriler, bir Denetleyici Kontrol ve Veri Toplama (SCADA) sistemi aracılığıyla kullanıcıya sunulur ve bu da yazılım geliştirmede ciddi bir ek yük anlamına gelmektedir. Bu nedenle, aşağıdaki özelliklere sahip bir sıcaklık izleme sistemine duyulan ihtiyacın arttığının en iyi göstergesidir:

- Fazla çaba sarf etmeden konuşlandırılabilir ve onlarca ve hatta yüzlerce sıcaklık ölçümü sağlayabilir.
- Bağımsız bir sistem olarak veya Dedektör Kontrol Sistemi (DCS) ortamının bir parçası olarak işlev görebilir veya bir DSS'ye entegre edilebilir.
- Kullanıcıya "tak ve çalıştır" olacak bir sistem sunabilir ve listenin 2. maddesinde gösterilen tüm seçenekler arasından seçim yapabilmesini sağlar.

9.2. LHC ve Parçacık Hızlandırıcılar

Bu kısım Büyük Hadron Çarpıştırıcısı (LHC) ve parçacık hızlandırıcılar hakkında genel bilgi vermektedir.

9.2.1. Parçacık Hızlandırıcılara Genel Bir Bakış

Bizleri çevreleyen Evreni anlayabilmek için teknolojik ilerlemeler insanlığın bitmeyen arayışıyla her zaman bağlantılı olmuştur. İnsanoğlu, doğada çıplak gözle görebileceğinden daha fazla şeylerin olduğunu anladığından bu yana, mikroskoplar elektronik mikroskoplara evrildi ve sonunda maddeyi atom altı parçacıklar düzeyinde gözlemlememizi sağlayan parçacık detektörlerine dönüştü. Parçacık hızlandırıcılar, Evren'in Büyük Patlama'dan sonraki saniyenin ilk kesirlerindeki koşullarını yeniden oluşturmak için geliştirilmiştir. Parçacık hızlandırıcıların altında yatan fizik teorisi esasen Einstein'ın görelilik teorisi olan bir enerji-kütle denkliğine dayanır; $E = m \cdot c^2$ ile ifade edilir. Hızlandırılmış parçacıklar kinetik enerji kazanır ve daha sonra parçacıklar hızlandırıcılar sayesinde neredeyse ışık hızına ulaşır. Böylece göreli etki nedeniyle enerji bir kütleye aktarılır ve bu da saçılan parçacıkların daha büyük bir kütleye sahip olmasına neden olur. Einstein'ın teorisiyle birlikte, Rutherford'un pozitif yüklü parçacık kaynağının enerjinin doğal radyoaktif maddelerden yayılan enerjiden aha fazla olduğu fikri, parçacık hızlandırıcılar aracılığıyla parçacık demetleri üretmeyi ve yeni parçacıklar keşfetmeyi mümkün kılmıştır.

1930'dan bu yana, her zamankinden daha yüksek enerjilere sahip çeşitli hızlandırıcılar inşa edilmiş ve farklı amaçlara hizmet etmek için tasarlanmıştır. Zaman geçtikçe, ulaşılan maksimum kütle merkezi enerjisi seviyesi katlanarak 100 keV'den 10 TeV'ye çıkarılmış ve bu da insanlığa yeni araştırma ve keşiflerin kapılarını açmaktadır. Yüksek enerji fiziğindeki keşifler dikkate alındığında, parçacık hızlandırıcıların görevi, yüklü parçacık ışın demetini, belirli bir hedefle çarpışmalarını sağlamak veya (iki)

ışının demetinin kafa kafaya çarpışmasını sağlamak için ışık hızına yakın bir hızda hızlandırmaktır.

Bahsedilen amaçları gerçekleştirmek amacıyla, yüklü parçacıkları en basit biçimde hızlandırmak için bir potansiyel farka ihtiyaç vardır. Bir DC kaynağının kutuplarına iki metal plakanın bağlanmasıyla potansiyel farkı oluşturulabilir ve böylece parçacıklar elektrik alanın etkisi altında hızlanmaya başlar. Bu hızlandırıcılar en basit elektrostatik hızlandırıcılar olarak bilinir. Fakat DC hızlandırıcılarda güç kaynağı ile parçacıkların erişebileceği çarpışma enerjisi sınırlıdır ve parçacıklar yüksek enerjilere ulaşamayacaktır. Bu sebeple DC hızlandırıcılar yerine AC tabanlı hızlandırıcılar geliştirilmiştir. AC hızlandırıcılar belirli bir rezonans aralığında çalıştığından ayrıca RF hızlandırıcılar olarak da adlandırılır.

Günümüzde AC tabanlı hızlandırıcının iki ana türü vardır —Doğrusal ve Dairesel. Doğrusal hızlandırıcılar, bir AC kaynağı ile bir iyon kaynağını birbirine bağlayan sıralı sürüklenme tüpleri şeklinde tasarlanmıştır. AC kaynağının farklı kutuplarına iki sıralı sürüklenme tüpü bağlanır ve birbirine zıt olarak yüklenir. Böylece iki sürüklenme borusu arasındaki boşlukta bir elektrik alanı oluşturulur, böylece parçacıklar hızlanmaya başlar. Doğrusal hızlandırıcıların yanı sıra dairesel hızlandırıcılar, parçacıklara enerji sağlamak için RF boşluklarını kullanarak yüklü parçacıkları hızlandırır. İki kutuplu mıknatıslar kullanılarak parçacıkların yolları bükülür ve belirli bir yörüngede tutulur. Bu işlem, parçacıklar nihai enerjiye ulaşana kadar RF boşluklarından birkaç kez tekrarlanır.

Bugünün hızlandırıcı fiziğine baktığımızda, dairesel hızlandırıcılar dünya çapında doğrusal hızlandırıcılardan daha fazla kullanılmaktadır çünkü doğrusal hızlandırıcıların dairesel hızlandırıcının enerjisine ulaşmak için muazzam bir uzunluğa sahip olması gerekir. Bunun yanında, dairesel hızlandırıcılar içinde parçacıklar birçok kez dolaştığı için birçok kez çarpışma fırsatı sağlanır. Bugün, en yaygın olarak kullanılan dairesel

hızlandırıcı türü ise senkrotrondur.

9.2.2. Büyük Hadron Çarpıştırıcısı

LHC, şimdiye kadar dünyada yapılmış en güçlü ve en büyük parçacık hızlandırıcısı olan senkrotondur . Cenevre yakınlarındaki İsviçre-Fransa sınırında yer almaktadır. 26,7 km'lik bir çevreye, yaklaşık 3 metre boya sahip olan ve Dünya yüzeyinin ortalama 100 metre bulunan uzanan devasa bir halka içinde yer almaktadır. LHC dairesel bir hızlandırcı türü olduğu için demetlerin kafa kafaya birbirine girmesini sağlayan bir çarpıştırıcıdır aynı zamanda.

LHC'nin ana hızlandırılmış parçacıkları protonlardır; bunun sebebi protonların son derece kararlı parçacıklar olmasıdır ve ayrıca LHC içinde belirli miktar protonların bir araya gelmesiyle oluşan demetler, Big Bang'inyavaş yavaş soğurmasında sonra oluşturulanlarla aynıdır.

LHC demetleri aslında sürekli bir proton akışı değildir; demet, zıt yönlerde hareket eden yaklaşık 2808 proton grubundan oluşur. 13 TeV kütle merkezi enerjisine ulaşana kadar zıt yönlerde hızlandırılırlar ve çarpıştıklarında neredeyse ışık (0.999 999 991c) hızındadırlar. Çarpışacak demetler arasında 25 ns'de bulunmaktadır ki bu da saniyede 40 milyon demet çarpıştığı anlamına gelir. Demet birkaç santimetre uzunluğundadır (parçacıkların hareket yönünde ölçülür); her proton grubunda yaklaşık $1,15 \cdot 10^{11}$ yüklü parçacık (proton) bulunur. Çarpışan iki proton grubu için, her çarpışma noktasında ortalama 50 çarpışma "yığını" elde edilir.

LHC çarpıştırıcısında proton-proton çarpışmalarının yanı sıra, farklı fizik çalışmaları için kurşun iyon çarpışmaları da gerçekleştirilir. LHC, 2010 yılında ilk 7 TeV çarpışmasının kaydedilmesiyle fizik verileri elde edip analiz etmeye başladı. LHC'nin çarpışma enerjisi, 2. Çalışması sırasında (2015 ile 2018 arasında), E_{CM} 13 TeV'ye yükseltilirken, demet yoğunluğu proton grubu başına $1{,}15 \cdot 10^{11}$ protona ve entegre par-

laklık ise 2.çalışma evresinin sonunda 189 fb^{-1}'a ulaştı.

9.3. Kompakt Müon Selonoid (CMS)

CMS detektörü, LHC'deki iki genel amaçlı parçacık detektör deneyinden biridir ve detektörü sayesinde CMS deneyi, enerjisi oldukça yüksek parçacıkları gözlemlemeyi ve SM'nin hassas ölçümlerini yapmamızı sağlamaktadır. SM çalışmalarının yanı sıra ekstra boyut, karanlık madde, SUSY vb. gibi diğer fizik çalışmalarını da yürütmektedir. CMS dedektörü LHC halkasının Etkileşim Noktası (IP) 5'te, Cessy, Fransa civarında bulunmaktadır. Detektör yerin 100 m altında bir oyuk içine yerleştirilmiştir ve deney burada gerçeklenmektedir. CMS detektörünün oyuk kısmı iki kısımdan oluşur; deneysel (UXC) ve yer altı (USC) oyukları. CMS dedektörü, UXC adı verilen deneysel oyukta bulunurken, yer altı mağarası (USC) alt dedektörlere güç verme, elektronik okuma, kontrol ve izleme gibi bazı hizmetlerin kurulumunu sağlar. (Collaboration et al., 2008).

14000 ton ağırlığa, 15 metre yüksekliğe ve 21 metre uzunluğa sahip olmasıyla bu özellikler ona nispeten kompakt bir yapı kazandırmıştır. Şimdiye kadar yapılmış en güçlü solenoid süper iletken mıknatıs, 3,8 T'lik bir manyetik alanla parçacıkları dedektörün içinde tutar ve detektör süper iletken mıknatısın yanında müon parçacıklarını hassas bir şekilde tespit etmek için müon odalarına sahiptir. Bu özellikler sebebiyle CMS - Kompakt Muon Selonoid olarak adlandırılır. CMS dedektörü alt katmanların bir araya gelmesiyle oluşturulmuştur ve bu katmanlar şunlardır: bir izleme sistemi (izleyici olarak da bilinir), elektromanyetik kalorimetre ve hadronik kalorimetre, süper iletken mıknatıs ve şekilde görüldüğü gibi müon sistemi. CMS dedektörlerinin katmanları, ardışık olarak izleyici, elektromanyetik kalorimetre, hadronik kalorimetre, süper iletken mıknatıs ve müon dedektör sistemleri ile birbirlerini çevrelemektedir. Nitekim dedektörlerin katmanları en içteki, ortadaki ve son olarak en dıştaki katman olarak da tanımlanabilir. (Collaboration et al., 2008).

En içteki katman, etkileşim noktasından saçılan parçacıkların yörüngesi hakkında bilgi almak amacıyla tamamen silikondan yapılmış bir takip sistemine sahiptir. Ara katmanlar, parçacıkların enerjisini emmek ve ölçmek için kalorimetrelerden, başka bir ifadeyle elektromanyetik ve hadronik kalorimetrelerden oluşur. Kalorimetrelerin ardından, 3,8 T'lik manyetik alan olan bir süper iletken mıknatıs, parçacıkların yolunu bükmek için kullanılır. Parçacıkların yörüngelerini bükmek, bu bükülmüş yörüngelerin yarıçapını ölçmemize yardımcı olur. Böylece parçacıkların momentumu, 41,7 MAmper-dönüşü taşıyan ve Niyobyum-Titanyum'dan (NbTi) oluşan güçlü bir mıknatıs kullanılarak hesaplanabilir. En dıştaki katman ise, diğer parçacıklara göre daha fazla enerji olan ve diğer katmanları delip geçen müonları tespit etmek için tasarlanmıştır. Bu katman, bir demir dönüşü "yoke" ile entegre olan bir müon detektör sistemidir esasen. (*The CMS magnet project: Technical Design Report*, 1997).

LHC'in Yükseltilmesi ve CMS Detektörün İyileştirilmesi Daha fazla verinin analiz edilebilmesi için 3. Çalışma evresinden sonra LHC 3. uzun dönem kapatma evresine girecektir ve bu süreçte detektörler eve LHC makinesi HL-LHC olarak adlandırılan deneye hazırlanacaktır. Bu deneydeki hedef, daha kapsamlı bir veri kümesini depolayıp benzeri görülmemiş olayların gözlemlenmesi için parlaklığı 10 kat daha artırmaktır. HL-LHC'de ortalama çarpışma sayısı 40–60'tan 140–200'e çıkaracak şekilde daha fazla çarpışma gerçekleştirilecektir. Nitekim, CMS dedektörünün yüksek parlaklık ve yaşlanma etkisiyle başa edebilmesi ve ayrıca daha sert radyasyon ortamında çalıştırılabilmesi için iyileştirmeye ihtiyacı vardır. Tüm alt dedektörler ve UXC kısmında bulunan elektronikler ve makineler CMS'nin HL-LHC yükseltmesi için hazırlanmaya başlamıştır. (Tsirou, 2020-12-05).

CMS dedektörünün izleme sistemi, etkileşim noktasına en yakın bölge olduğu için çok daha fazla radyasyona maruz kalmaktadır. Bu yüzden izleyici kısmı, yüksek radyasyon dozuna dayanabilen ve yüksek bir veri hızını gerçekleştirebilmesi için tamamen yenilenecektir. Bu kapsamda, izleyicinin ön uç elektronik kısmı, yapısı hiç değiştirilmeden

izleyicinin okuma, soğutma ve güç sistemi yenilenecektir. Benzer şekilde, CMS kalorimetreleri, HL-LHC tarafından getirilen iyonlaştırıcı yüksek radyasyon dozları altında çalışmak üzere bir yükseltmeye tabi tutulacaktır. ECAL ve HCAL'nin uç kapakları, ışın huzmesi yoluna (*The Phase-2 Upgrade of the CMS Barrel Calorimeters*, 2017) yakın olmaları nedeniyle $1.5 \cdot 10^{15}$ neq/cm^2 üzerinde radyasyon dozlarına maruz kalacaktır. Bu yüksek radyasyon seviyesi, ECAL kristallerine, dedektör üzerindeki soğutma devrelerine ve ana kartlara ve aynı zamanda HCAL foto dedektörlerine ve döşeme yanıtına da zarar verecektir. Bu yüzden, iki uç başlığın (EE ve HE) yerini alacak şekilde, yüksek tanecikliliğini koruyacak yeni bir uç kalorimetresi tasarlanmaktadır; Yüksek Tanecikli Kalorimetre (HGCAL) (*The Phase-2 Upgrade of the CMS Endcap Calorimeter*, 2017).

Müon sistemine bakıldığında, sistemin uç kapakları bakımdan geçmelidir. Faz 2 ve HL-LHC deneyleri ile birlikte gelen yüksek radyasyonla ilgili zorlukları ele alabilecek GEM dedektörü olarak adlandırılan yeni bir müon sistemi tasarlandı. Kritik ileri bölgede hassas müon takibini ve tanımlanması nı gerçekleştiren ek yedekli tetikleme sistemleri ve ölçüm noktaları GEM dedektörü tarafından yapılması hedeflenmektedir. Buna ek olarak, yeni RPC modülleri ile daha fazla iyileştirme ve geliştirme yapılacaktır (*The Phase-2 Upgrade of the CMS Muon Detectors*, 2017).

9.4. CMS'in Detektör Kontrol ve Güvenlik Sistemleri

1996 yılına dayanan LHC dedektörlerinin tasarımı, silikon malzemesinin radyasyona karşı dayanıklı olması nedeniyle silikon ile yapılmaktadır. Silikon teknolojisindeki gelişmeler artıkça, LHC dedektörleri, izleme sistemlerinde ve hatta CMS HGCAL örneğinde olduğu gibi kalorimetrelerin bazı bölümlerinde silikonu daha sık kullanmaya başladılar. Fakat, radyasyon dozu arttıkça Si tükenme voltajı da yükseltmektedir ki bu da Silikon tabanlı alıgıçların sıcaklık kontrollü ve izlenen koşullarda çalışması gerekir. (Tsirou, 2020-12-05).

Bunun sebebi ise esasen şudur ki: radyasyonun malzeme hasarı üzerindeki etkisi, güçlü bir şekilde sıcaklıktan, T kaynaklanmaktadır. Hasarın zamanla geri kazanılabileceği veya zamanla tükenme geriliminde bir artışa yol açabilecek bazı tavlama etkileri de vardır. "ters tavlama" olarak bilinen ikinci etki, dedektör daha düşük sıcaklıklarda çalıştırılırsa önlenebilir. Aslında bakarsak düşük çalışma sıcaklığı, kaçak akımı ve ısı oluşumunu azalttığı için de yararlıdır. Buna karşılık, soğutma sistemi sensörün kendi kendine ısınmasını telafi edemezse, akım ve sıcaklık kontrolsüz bir şekilde artacak ve dedektörün kararsız hale gelmesine neden olacaktır. "termal kaçış" olarak bilinen bu fenomen, sıcaklık arttıkça kaçak akımın arttığı bir pozitif geri besleme döngüsüdür. (Tsirou, 2020-12-05).

Son zamanlarda, LHC'nin parlaklığında dikkate değer bir artış olmuştur. Nitekim bu durum ışınımı da artırarak alt dedektörlerin daha da düşük sıcaklıklarda çalışmasını gerektirmiştir. Örneğin, CMS dedektörünün çalışma sıcaklığı son on yılda -10°C'den -20°C'ye değişti. Bu, parlaklıktaki artışın beraberinde bizlere LHC dedektörlerinin çalışma sıcaklığında önemli bir sıcaklık düşüşün olması gerektiğini göstermektedir. Ayrıca, LHC dedektörlerinin katmanlı bir yapıya sahip olması nedeniyle, Si dedektörleri, farklı sıcaklıklarda çalıştırılan diğer Si olmayan dedektörlerine de komşudur. Örnek vermek gerekirse, son iki yıl boyunca, CMS Si-İzleyici -20°C'de çalışırken, Namlu ECAL -17°C'de tutuyor. Bu nedenle , sıcaklık ölçümü, Si-detektörün çevresinde ve servisleri de dahil çeşitli bölümlerinde yapılmalıdır. (Tsirou, 2020-12-05).

LHC dedektörlerinde bahsedilen parametrelerin kontrolü ve güvenliği, sıcaklık değerlerini devreye sokan DSS ve DCS olmak üzere iki ana sistemden oluşur. DSS'nin amacı, güvenlik operasyonlarını garanti etmektir ve donanım, sistemi birbirine kilitleyebilir. Öte yandan, DCS soğuk ve kuru sistemlerin kontrolünden sorumludur. Örneklendirirsek, CMS DCS, HGCAL izleme sisteminden olağan dışı bir çıkış gerçekleştirirse, CMS DSS'ye bir alarm gönderir ve karşılığında tüm sistemleri kilitler. Sonuç ola-

rak, DCS'nin DSS üzerinde yerleşik bir ek yazılım katmanı olduğunu söyleyebiliriz. (Barney, n.d.).

Daha önce de bahsedildiği gibi CMS alt dedektörlerinin ömürlerini sürdürebilmeleri için soğuk ve kuru ortamlar gibi koşullarda çalışması gerekmektedir. Bu çalışma koşulları, CMS DSS'yi bağımlı olarak besleyecek şekilde bir soğuk dedektör sistemi tarafından izlenir ve kontrol edilir. Bir soğuk dedektör, hepsi farklı işlevlere sahip olan soğutma, kuru gaz ve algılama sistemleri olmak üzere üç ana sistemden oluşur. CMS soğuk dedektör sistemi, ana CMS soğuk alt dedektörleri –HGCAL, İzleyici ve MTD ve kısmen de ECAL için tasarlanmıştır ve birbirinden bağımsız çalışan ayrı soğuk alt dedektör sistemlerine sahiptir. Bunun nedeni, farklı zamanlarda devreye alınmaları ve kurulumlarının yapılmış olmasıdır. Fakat, her bir soğuk alt dedektörü aynı tür altyapı ve politika ile tasarlandı. Sonuç olarak, soğuk alt dedektörleri servislerini yapmakta olup, alt dedektörleri tek bir CMS soğuk izleme işlemcisi tarafından izlenebilmekte ve herhangi bir arıza durumunda işlemci ana CMS soğuk dedektörüne rapor gönderebilmektedir. Tez çalışması boyunca geliştirilen sistem bu soğuk alt detektörlerin sıcaklığını izlemek ve kontrol etmek için tasarlanmıştır. (Tsirou & Verdini, 2020-10-23).

9.5. Çok Kanallı Sıcaklık Sensörlerini Okuma Sistemi

Soğutma sistemlerinde en önemli parametre olan sıcaklık, CMS'nin Si tabanlı alt dedektörlerinin (İzleyici, HGCAL, MTD) okuma çiplerine gömülü sıcaklık sensörleri ile ölçülmektedir. Bunun dışında, dedektörün çevresindeki ve dedektörün kapalı olduğu taraftaki sıcaklığı izlememiz gerektiğidir. Bu nedenle, Si tabanlı alt dedektör ortamı için okuma çiplerine gömülü sıcaklık sensörleri yerine daha fazla izleme RTD'si talep edilmektedir. Bu izleme ve kontrol prosedürleri, geleneksel olarak PLC tabanlı sistemler aracılığıyla gerçekleştirilir. PLC'lerin veri toplama, izleme ve kontrol süreçleri için oldukça sağlam sistemler olduğu bilinen bir gerçektir.

Bununla birlikte, ticari kullanıma hazır COTS elektronikler olarak bilinen PLC tabanlı sistemler, izlenecek kanal sayısı arttıkça uygun maliyetli ürünler değildir. Kanal sayısı artırıldığında PLC tarafından okunan kanal başına maliyet 50 CHF'dir. Ayrıca, sıcaklık okuma ve izleme için maliyetin yanı sıra kapladığı alan da göz önüne alındığında, bu sorunun, sensörlerin kesinlikle izlenmesi gerektiği ve dolayısıyla da kontrol için bir PLC'ye bağlanacağı durumlarda güvenilir bir çözüm bulmamıza neden olmuştur.

Bu optimizasyon probleminde amaç fonksiyonlarımız olan maliyet ve kapladığı alan en son teknolojiler kullanılarak minimize edilmelidir. Gömülü sistemlerin ve Nesnelerin İnterneti'nin (IoT) büyük önemi ile birlikte, sıcaklık izleme için Çok Kanallı Sıcaklık Okuma Sistemi (MTRS) olarak adlandırılan gömülü tabanlı ve uygun maliyetli yeni bir geliştirme önerdik

MTRS'nin geliştirilmesine başlamadan önce, sıcaklık sensörünün belirlenmesi gerekir. Sıcaklık sensörlerinin radyasyona dayanıklı, güvenilir, dedektör koşullarıyla uyumlu ve DSS ve DCS'ye entegre edilebilir olması gerektiği göz önüne alındığında, RTD 4 kablolu sıcaklık sensörünün optimum tercih olduğu sonucuna varılmıştır. Bu nedenle kalibrasyon yapmamıza ihtiyaç olmadığını ve herhangi bir bozulma bile göstermediğini anladık. RTD seçiminde bahsetmeye değer bir diğer nokta, bunların çok küçük, her zaman kullanılabilir ve uygun fiyatlı COTS ürünleri olmaları ve aynı zamanda -200 °C ila 850 °C gibi düşük bir değerde çalışmasıdır. . Ayrıca, uç konektörlerle birbirine geçme nedeniyle tüm seri dirençlerin kompanzasyonu ile yüksek ölçüm doğruluğu sağlar.

RTD sensörünün seçim aşamasının takibinde MTRS çalışmasının yapılabilmesi için aşağıdaki adımlar atılmıştır;

- Analog Device tarafından geliştirilen bir mikrodenetleyici ile LTC2984 yongalarının değerlendirilmesi ve test edilmesi,
- MTRS okuma kartlarının Aşama I'ini tasarlanması, okunması ve test edilmesi

- Ortaya çıkan sorunları ele almak için MTRS okuma kartlarının Aşama II'sini yeniden tasarlanması ve test edilmesi.

LTC2984'e bağlanacak RTD sensörlerin konfigürasyon yapıldıktan sonra, okumanın değerlendirilmesi C ile yazılmış bir program tarafından gerçekleştirildi. Program, Seri Çevresel Arayüzü (SPI) üzerinden DC2420 ile haberleşen DC2026 Linduino'ya gömüldü. QuikEval yazılımı, bir arayüzde takılı RTD sensörleri tarafından ölçülen sıcaklıkların görselleştirilmesi yapıldı. Sonuç olarak, LTC2984 çipi değerlendirildi ve çip üzerinde 20 kanal kullanılarak altı RTD sensörün bağlanabileceği görüldü.

LTC2984'e bağlı maksimum sensör sayısı işlevsel olarak doğrulandıktan sonra, bir sonraki aşama bir okuma devresi tasarlamaktır. Hem PCB yerleşimi hem de okuma devresinin şematik çizimi Altium Designer kullanılarak yapılmıştır. Kart iki VME konektörü içerir; birinci VME konektörü (J1), okuma kartına 24 adet 4 kablolu RTD sensörünün bağlantısını sağlarken, ikinci VME konektörü (J2), okuma kartı ile Raspberry Pi 4 şerit kablolar arasındaki iletişim için kullanılır.

J2'nin pinleri, kart seçim pinleri, çip seçim pinleri ve Master Giriş Slave Çıkışı (MISO), Master Çıkış Slave Girişi (MOSI) ve Clock (CLK) gibi SPI iletişim girişleriyle bağlantılıdır. Esasen, bir VME DIN41612 konektörü 96 pinden oluşur ve bu nedenle tercih edilen RTD sensörünün dört kablosu olduğundan sadece 24 sensörü bağlamamıza izin verir. Böylece, dört LTC2984 çipi dijital sıcaklık ölçümünü yerine getirebilmesi amacıyla kart tasarımına eklenmiştir. Çiplere ek olarak voltaj düzenlemelerini telafi etmek için bir filtre görevi yapan seramik kapasitörler kart üzerine entegre edilmiştir.

Bunların dışında, hangi kart ve çipin seçileceğini belirtmek için iki entegre devre (IC) eklendi. SN74HC688PWT IC, 8 girişli bir anahtarla birlikte kartı seçmeyi amaçlarken, SN74ACT32D IC, çip seçimi için eklenmiştir. Elektronik enstrümantasyonları yerleştirdikten sonra, PCB kartı, raf ünitelerinin boyutu göz önünde bulundurularak Eurocard (3U boyutunda) koşulları altında tasarlanmıştır. Böylece MTRS'nin ilk

PCB tasarımı tamamlanmıştır.

9.5.1. MTRS Aşama 1 Kartlarından Verilerin Elde Edilmesi

MTRS kartının okuması, bir mikro denetleyici veya mikroişlemci ile gerçekleştirilebilir. Buradaki önemli nokta, karttan alınan sensör değerlerinin herhangi bir CMS soğuk dedektörün DCS veya DSS'sine aktarılması gerektiğidir. Bu nedenle veri aktarımı için projede bir sunucuya ihtiyaç duyulmuştur. Soket sunucu/istemci ve OPC sunucusu geliştirmek için yeterli bellek alanına ihtiyacımız olduğundan, mikrodenetleyici olmayan çip üzerine geliştirilmiş bir sistem (SoC) olan RPi 4B+ kullanılmasına karar verildi; dolayısıyla bir sunucuyu kendi başına dağıtmayı mümkün kılar. Bu sayede MTRS projesinin veri toplaması ve iletimi, kontrolör olarak görev yapan Raspberry Pi 4 B+ tarafından gerçekleştirilmiştir.

Verilerin RPi tarafından nasıl elde edildiğine bakıldığında, tasarlanan ve üretilen PCB kartının giriş olarak iki konektörü vardır; bunlardan biri 24 RTD sensöre bağlı, diğeri ise şerit kablo ile RPi'ye bağlı olup SPI iletişimini sağlamayı sağlamaktır ve o anda hangi kart ve çipin okunacağını seçmek içindir.

Çiplerden sensör verilerini almak için, SPI protokolü ile sağlanmıştır. SPI iletişimini gerçekleştirmek için dee hem bcm2835 hem de wiringPi kütüphanesi kullanılarak okuma programı RPI üzerinde C dilinde yazılmıştır. SPI fonksiyonları RPi üzerinden kurulduktan sonra kasa içine yerleştirilen 10 karttan sırayla kart seçilir ve her kartta bulunan 4 çipten biri seçilir. Bunlara takiben, LTC2984'e bağlı her bir RTD'ye karşılık gelen kanalların yapılandırılması, çipin RAM'ine 32-bit kanal atama kelimesi ile programlanarak etkinleştirilir. Sözcük, RTD tipi, algılama direnci kanal işaretçisi, sensör konfigürasyonu, uyarma akımı, RTD eğrisi ve özel RTD veri işaretçisi gibi RTD ve algılama direnci ile ilgili bilgilerden oluşur. Böylece seçilen kart üzerindeki her çip için kanalları konfigüre edilir. Kanal yapılandırılmasından sonra veriler 6 kanaldan sırayla

okunur böylece bir çipin okunması tamamlanır. Sırasıyla kart üzerindeki kalan üç çip de bu şekilde okunur ve bir karttan okunması tamamlanınca sırasıyla kasadaki diğer kartlardan verilerin elde edilmesi gerçekleştirilir.

9.6. MTRS Aşama 1'nin Sonuçları ve Getirdiği Problemler

9.6.1. MTRS Aşama 1'nin Sonuçları ve Değerlendirilmesi

MTRS kartlarının ilk üretimininden sonra sıcaklık okuma kartlarından veri edinimi sırasında, RPi ile bir veya daha fazla kart arasında iletişim sorunlarıyla meydana geldi. İletişim kurulmuş olmasına rağmen, birkaç sensör hatasıyla ("eksik" sıcaklık sensörü) karşılaştık. Yazılan okuma programı ile kasa içine yerleştirilmiş 5 kartı sırayla okurken bazen bu kart üzerindeki çiplerden veriler alınamadı bazense de alınabildi. Başka deyişle, okuma sistemimiz stabil çalışamıyordu ve bunun sebebi RPi'de *chip-select* işlevlerini (ve ardından okumayı) öldüren çok sayıda yüksek frekanslı gürültü vardı. Dışarıdan filtre devreler kuralmasına rağmen bu gürültüler önlenemedi. Farklı bir yöntem denendiğinde; programa zaman gecikmeleri eklendiğinde 5 sıcaklık okuma kartı RPi ile istikrarlı iletişimi sürdürmeyi başardı. Fakat zaman gecikmeleri yerine daha etkili bir yaklaşımla stabil bir okuma gerçekleştildi.

Bu yöntemde, bir Arduino bir sıcaklık okuma kartına bağlandığında, şemanın mükemmel çalıştığı gerçeğine ulaşıldı. Ancak Arduino, doğrudan Ethernet bağlantısı sunmadığından. Arduino'nun Modbus protokolü üzerinden (endüstriyel elektronik cihazları bağlamak için yaygın olarak bulunan, çok hata ayıklanmış ve standart bir iletişim protokolüdür) RPi 4B+'ya bağlanmasının test edilmesine karar verildi. Arduino, standard Arduino Modbus kütüphanesini kullanarak, Uzak Terminal Birimi protokolü ile RS485 üzerinden seri iletişim sayesinde RPi'ye veri göndermeyi başarabildi.
RS485'in tercih edilmesinin nedeni Arduino ile Raspberry Pi 4B+ arasında filtre görevi görmesiydi. Böylece RPi 4B+'ın sıcaklık çiplerine doğrudan erişimi ortadan kalkıyor

ve robust bir veri elde edinimi sağlanabiliyor. Modbus ile Master - RS485 Modbus arayüzü olarak çalışır. MTRS kartının ilk versiyonu bir girişten Arduino'ya ve ikinci girişten 24 RTD sensörüne bağlandı. Sensörler, ECAL için chiller'den gelen iki borunun etrafına yerleştirildi. MTRS kartına bir/iki Arduino bağlandığında, herhangi bir iletişim hatası gözlemlenmedi ve bu yöntem bize daha etkili bir okuma sistemi sağlamıştır.

9.6.2. MTRS Aşama-2 Tasarlanması

Arduino Nano ile okuma sadece bağımsız tek bir kartın okuması içindi ve çok kartlı okuma sisteminde bir sunucu aracalığuyla verilerin PLC DSS veya PLC DCS sistemlerine iletilmesi için RPi kullanılması gerekir. Bu sebeple MTRS Aşama 1 kartına farklı entegreler eklenerek bahsedilen yaklaşım tabanlı Aşama 2 kartı tasarlandı. Bu tasarımda ıcaklık kartının kendisine yalnızca Atmega328P entegresi (ve zaman damgası için) ve RS485 çipi yerleştirmeye karar verildi.

Kartın ikinci versiyonunun tasarımında her kart, dört LTC2984 yongası kullanarak 24 adede kadar RTD sensörünü okuyabilmektedir. LTC2984 yongalarını seçmek ve adreslemek için bir ATMEGA328P-U mikro denetleyici kullanıldı. Veriler ATMEGA SPI veri yolu üzerinden okunur. ATMEGA I^2C veri yolu, kart anahtarlarının durumunu okumak için kullanılır ve ATMEGA UART, bilgileri dış dünyaya iletmek için kullanılır, aynı zamanda RS485 protokolü üzerinden RPi'ye veri aktarımını başlatmak için kullanılır. Böylece tasarlanan Aşama 2 kartıyla ve önceden C'de yazılan okuma programıyla verilerin başarıyla edindiği gözlenmiştir.

9.7. RPi'den DCS'e Veri Akışı

C'de geliştirilen bir program ile MTRS'nin DAQ'sunu sağladıktan sonra, sensör verileri ve bayraklarının OPC UA sunucusuna gönderilmesi gerekir, böylece OPC UA istemcilerine, yani CMS alt dedektör kontrol sistemlerine yayınlayabilir. OPC UA, Python

kullanılarak geliştirildiği ve RPi üzerinde yürütüldüğü için, C tabanlı programdan OPC UA sunucusuna veri akışı için bir arayüze ihtiyacımız var. Bu nedenle, bir API TCP-/IP ağı için iletişim fonksiyonlarını tanımlayan bir soket arayüzü geliştirilmesine karar verildi. Soket herhangi bir dilde geliştirilmesine izin verdiğinde, C'de geliştirilen bir sunucu, verileri Python'da yazılmış bir istemciye OPC UA sunucusuna gönderir. Soket istemcisinin ana görevi, veri almak ve okumak için istekler göndermek ve ardından bunları OPC UA sunucusuyla paylaşmaktır, soket sunucusu ise sensör verilerini soket istemcisine iletmeyi sağlar. Bu çalışmada soket sunucusu ve soket istemcisi arasında güvenilir bir aktarım sağlamak için TCP protokolü kullanılarak soket oluşturulmuştur. Python'da OPC UA sunucu üzerine yazılan soket istemci verileri aldıktan sonra verileri OPC UA sunucu ile paylaşır. OPC UA sunucu, OPC UA istemci istek gönderdiğinde bu verileri onunla paylaşarak veriler izlenmeye başlar. Bu projede OPC UA istemci olarak FreeOPCua'nin GUI indirilip terminalden kurulmuş ve veriler bu arayüz üzerinden gözlenmiştir.

9.8. Sonuç

Upgrade 2 ve HL-LHC deneyleri nedeniyle çarpışma sayısının artması ile birlikte mevcut parlaklık da artacaktır. Tamamen veya kısmen olmak tasarlanan Si tabanlı CMS dedektör alt katmanlarında, yüksek parlaklık nedeniyle tükenme voltajı artacaktır. Bu nedenle, bu düşük sıcaklık derecelerinde çalışmayı sağlamak için sıcaklığı izlenmesini ve kontrol edilmesini gerektirmektedir. Sıcaklık izleme şimdiye kadar PLC tarafından gerçekleştirilmesinde rağmen, izleme için PLC tabanlı sistemler uygun maliyetli değildir ve dedektör dışı tarafta büyük yer kaplamaktadır. Bu tez, yukarıda bahsedilen sorunların üstesinden gelmek için yeni bir sıcaklık izleme sisteminin tasarımı ve geliştirilmesine odaklanılmıştır.

Yeni MTRS geliştirme süreci boyunca bu çalışmada gerçekleştirilen aşamalar;

- LTC2984 yongası, DC2420 kiti kullanılarak test edilir ve değerlendirilir. Çipin kanallarını optimize edilerek LTC2984 çipi başına altı sensör kullanmaya karar verildi.
- Dört telli PT1000/100 RTD sensörlerini izlemek için 4 LTC2984 çipinden oluşan özel bir sıcaklık sensörü PCB kartı tasarlanmıştır. Her kart 24 adede kadar RTD sensörünü izleyebilmesi, 5 V ve 150 mA'da çalışabilmesi sağlanmıştır. Bu kart bağımsız olarak da çalışabilirken aynı zamanda bir grubun parçası da olabileceği gösterilmiştir.
- PCB kartlarını yeniden tasarlayarak kartlarda ortaya çıkan bazı gürültü ve iletişim sorunlarının üstesinden gelinmiştir.
- Kartlar dört farklı iletişim protokolünde test edilmiştir:
  - Modbus üzerinden yalnızca tek bir kart için bağımsız,
  - Bir aracı işlemci ve TCP/IP İstemci-Sunucu protokolü kullanan bir veya daha fazla kart,
  - Ek olarak aracı işlemci üzerinde bir OPC-UA sunucusu çalıştırmak ve istemci olarak SCADA sistemlerine erişmek,
  - PLC'ye özel- PLC donanımında yaygın olan bir Modbus CP kullanarak Modbus iletişimini yürütmek, böylece sıcaklık verilerini PLC tarafından oluşturulan (DCS için kullanılan) verilerle bütünleştirmek.
- Fiyat ve kurulum ek yükü, donanım ve yazılım, kartları CMS alt dedektörlerinin büyük RTD sensör tabanlı izlemesi için mevcut PLC merkezli çözümlere arzu edilen bir alternatif haline getiriyor.

REFERENCES

Aad, G., Butterworth, J., Thion, J., Bratzler, U., Ratoff, P., Nickerson, R., ... others (2008). The atlas experiment at the cern large hadron collider. *Jinst*, *3*, S08003.

Aamodt, K., Quintana, A. A., Achenbach, R., Acounis, S., Adamová, D., Adler, C., ... others (2008). The alice experiment at the cern lhc. *Journal of Instrumentation*, *3*(08), S08002.

Akgun, B. (2021-05-03). personal communication.

Alves Jr, A. A., Andrade Filho, L., Barbosa, A., Bediaga, I., Cernicchiaro, G., Guerrer, G., ... others (2008). The lhcb detector at the lhc. *Journal of instrumentation*, *3*(08), S08005.

The Atomic Age, A Linda Hall Library Exhibition. (Unknown). Retrieved 10/03/2021, from `https://atomic.lindahall.org/what-is-an-atom-smasher.html`

Automation, U. (n.d.-a). *Node and object model.* Retrieved 12/05/2021, from `https://documentation.unified-automation.com/uasdkcpp/1.4.2/html/L2UaAddressSpaceConcepts.html`

Automation, U. (n.d.-b). *Opc node class identifiers.* Retrieved 12/05/2021, from `http://documentation.unified-automation.com/uasdkdotnet/2.5.6/html/L2UaNodeIds.html`

Automation, U. (n.d.-c). *Opc ua structure.* Retrieved 12/05/2021, from `http://documentation.unified-automation.com/uasdkdotnet/2.4.2/html/L2OpcUaOverview.html`

Barney, D. (n.d.). *Hgcal dss and dcs specifications.*

Bauer, G., Behrens, U., Bowen, M., Branson, J., Bukowiec, S., Cittolin, S., ... Sumorok, K. (2012, dec). Status of the CMS detector control system. *Journal of Physics: Conference Series*, *396*(1), 012023. Retrieved from https://doi.org/10.1088/1742-6596/396/1/012023 doi: 10.1088/1742-6596/396/1/012023

Brüning, O., & Rossi, L. (2019). The high-luminosity large hadron collider. *Nature Reviews Physics*, *1*(4), 241–243.

Brüning, O. S., Collier, P., Lebrun, P., Myers, S., Ostojic, R., Poole, J., & Proudlock, P. (2004). *LHC Design Report*. Geneva: CERN. Retrieved from http://cds.cern.ch/record/782076 doi: 10.5170/CERN-2004-003-V-1

Burnet, J.-P. (2016). Requirements for power converters. *arXiv preprint arXiv:1607.01597*.

Béjar Alonso, I., Brüning, O., Fessia, P., Rossi, L., Tavian, L., & Zerlauth, M. (2020). *High-Luminosity Large Hadron Collider (HL-LHC): Technical design report* (I. Béjar Alonso, Ed.). Geneva: CERN. Retrieved from https://cds.cern.ch/record/2749422 doi: 10.23731/CYRM-2020-0010

Caron, J.-L. (1997, Sep). *LHC layout. Schema general du LHC.* Retrieved from https://cds.cern.ch/record/841573 (AC Collection. Legacy of AC. Pictures from 1992 to 2002.)

Chatrchyan, S., Hmayakyan, G., Khachatryan, V., Sirunyan, A. M., Adolphi, R., Anagnostou, G., ... Trub, P. (2008). The CMS experiment at the CERN LHC. The Compact Muon Solenoid experiment. *JINST*, *3*, S08004. 361 p. Retrieved from https://cds.cern.ch/record/1129810 (Also published by CERN Geneva in 2010) doi: 10.1088/1748-0221/3/08/S08004

Cid-Vidal X. and Cid R. (2010). *Taking a closer look at lhc - magnetic multipoles.* Retrieved 12/05/2021, from https://www.lhc-closer.es/taking_a_closer_look_at_lhc/0.magnetic_multipoles

Cittolin, S., Rácz, A., & Sphicas, P. (2002). *CMS The TriDAS Project: Technical Design Report, Volume 2: Data Acquisition and High-Level Trigger. CMS trigger and data-acquisition project*. Geneva: CERN. Retrieved from https://cds.cern.ch/record/578006

The CMS hadron calorimeter project: Technical Design Report. (1997).

The CMS magnet project: Technical Design Report. (1997). Geneva: CERN. Retrieved from https://cds.cern.ch/record/331056

COCKCROFT, J., & WALTON, E. (1932). Disintegration of Lithium by Swift Protons. *Nature*, *129*(3261), 649–649. doi: 10.1038/129649a0

Collaboration, C., Chatrchyan, S., Hmayakyan, G., Khachatryan, V., Sirunyan, A., Adam, W., ... others (2008). The cms experiment at the cern lhc. *JInst*, *3*, S08004.

collaboration, C., et al. (1997). The electromagnetic calorimeter project. *Technical Design Report, CERN/LHCC*, *375*, 97–23.

Coner, D. E. (1995). *Internetworking with tcp/ip: principles, protocols, and architecture*. Prentice Hall.

De Broglie, L. (1924). *Recherches sur la théorie des quanta* (Unpublished doctoral dissertation). Migration-université en cours d'affectation.

Device, A. (n.d.-a). *Dc2399 and dc2210 ltc2984 digital temperature measurement system.* Retrieved 12/05/2021, from https://www.analog.com/media/en/technical-documentation/user-guides/DC2420F.PDF

Device, A. (n.d.-b). *The ltc2984–multi-sensor high accuracy digital temperature measurement system with eeprom.* Retrieved 12/05/2021, from https://www.analog.com/media/en/technical-documentation/

data-sheets/2984fb.pdf

Drollinger, V. (2006, Apr). Getting ready for Physics at the LHC with the CMS Detector. , 187-192. 5 p. Retrieved from http://cds.cern.ch/record/942395 (presented at Lake Louise Winter Institute 2006, 17-23 February 2006, Alberta, Canada) doi: 10.1142/9789812772541_0020

Eidelman, S., Hayes, K., Olive, K. e., Aguilar-Benitez, M., Amsler, C., Asner, D., ... others (2004). Review of particle physics. *Physics letters B*, *592*(1-4), 1–5.

Electronics, P. (n.d.). *Thermal management.* Retrieved from https://www.powerelectronics.com/technologies/thermal-management/article/21862807/universal-temperature-sensor-ic-with-eeprom-targets-modular-custom-sensor-systems

ETH – Institute for Theoretical Physics – Particle Physics Phenomenology 1 – HS 2010. (2010). Retrieved 18/05/2021, from https://edu.itp.phys.ethz.ch/hs10/ppp1/

Evans, L., & Bryant, P. (2008). Lhc machine. *Journal of instrumentation*, *3*(08), S08001.

Evans, L. R., & Bryant, P. (2008). LHC Machine. *JINST*, *3*, S08001. 164 p. Retrieved from http://cds.cern.ch/record/1129806 (This report is an abridged version of the LHC Design Report (CERN-2004-003)) doi: 10.1088/1748-0221/3/08/S08001

Fartoukh, S. (2014). Pile up management at the high-luminosity LHC and introduction to the crab-kissing concept. *Physical Review Special Topics - Accelerators and Beams*, *17*(11). doi: 10.1103/physrevstab.17.111001

Fayet, P., & Ferrara, S. (1977). Supersymmetry. *Physics Reports*, *32*(5), 249–334. doi: 10.1016/0370-1573(77)90066-7

Focardi, E. (2008). *Tracker cooling plant.* Retrieved 12/05/2021, from https://

slideplayer.com/slide/10173592/

Foundation, O. U. (n.d.-a). *Brief history of opc ua.* https://opcfoundation.org/about/what-is-opc/. ((Accessed on 12/05/2021))

Foundation, O. U. (n.d.-b). *Freeopcua python-opcua github repository.* Retrieved 12/05/2021), from https://github.com/FreeOpcUa/python-opcua

Foundation, O. U. (n.d.-c). *Opc alarm and events.* Retrieved 12/05/2021, from https://opcfoundation.org/developer-tools/specifications-classic/alarms-and-events/

Foundation, O. U. (n.d.-d). *Opc data access.* Retrieved 12/05/2021, from https://opcfoundation.org/developer-tools/specifications-classic/data-access/

Foundation, O. U. (n.d.-e). *Opc ua freeopcua c++ github repository.* Retrieved 12/05/2021, from https://github.com/FreeOpcUa/freeopcua

Foundation, O. U. (n.d.-f). *Opc ua open62541 github repository.* Retrieved from https://github.com/open62541/open62541

Foundation, O. U. (n.d.-g). *What is opc ua.* Retrieved 12/05/2021, from https://opcfoundation.org/about/opc-technologies/opc-ua/

García, M. V., Irisarri, E., Pérez, F., Marcos, M., & Estévez, E. (2017). Engineering tool to develop cpps based on iec-61499 and opc ua for oil&gas process. In *2017 ieee 13th international workshop on factory communication systems (wfcs)* (pp. 1–9).

Halyo, V., Hunt, A., Jindal, P., LeGresley, P., & Lujan, P. (2013, May). GPU Enhancement of the Trigger to Extend Physics Reach at the LHC. *JINST*, *8*, P10005. 13 p. Retrieved from http://cds.cern.ch/record/1550044 (Comments: 13 pages 8 figures) doi: 10.1088/1748-0221/8/10/P10005

Jeitler, M. (2013). Upgrade of the trigger system of cms. *Nuclear Instruments and Methods in Physics Research Section A: Accelerators, Spect-*

rometers, Detectors and Associated Equipment, *718*, 11-15. Retrieved from https://www.sciencedirect.com/science/article/pii/S0168900212009941 (Proceedings of the 12th Pisa Meeting on Advanced Detectors) doi: https://doi.org/10.1016/j.nima.2012.08.091

Kahle, K., Steerenberg, R., & Pandolfi, S. (2017, Aug). LHC report: Something in the nothing. Retrieved 16/05/2021, from http://cds.cern.ch/record/2281882

Kalita, L. (2014). Socket programming. *International Journal of Computer Science and Information Technologies*, *5*(3), 4802–4807.

Karimeh, Wassef, Chammoun, Maroun, Shvetsov, Ivan, Tsirou, Andromachi, & Verdini, Piero Giorgio. (2020). Status and future of the cms tracker dcs. *EPJ Web Conf.*, *245*, 01005. Retrieved from https://doi.org/10.1051/epjconf/202024501005 doi: 10.1051/epjconf/202024501005

Karimäki, V., Mannelli, M., Siegrist, P., Breuker, H., Caner, A., Castaldi, R., ... Cattai, A. (1997). *The CMS tracker system project: Technical Design Report*. Geneva: CERN. Retrieved from https://cds.cern.ch/record/368412

Langacker, P. (1986). The standard model and beyond. In *Aip conference proceedings* (Vol. 150, pp. 142–164).

Large Hadron Collider (LHC) Lecture. (2016). Retrieved 18/05/2021, from http://boson.physics.sc.edu/~venkat/spring2016/Lecture01.pdf/

Layter, J. G. (1997). *The CMS muon project: Technical Design Report*. Geneva: CERN. Retrieved from https://cds.cern.ch/record/343814

Luciano, M. (2017). *Advanced detector technology.* Retrieved 12/05/2021, from https://indico.cern.ch/event/598530/contributions/2547226/attachments/1517190/2368223/HCP2017_LMusa_L2.pdf

Mahnke, W., Leitner, S.-H., & Damm, M. (2009). *Opc unified architecture*. Springer Science & Business Media.

Mandelstam, S. (1958). Determination of the pion-nucleon scattering amplitude from dispersion relations and unitarity. general theory. *Physical Review*, *112*(4), 1344.

Mobs, E. (2018, Aug). The CERN accelerator complex - August 2018. Complexe des accélérateurs du CERN - Août 2018. Retrieved from `https://cds.cern.ch/record/2636343` (General Photo)

Murnane, D. (2014). *Supersymmetric dark matter searches with cms data* (Doctoral dissertation). doi: 10.13140/RG.2.2.13923.50724

Myers, S. (2012). The engineering needed for particle physics. *Philosophical Transactions of the Royal Society A: Mathematical, Physical and Engineering Sciences*, *370*(1973), 3887–3923. doi: 10.1098/rsta.2011.0053

Ogur, S. (2020-09-12). personal communication.

Ogur, S., & Yildiz, V. (2020-09-12). personal communication.

Opc historical data access. (n.d.). Retrieved 12/05/2021, from `https://opcfoundation.org/developer-tools/specifications-classic/historical-data-access/`

Orfanelli, S. (2016). *An innovative beam halo monitor system for the cms experiment at the lhc: Design, commissioning and first beam results* . Retrieved from `https://cds.cern.ch/record/2231966` (Presented 11 Feb 2016)

The Phase-2 Upgrade of the CMS Barrel Calorimeters (Tech. Rep.). (2017, Sep). Geneva: CERN. Retrieved from `https://cds.cern.ch/record/2283187` (This is the final version, approved by the LHCC)

The Phase-2 Upgrade of the CMS DAQ Interim Technical Design Report (Tech. Rep.). (2017, Sep). Geneva: CERN. Retrieved from `https://cds.cern.ch/record/2283193` (This is the CMS Interim TDR devoted to the

upgrade of the CMS DAQ in view of the HL-LHC running, as approved by the LHCC.)

The Phase-2 Upgrade of the CMS Endcap Calorimeter (Tech. Rep.). (2017, Nov). Geneva: CERN. Retrieved from https://cds.cern.ch/record/2293646

The Phase-2 Upgrade of the CMS Muon Detectors (Tech. Rep.). (2017, Sep). Geneva: CERN. Retrieved from https://cds.cern.ch/record/2283189 (This is the final version, approved by the LHCC.)

The Phase-2 Upgrade of the CMS Tracker (Tech. Rep.). (2017, Jun). Geneva: CERN. Retrieved from https://cds.cern.ch/record/2272264

PHYS3002 : NUCLEI AND PARTICLES Lecture Notes. (2015). Retrieved 18/05/2021, from http://www.personal.soton.ac.uk/ab1u06/teaching/phys3002/course/13_accelerators_a.pdf

Rossi, L., & Brüning, O. (2015). Introduction to the HL-LHC Project. *Adv. Ser. Dir. High Energy Phys.*, *24*, 1-17. Retrieved from https://cds.cern.ch/record/2130736 doi: 10.1142/9789814675475_0001

Siemens. (n.d.). *Simatic wincc oa from siemens.* Retrieved from https://new.siemens.com/global/en/products/automation/industry-software/automation-software/scada/simatic-wincc-v7.htmldefault.aspx.error.html

Stevens, W. R., Rudoff, A. M., & Fenner, B. (2003). *Unix network programming volume 1: The sockets networking api* (Vol. 3). Addison-Wesley Professional.

TDR, C. (2006). Cms physics: Technical design report v. 2: Physics performance. *Cern Geneva1*.

Tsirou, A. (2020-12-05). personal communication.

Tsirou, A., Tekis, H., & Verdini, P. G. (2019). *The first pcb design of the mtrs*

boards:eda-04119-v1. Retrieved 12/05/2021, from https://edms.cern.ch/ui/#!master/search/view?objecttype=document&query=EDA-04119-V1&latestversion=false&hideobsolete=true&dadvanced=false&global=true

Tsirou, A., Tekis, H., & Verdini, P. G. (2020). *The second pcb design of the mtrs boards*. Retrieved 12/05/2021, from https://edms.cern.ch/ui/#!master/search/view?objecttype=document&query=EDA-04119-V2.0&latestversion=false&hideobsolete=true&dadvanced=false&global=true

Tsirou, A., & Verdini, G., P. (2020-10-23). personal communication.

Wenninger, J. (n.d.). *The LNF Spring School Lecture Note: "LHC: construction and operation"*.

Yousaf Shah, S., Tsirou, A., Verdini, P. G., Hartmann, F., Masetti, L., Dirkes, G. H., ... Fahrer, M. (2009). The CMS Tracker Detector Control System. *Nuclear Instruments and Methods in Physics Research Section A: Accelerators, Spectrometers, Detectors and Associated Equipment*, *604*(1-2), 281–283. doi: 10.1016/j.nima.2009.01.093

APPENDIX 1. EDA-04119-V1-0 SCHEMATIC DRAW

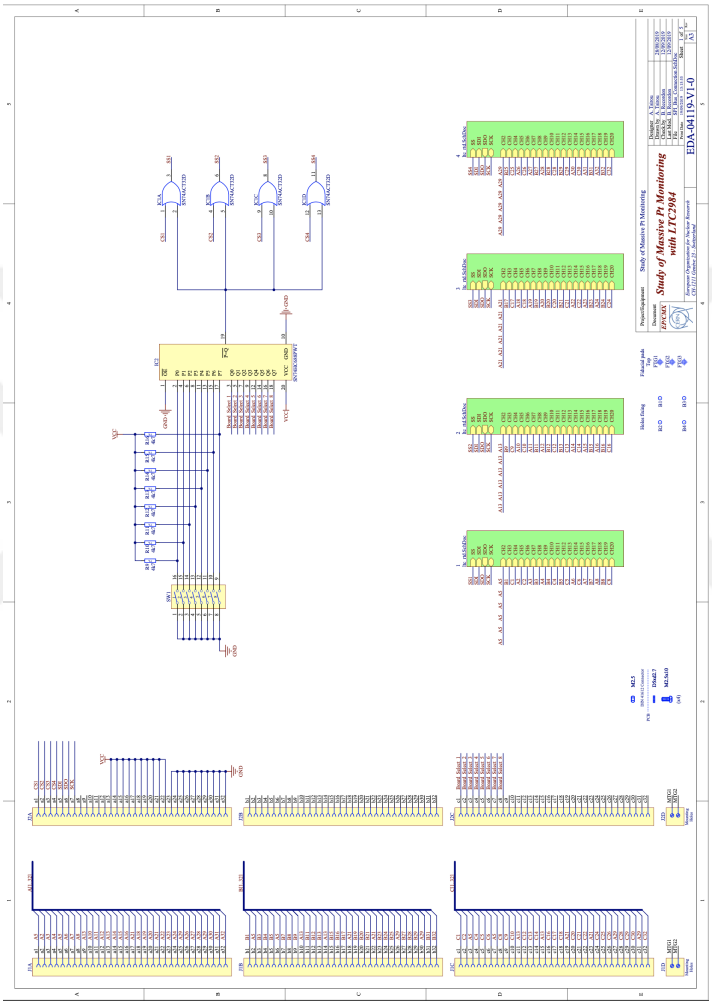


Figure 9.1: MTRS Phase 1 circuit design for SPI communication, board and chip selections.

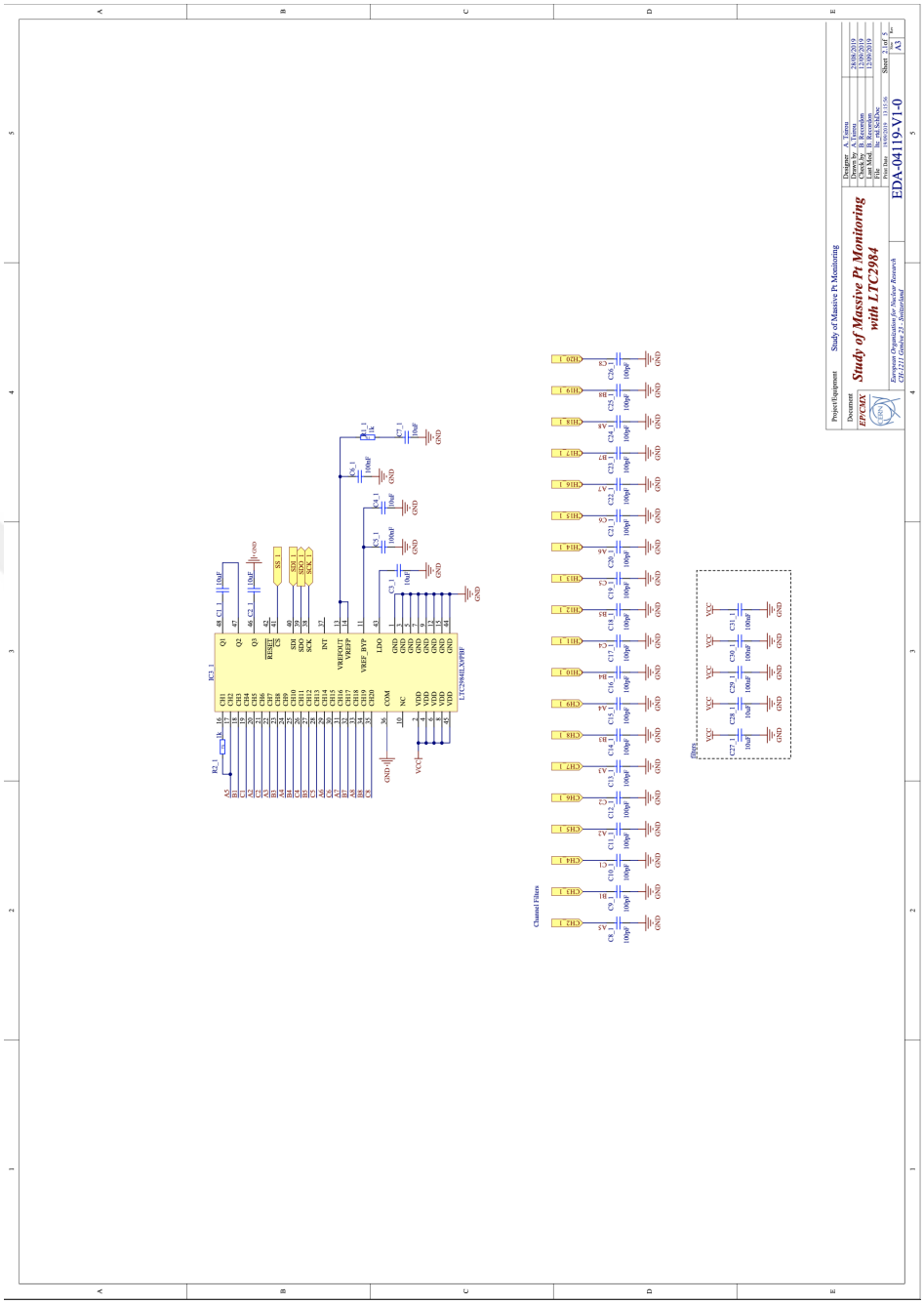
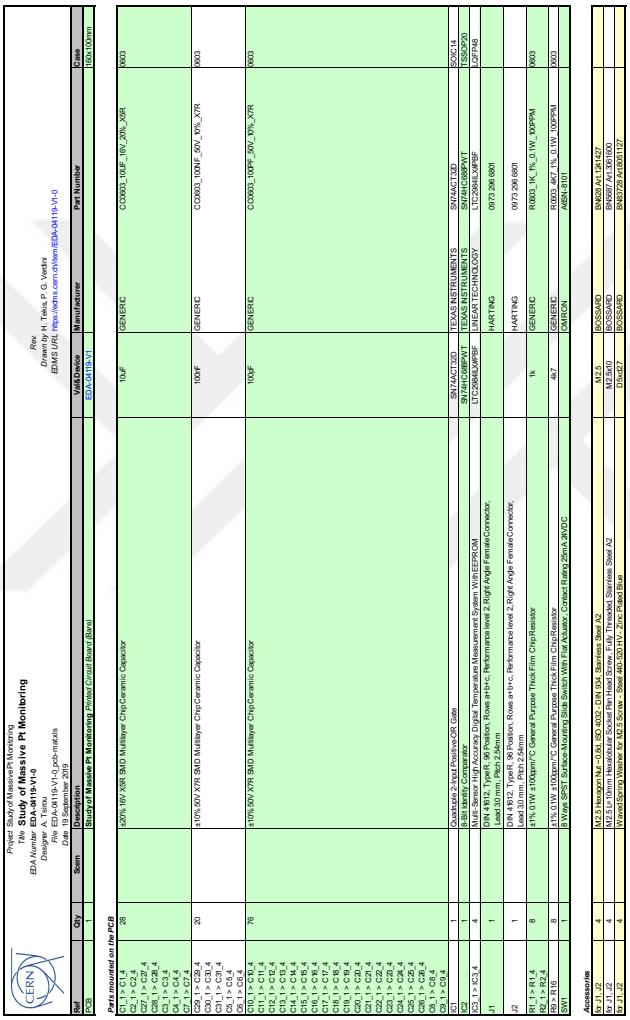


Figure 9.2: A LTC2984 IC connections by two VME connectors (Raspberry Pi and sensors) in MTRS Phase 1.

APPENDIX 2. EDA-04119-V1-0 PCB MATERIALS



EDA-04119-V1-0_pcb-mat.xls

Project: Study of MassivePt Monitoring
Title: **Study of Massive Pt Monitoring**
EDA Number: **EDA-04119-V1-0**
Owner: A. Pezzotta
File: EDA-04119-V1-0_pcb-mat.xls
Date: 19 September 2019

Rev:
Drawn by: H.T.Teles, P. G. Verdini
EDMS URL: https://edms.cern.ch/item/EDA-04119-V1-0

Ref	Qty	Seen	Description	Valid Device	Manufacturer	Part Number	Case
PCB	1		**Study of Massive Pt Monitoring** Printed Circuit Board (Bare)	EDA-04119-V1			100x100mm
Parts mounted on the PCB							
C1_1 > C1_4 C2_1 > C2_4 C27_1 > C27_4 C28_1 > C28_4 C3_1 > C3_4 C4_1 > C4_4 C7_1 > C7_4	28		±20% 16V X5R SMD Multilayer Chip Ceramic Capacitor	10uF	GENERIC	CC0603_10UF_16V_20%_X5R	0603
C29_1 > C29_4 C30_1 > C30_4 C31_1 > C31_4 C5_1 > C5_4 C6_1 > C6_4	20		±10% 50V X7R SMD Multilayer Chip Ceramic Capacitor	100nF	GENERIC	CC0603_100NF_50V_10%_X7R	0603
C10_1 > C10_4 C11_1 > C11_4 C12_1 > C12_4 C13_1 > C13_4 C14_1 > C14_4 C15_1 > C15_4 C16_1 > C16_4 C17_1 > C17_4 C18_1 > C18_4 C19_1 > C19_4 C20_1 > C20_4 C21_1 > C21_4 C22_1 > C22_4 C23_1 > C23_4 C24_1 > C24_4 C25_1 > C25_4 C26_1 > C26_4 C8_1 > C8_4 C9_1 > C9_4	76		±10% 50V X7R SMD Multilayer Chip Ceramic Capacitor	100pF	GENERIC	CC0603_100PF_50V_10%_X7R	0603
IC1	1		Quadruple 2-Input Positive-OR Gate	SN74AHCT32D	TEXAS INSTRUMENTS	SN74AHCT32D	SOIC14
IC2	1		8-Ch Analog Multiplexer	SN74HC4051PWT	TEXAS INSTRUMENTS	SN74HC4051PWT	TSSOP16
IC3_1 > IC3_4	4		Multi-Sensor High Accuracy Digital Temperature Measurement System With EEPROM	LTC2984IUKPBF	LINEAR TECHNOLOGY	LTC2984IUKPBF	LQFP48
J1	1		DIN 41612, Type/R, 96 Position, Rows a+b+c, Performance level 2,Right Angle Female Connector, Lead 30 mm, Pitch 2.54mm		HARTING	09 73 296 6801	
J2	1		DIN 41612, Type/R, 96 Position, Rows a+b+c, Performance level 2,Right Angle Female Connector, Lead 3.8 mm, Pitch 2.54mm		HARTING	09 73 296 6801	
R1_1 > R1_4 R2_1 > R2_4	8		±1% 0.1W ±100ppm/°C General Purpose Thick Film ChipResistor	1k	GENERIC	R0603_1K_1%_0.1W_100PPM	0603
R3 > R16	8		±1% 0.1W ±100ppm/°C General Purpose Thick Film ChipResistor	4k7	GENERIC	R0603_4K7_1%_0.1W_100PPM	0603
SW1	1		8 Ways SPST Surface-Mounting Slide Switch With Flat Actuator, Comes Rating 25mA 28VDC		OMRON	A6B4-8101	
Accessories							
for J1, J2	4		M2.5 Hexagon Nut –Obl. ISO 4032 - DIN 934 ,Stainless Steel A2	M2.5	BOSSARD	BN828 Art.1361427	
for J1, J2	4		M2.5 x 10mm Hexalobular Socket Pan Head Screw, Fully Threaded, Stainless Steel A2	M2.5x10	BOSSARD	BN5697 Art.1361690	
for J1, J2	4		Wave/Spring Washer for M2.5 Screw - Steel 460-540 Hv - Zinc Plated Blue	10wa27	BOSSARD	BN5728 Art.1361127	

Dimensions: 100 x 100mm		
Through Pins	196	
SMD pins on Top	522	
SMD pins on Bottom	0	
Total number of pins	718	

Figure 9.3: Materials used for PCB design of MTRS Phase 1.

APPENDIX 3. EDA-04119-V2-0 SCHEMATIC DRAW

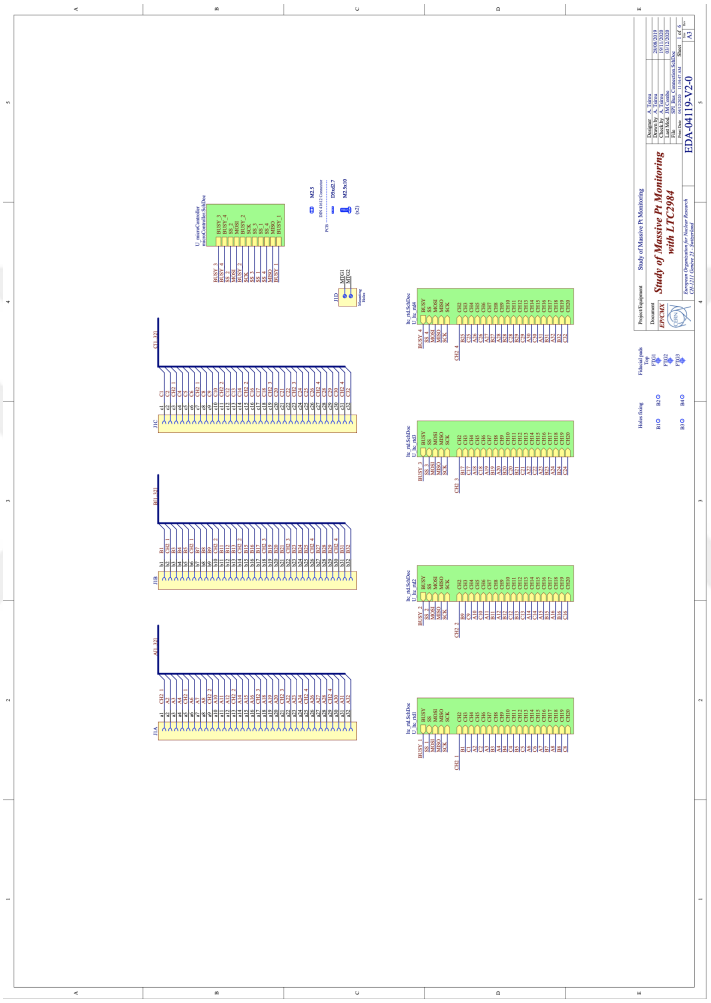


Figure 9.4: VME sensor connections by four LTC2984 ICs, and ATMEGA328P SPI, UART and I^2C connections with four LTC2984 chips in MTRS Phase 2 circuit design.

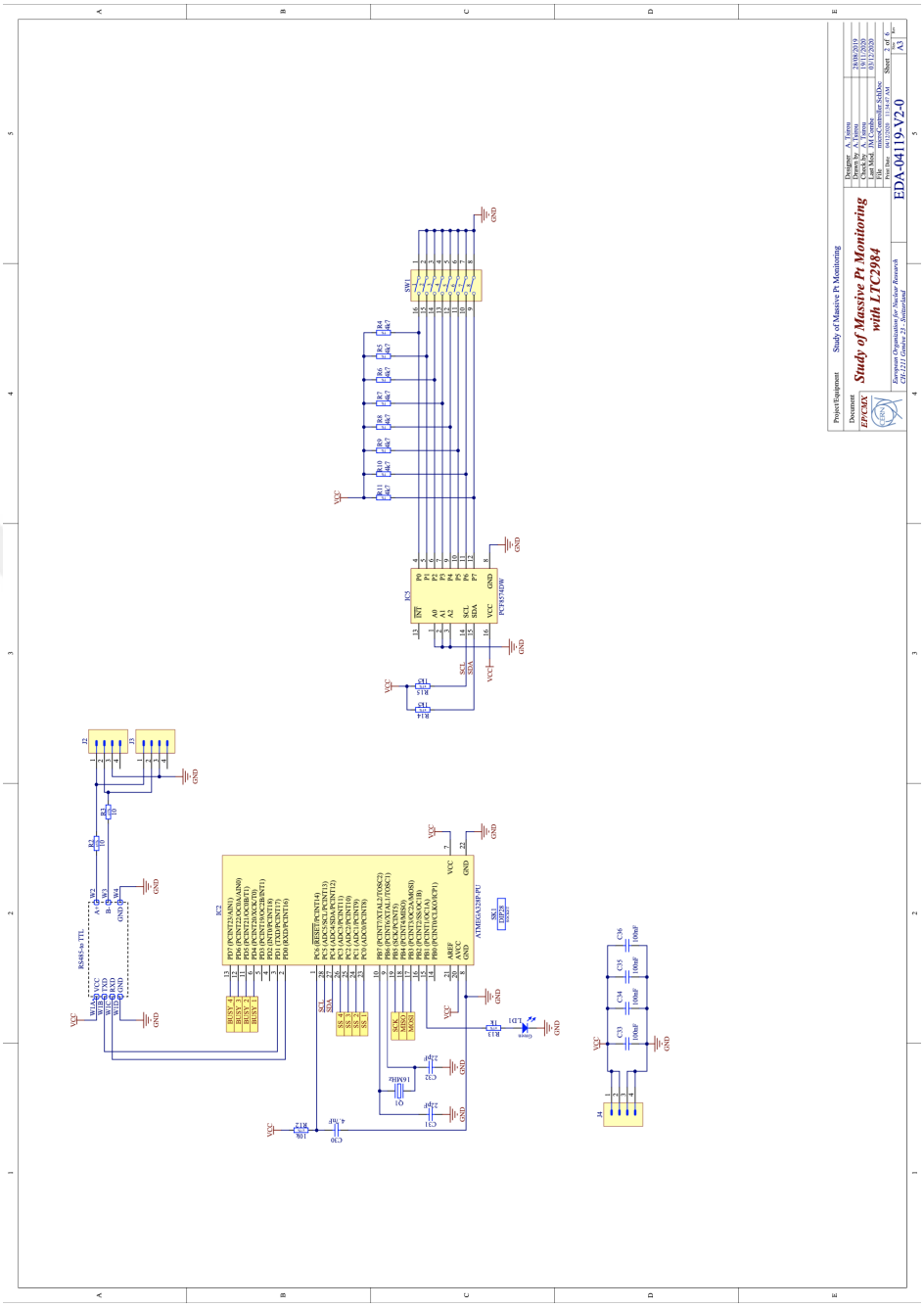


Figure 9.5: MTRS Phase-2 circuit design continues with connections between ATMEGA328 and RS485 TTL circuit.

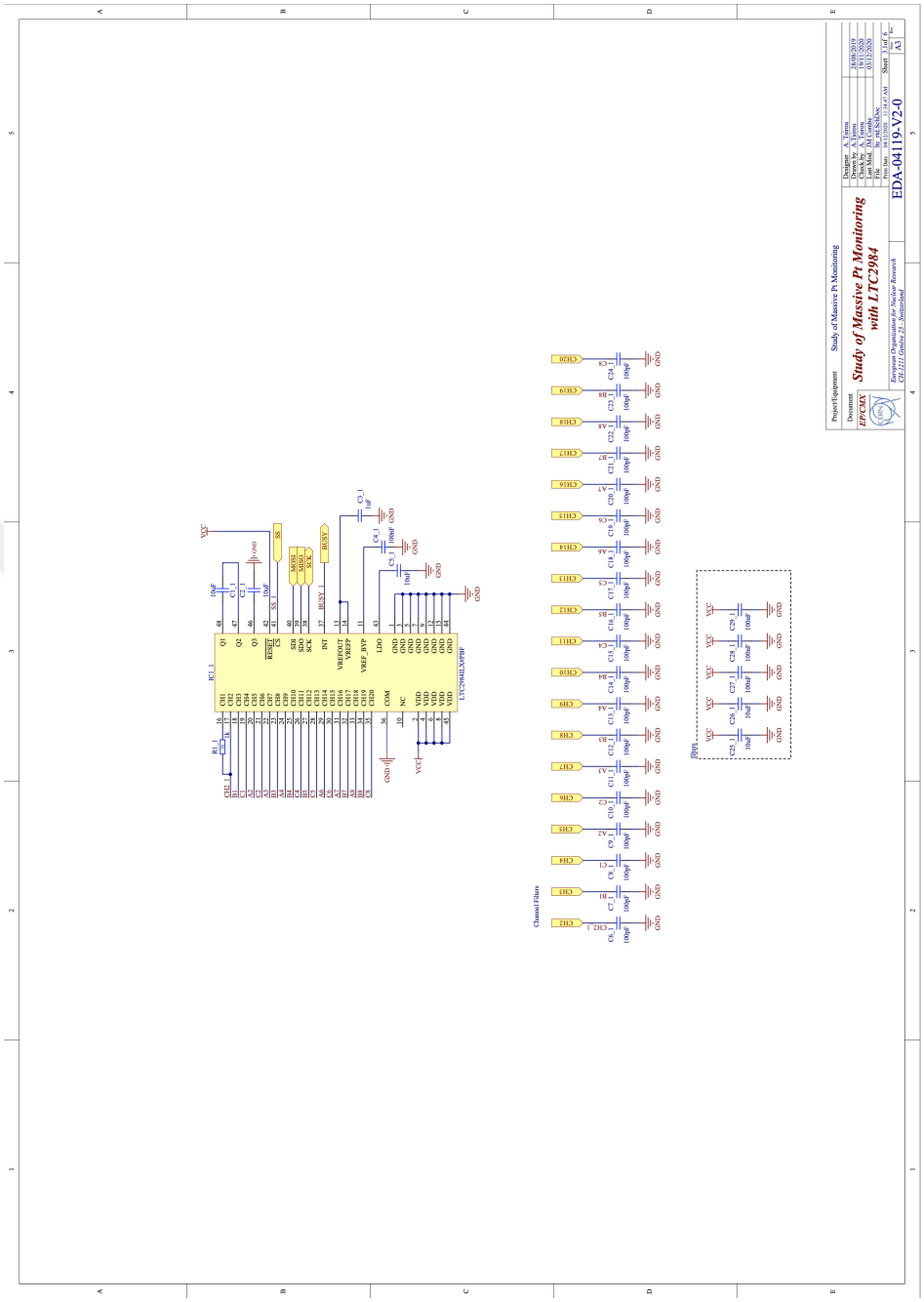


Figure 9.6: A LTC2984 IC connections by VME connectors (sensor connections) and ATMEGA328P in MTRS Phase 2.

CURRICULUM VITAE

PERSONAL INFORMATION

Name, Last Name : Hatice TEKİŞ

EDUCATION

Bachelor of Science : July 2017, KTO Karatay University, Faculty of Engineering, Computer Engineering

: July 2017, KTO Karatay University, Faculty of Engineering, Electrical and Electronics Engineering (Double Major)

Master of Science : June 2021,KTO Karatay University, The School of Graduate Studies, Electrical and Computer Engineering

Languages : English

WORK EXPERIENCES

Internships:

Date	**Title**	**Institution**
Jan. 2020–Mar. 2021	Technical Student	CERN,
Jun. 2019–Sept. 2019	Summer Student	CERN,
Sept.2016–Jul. 2017	Student Assistant	KTO Karatay University,
Jul. 2016–Aug. 2016	Engineering Intern	HAVELSAN,
Nov. 2015–Jul. 2016	Student Assistant	KTO Karatay University,
Jun. 2015–Jul.2015	Engineering Intern	Anadolu Birlik Holding.

The Organization Where S/he Works:

Date	**Title**	**Institution**
Nov. 2019–Present	Research Assistant	KTO Karatay University,
Oct. 2017–Nov. 2019	Project Assistant	KTO Karatay University.

Date of Approval: the 7thof June 2021.